The Fire Safety of Granular Propellant Handling Facilities

Frederick Paquet

A Thesis

in

The Department

of

Mechanical and Industrial Engineering

Presented in Partial Fulfillment of the Requirements

for the Degree of

Doctor of Philosophy (Mechanical Engineering) at

Concordia University

Montréal, Québec, Canada

January 2017

CONCORDIA UNIVERSITY

School of Graduate Studies

This is to certify that the thesis prepared

By: **Mr. Frederick Paquet**

Entitled: **The Fire Safety of Granular Propellant Handling Facilities**

and submitted in partial fulfillment of the requirements for the degree of

Doctor of Philosophy (Mechanical Engineering)

complies with the regulations of this University and meets the accepted standards with respect to originality and quality.

Signed by the Final Examining Committee:

_____ Chair
Dr. Catherine Mulligan

_____ External Examiner
Dr. Andrew Higgins

_____ External to Program
Dr. Liangzhu Wang

_____ Examiner
Dr. Lyes Kadem

_____ Examiner
Dr. Gerard Gouw

_____ Examiner
Dr. Sek Kwan Chan

_____ Supervisor
Dr. Hoi Dick Ng

Approved by _____
Martin D. Pugh, Chair
Department of Mechanical and Industrial Engineering

_____ 2017

_____
Amir Asif, Dean
Faculty of Engineering and Computer Science

Abstract

The Fire Safety of Granular Propellant Handling Facilities

Frederick Paquet, Ph.D.

Concordia University, 2017

This thesis examines an industry-related problem in the field of solid granular propellant combustion. Through a literature review, it has been found that the safety aspects of propellants installations have not been well defined and studied. Such lack of standard could potentially lead to industrial accidents of varying magnitudes. The present project studies the flame propagation, heat output and pressure generated by the combustion of a range of propellants configurations. An experimental approach is first used to obtain a reliable set of data. Models are then obtained through the comparison of the empirical data with theoretical considerations, scaling and numerical simulations. Using the generated models, it shall eventually be possible to apply the findings in conceiving a set of guidelines for the safe design of propellant installations.

Flame propagation is central to the study of propellant combustion. Through the examination of video recordings from an array of propellant fire tests, it is possible to observe three main flame propagation modes: radiation heat transfer (ideal case), contact with burning projections and engulfment by a fireball. The maximum event dimensions depend on the dominant mode. A decision tree scheme is used to breakdown the possible events in the various propagation modes and assign conditions for their occurrence. Application of the methodology on a small scale flame propagation test shows that it is possible to scale the results to larger scale cases and obtain propagation rate estimates.

In both the radiant heat flux and pressure generation cases, theoretical forms are derived based on previous work and theoretical principles. Statistical analyses of the experimental results show good agreement with general theoretical forms. It is shown that one must, however, be attentive to possible collinearities and variable factors when interpreting statistical results. By taking into account the theoretical expectations, it is possible to estimate these additional factors and obtain models that are more generally applicable. It is also shown that the general models rely heavily on the combustion rate of the propellant configuration. This shows that the flame propagation analysis is an important part of estimating the various fire safety parameters of granular propellants.

In memory of Roy Albion Nichols

Acknowledgments

The author wishes to acknowledge the important contribution made by General Dynamics - Ordnance and Tactical Systems Canada, Valleyfield for providing the propellant samples, test enclosures and testing facilities. The author also thanks the contribution of Francois Cottin, Simon Durand, Etienne Comtois, and Pierre Lavigne in planning and performing the testing. The help of Janet Nichols is also acknowledged in the final review of the manuscript. Part of this work was supported by the Natural Science and Engineering Research Council of Canada (NSERC) through Engage grant number EGP 415114-11.

On a more personal note, I would like to thank my supervisor, Dr. Hoi Dick Ng, for allowing me to complete this endeavor. Given my special part-time status, due to other professional obligations, his patience and support were exemplary. I also would like to acknowledge the support of Daniel Lepage, Pierre-Yves Paradis and Marc Boileau for allowing me to perform this work as part of my employment at General Dynamics - Ordnance and Tactical Systems Canada, Valleyfield. The support given by Dr. Dominic Groulx of Dalhousie University in reviewing parts of this manuscript was greatly appreciated.

Thanks to my family for their unwavering support in this lengthy effort. The constant encouragement by my grandparents, parents and sister will never be forgotten. Of special note is the contribution of my father, Mario Paquet, in giving me the love of science and keeping me on the right path from time to time. Finally, I would like to thank my wife for her constant care and patience.

Table of Contents

List of Figures

List of Tables

List of Symbols

Symbol	**Description**	**Unit** (SI - mks)
α_i	Calculation constants	(multiple)
γ	Heat capacity ratio	(dimensionless)
γ_f	Effective heating length	(m)
Δt	Time increment	(s)
ϕ	Edge half angle	(rad)
θ	Elevation angle	(rad)
Ω	Thermodynamic state function	(operator)
ρ_{air}	Air density	(kg/m^3)
ρ_{bulk}	Solid propellant bulk density	(kg/m^3)
ρ_{gas}	Combustion gases density	(kg/m^3)
ρ_{solid}	Solid propellant absolute density	(kg/m^3)
σ	Stefan-Boltzmann constant	(W m^{-2} K^{-4})
τ	Emissivity	(dimensionless)
τ_{OD}	Optical thickness	(dimensionless)
$\bar{\tau}$	Time ratio	(dimensionless)
χ	Combustion - transmission ratio	(dimensionless)
a_i	Exponential constant	(dimensionless)
A	Venting area	(m^2)

A_{base}	Fire base surface area	(m^2)
b	Covolume	(m^3/kg)
B	Vector of unknown exponents	(dimensionless)
c	Charge density	(kg/m^3)
c_τ	Fraction of energy transmitted	(dimensionless)
c_{air}	Sound velocity in air	(m/s)
c_p	Solid propellant heat capacity	(J/kg K)
C	Constant	(dimensionless)
C_D	Discharge coefficient	(dimensionless)
C_v	Combustion gases heat capacity	(J/kg K)
d_t	Thickness	(m)
D_{ini}	Propellant stack diameter	(m)
D_{flame}	Flame diameter	(m)
E	Propellant heat of explosion	(J/kg)
F_{1-2}	Configuration factor	(dimensionless)
F_n	n^{th} Configuration factor	(dimensionless)
g	Gravitational acceleration	(m/s^2)
$\bar{h}$	Burning propellant height ratio	(dimensionless)
h_{test}	Test burning propellant height	(m)
H	Flame height	(m)
H_{stack}	Propellant stack height	(m)
I_i	Intensity at point i	(W/m^2)
k	Thermal conductivity	(W/m K)
k_1, k_2	Constant factors	(multiple)
k_B	Boltzmann constant	(J/K)
k_i	Slope of the maximum pressure with mass	(Pa/kg)

k_{st}	Deflagration index	(Pa m/s)
$\bar{L}$	Characteristic length	(m)
m	Solid propellant mass	(kg)
m_{air}	Mass of air in enclosure	(kg)
m_e	Total enclosure gas mass	(kg)
m_{max}	Maximum gas mass in enclosure	(kg)
$\dot{m}_e$	Total mass rate of change	(kg/s)
$\dot{m}_{gen}$	Mass combustion rate	(kg/s)
$\dot{m}_{vent}$	Gas mass venting rate	(kg/s)
M_w	Molecular weight of combustion gases	(kg/mol)
N	Number of moles	(mol)
p_i	Enclosure pressure	(Pa)
p_o	Outside pressure	(Pa)
p_{red}^{LP}	Low pressure asymptote reduced pressure	(Pa)
P	Pressure	(Pa)
P_m	Maximum unvented pressure	(Pa)
P_{max}	Maximum vented pressure	(Pa)
P_{red}	Reduced pressure	(Pa)
$\dot{P}_{max}$	Maximum vented pressure rate of change	(Pa/s)
q	Heat flux	(J/m^2)
q_{in}	Surface heat flux	(W/m^2)
$\dot{q}''$	Radiant heat flux	(W/m^2)
$\mathbf{Q}$	Vector of maximum radiant heat fluxes	(W/m^2)
$\bar{Q}$	Scaled power	(W/kg)
$\dot{Q}_m$	Fire power	(W)
$\dot{Q}_r$	Total radiated power	(W)

$\dot{Q}_s$	Surface emissive power	(W/m^2)
r_{fire}	Distance from the fire	(m)
r_{flame}	Flame radius	(m)
r_x	Horizontal flame propagation rate	(m/s)
r_y	Vertical flame propagation rate	(m/s)
r^2	Square of the correlation coefficient	(dimensionless)
R	Ideal gas constant	(Pa m^3 / mol K)
R_{fire}	Fireball radius	(m)
R_{flame}	Flame radius	(m)
R_i	Distance at point i	(m)
R_{ini}	Propellant stack radius	(m)
R_{sphere}	Equivalent sphere radius	(m)
S_u	Flame velocity	(m/s)
t	Time	(s)
t_{burn}	Propellant grain burning time	(s)
t_{burnx}	Horizontal burning time	(s)
t_{burny}	Vertical burning time	(s)
t_{ig}	Ignition time	(s)
t_{ind}	Induction time	(s)
t_{proj}	Propellant grain projection time	(s)
t_{ss}	Steady state time	(s)
t_{tot}	Total event time	(s)
T	Temperature	(K)
T_f	Surface flame temperature	(K)
T_{ig}	Ignition temperature	(K)
T_{inf}	Surrounding temperature	(K)

T_o	Maximum thickness temperature	(K)
T_{OD}	Transmittance	(dimensionless)
T_s	Surface temperature	(K)
u, v, w	Unit vector components	(m)
U	Gas rising velocity	(m/s)
v	Gas venting velocity	(m/s)
v_g	Propellant grain velocity	(m/s)
V	Volume	(m^3)
$\bar{V}$	Burning propellant volume ratio	(dimensionless)
V_{cyl}	Cylindrical fire plume volume	(m^3)
V_N	Burning rate normal to the strand edge	(m/s)
V_{test}	Test burning propellant volume	(m^3)
V_u	Burning rate in the vertical direction	(m/s)
x	Spatial dimension	(m)
X	Charge covolume ratio	(dimensionless)
$\mathbf{X}$	Matrix of independant variables	(multiple)

Chapter 1

Introduction

> "It is not a description of a mechanism, or anything concrete; it is just a strange fact that we can calculate some number and when we finish watching nature go through her tricks and calculate the number again, it is the same."
>
> Richard Feynman - Lectures on physics (1961)

Throughout human history, energy transformation has been an important factor in the advancement of technologies. Some of the most fundamental inventions have been designed to harness a certain form of energy and release it as another. The discovery of fire is an example where a substance undergoes some transformation which emits heat and other products. The wheel was invented to transform rotational energy into translational energy. In the last example, both the input and output are forms of mechanical energy. More modern examples include the transformation of mechanical energy to electrical energy through various types of turbines and the generation of heat from the energy contained in atoms through nuclear reactions.

Although it was realized very early that energy can be transformed, it would not be until

the Renaissance and the birth of modern science that a formal description of these phenomena was obtained [1]. Various conservation laws have resulted in what is now known as the First Law of Thermodynamics. This law states that energy is always conserved. The term energy is itself difficult to define. In the present context, one of the best definitions would be that of Richard Feynman [2]: "property of objects, transferable among them via fundamental interactions, which can be converted into different forms but not created or destroyed". The previous definition does not directly define what energy is, but clearly states how it is perceived. From an engineering standpoint, this definition of energy is sufficient, as shown by the large number of applications derived from it.

Energy transformation is the main goal of any propellant. The presence of the verb to "propel" in the word propellant implies that the product is mechanical energy. This transformation is achieved by two main ways: the expansion of a pressurized gas, such as would be found in a spray bottle, or the completion of a combustion reaction. The latter requires that the product be a high temperature mixture of gaseous products. The reactants of a propellant combustion reaction can be of any physical phase but solids and liquids are often used. The heat liberated by the chemical reaction along with a change of phase from solid or liquid to gas can potentially generate high pressures in a closed volume. The resulting pressure can subsequently be used to perform mechanical work [3]. The following are three widely used applications of propellants:

- Rockets: the high-pressure and temperature gases generated inside a partially closed volume are allowed to eject in a controlled fashion. By the conservation of momentum (or Newton's third law), the high energy gas flow will produce an equivalent thrust on the rocket.

- Guns: high pressure and temperature gases generated inside a closed volume are used to push a free moving projectile outside of a known length tube.

- Airbags: the high pressure and temperature gases generated inside a closed volume are allowed to vent inside a larger chamber composed of a flexible boundary, thus inflating the airbag. In this case, the gas generation and flow rates must be carefully controlled such that the inflation time be as specified (for example, faster than a collision but not fast enough to harm the user).

Because these applications differ considerably in their mechanical work requirement, the associated propellants will also differ. The data given in Table 1.1 shows the mechanical power required for a few of these applications [4] [5] [6]. One must thus be able to control the energy transformation very precisely. As the next section will show, this is performed by careful consideration of the propellant chemistry and geometry.

Table 1.1: Mechanical energy needed for various propellant applications

Application	Mechanical Energy (MJ)	Deployment time (s)
Space shuttle booster (rocket)	319,000	145
Typical airbag	8	0.06
Hunting riffle	4	0.01
Artillery gun	2000	0.03

1.1 Solid propellant combustion elements

Solid propellants are used in applications requiring high mechanical energies released in short times. In essence, all applications using propellants basically require large impulses. Being solid with a granular geometry, propellants are characterized by their composition and by the geometrical shape of the grains. The composition is important in establishing the required energy content to be released. It is also helpful in insuring that the energy release will not harm the application in any unwanted ways. For example, various chemicals can be used to reduce the erosivity of combustion gases with respect to the applications or to simply reduce the luminous flash associated with the combustion [3]. The

chemical makeup is also responsible for a very important property known as the burning rate of the composition. The burning rate of a propellant is the rate at which the solid to gas transformation takes place. In solid propellants, this burning rate is usually observed as the velocity of the receding surfaces during combustion [7]. Using a specific geometrical grain shape is a way to control the surface area of the propellant during the combustion. Since propellant combustion is a surface phenomena, controlling the surface will control the resulting solid to gas conversion rate. The grain geometry is also important in obtaining a product that is easy to handle in various applications. The chemical and geometrical aspects of propellants are discussed next, in detail.

1.1.1 Propellant combustion thermodynamics

As stated previously, the propellant composition is paramount in establishing the energy available for future release. Two main ingredients are used to control the energetic content of granular propellants: nitrocellulose, nitroglycerin [8]. Nearly all compositions use nitrocellulose, as this ingredient is practical to create the various geometrical shapes used. Propellants that use nitrocellulose as the only energetic component are called single bases. When additional energy is needed, nitroglycerin is usually added in the composition. This creates what is known as a double base. In addition to having higher energy, double bases will generally also have higher burning rates. In some cases, a third energetic component, nitroguanidine, is used to address the thermodynamic properties of the combustion gases. These propellants, known as triple bases, are useful for applications requiring higher energies and lower burning temperatures. Other energetic components are also sometimes used but in a far less frequent manner. Examples include RDX (Hexogen, cyclotrimethylene trinitramine), DEGDN (Diethylene Glycol Dinitrate) and HMX (Octogen, cyclotetramethylene tetranitramine) [3]. In all these cases, inert ingredients are often used to control the energy and burning rate more precisely. The combination of inert and

energetic components are chosen so as to satisfy the requirements of the application and optimize the manufacturing process.

Propellants are used in applications requiring high mechanical energies. The mechanical energies are obtained by the force applied through the pressure inside a closed volume. To obtain the required pressure, two mechanisms are at play: the release of thermal energy and a transformation from solid to gas [4]. In the former case, the heat liberated by the combustion of a solid is absorbed by the gas inside the closed chamber, thus increasing the pressure. In the latter case, it is a fact that small quantities of gases at standard conditions will occupy a large volume. For example, a 1 m^3 chamber will contain roughly 1.2 kg of air [9]. The same volume will hold approximately one ton of solid propellant, an increase by a factor of 1000 [4]. Since most equations of states for common gases show a direct relation with the quantity inside a volume, it is easy to see that enormous pressures can be generated by a transformation from solid to gas. The combination of both the energy release and a phase transformation thus creates the proper conditions for the generation of high mechanical energies. Given the type of phenomena at play during the above described combustion processes, it is important to better understand the thermodynamic variables used in modelling these events along with the relations between these variables.

Propellant combustion gases usually follow an equation of state known as the Nobel-Abel equation [7]:

$$P(V - b) = NRT \tag{1}$$

where b is known as the covolume of the combustion gases. The Nobel-Abel equation of state points to two important properties of propellant combustion gases: covolume and flame temperature. Covolume is a factor representing the actual volume taken by the gas molecules due to their nonideal behaviour [7]. It is not the volume of the individual molecules, but the apparent volume of interaction of these molecules. This volume of interaction becomes important at high temperatures and pressures. The flame temperature

is the temperature at which the gases are heated due to the release of the combustion energy [10]. This quantity is usually given either for constant volume or constant pressure settings in standard conditions. For the majority of common propellants, flame temperature will vary from 2500 to 3500 K. A commonly used related quantity is known as the propellant force. The force is simply the product RT, where R is the combustion gas constant and T is the flame temperature [4]. Scaled appropriately, the force is expressed in units of energy per unit mass. Therefore, one must be careful not to mix the concepts of propellant force and heat of explosion. The former only includes the energetic component contribution while the latter includes both the energetic and mass conversion components. For example, a typical double base will have a force of around 1000 J/g while its heat of explosion will be roughly 5000 J/g [4].

Other thermodynamic properties of note are the heat capacities and densities of the combustion gases. These properties depend on the configuration and chemical makeup of these gases. Computational codes are often used to obtain these thermodynamic parameters. Given a known set of ingredients, the codes can calculate a set of reaction products along with their concentrations and all relevant properties (from tabulated experimental data or fitted equations). Examples of such codes are NASA-CEA (National Aeronautics and Space Administration - Chemical Equilibrium with Applications) [11], Chemkin [12] and Cheetah [13]. Note that these codes provide the thermochemical parameters of the propellant combustion gases and also address the reaction kinetics. Due to the large number of possible reactions and their dependence on the external conditions, it is much harder to calculate reaction rates than it is to compute equilibrium conditions. Therefore, it is not currently possible to calculate the burning rate of a composition based only on its chemical makeup [14].

When using a closed volume, the ratio of the propellant mass on the volume is known as the charge density [4]. In most applications, the charge density is high enough that it is

warranted to assume combustion gases that have flame values. When performing calculations on such cases it is customary to neglect the air originally present in the application. In cases where this density has lower values, the previous assumption is no longer valid as the variables will take values between that of the standard properties and flame values. The effect of air thus cannot be neglected anymore as some mixing will occur. The situation becomes even more complex when the combustion gases are allowed to escape in the atmosphere, such as would be the case in open air burnings and vented enclosure fires.

1.1.2 Combustion rate

During the manufacturing process, the chosen chemical ingredients are initially mixed together with or without the aid of processing solvents. Following the mixing step, the composition is extruded through a set of dies in order to shape the product to a desired geometry. The extruded strands are then cut in a rotary cutting machine to a specific length [8]. The geometry given to the formulation is of great importance to its combustion behaviour as it controls the available surface area. Since the combustion occurs at the surface of the propellant, the total area can change during the combustion. In some cases it is useful to have a progressive gas generation rate by using a geometry where the surface area increases with the advancing combustion [8]. Propellants are often tested in constant volume closed vessels prior to being used in their applications. The energy and gas generation rate of a sample are characterized by measuring the maximum pressure obtained and the time rate of change of the pressure signal, respectively [4].

Propellant grains are usually cylindrical, spherical or rectangular in shape. In order to control the surface progression during combustion, cylindrical grains contain a number of cylindrical holes which are centered and parallel to the radial axis. These holes are known as perforations. As the number of perforations is increased, the surface of the grain will also increase as combustion progresses. Typically, the commonly used grain geometries

feature 0, 1, 7, or 19 perforations [7]. The number of perforations used depends on the requirements of the application. A diagram showing these commonly used geometries is shown on Figure 1.1. If the grain surface area progression is guided by the number of perforations, its surface area magnitude is decided by the actual dimensions of the grain. The spacing between each cylindrical surface of the grain (perforations and outer diameter) is a quantity known as the web of the propellant [7]. These spacings are usually made equal so as to give each propellant a single web. As the surfaces recede during combustion, they will meet at a point equal to half of the web (often denoted as the sliver point). Lines representing the web are shown on Figure 1.1 for various configurations. From the knowledge of the web and number of perforations, it is possible to determine the diameter of the propellant grain. The length of the grain is chosen to provide a final control of the bulk density of the product. The goal is to precisely control the rate of energy release and tailor its evolution in time to the requirements of various applications.

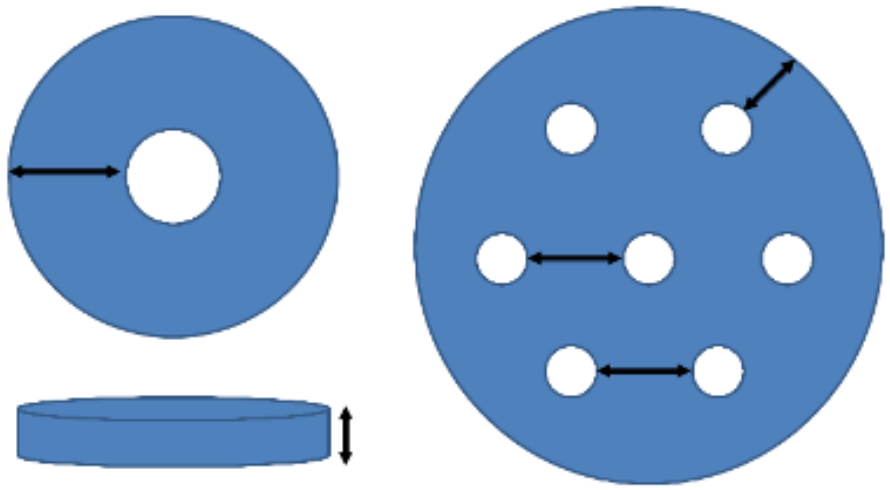

Figure 1.1: Typical grain geometries for propellants. These geometries are often referred as disc (lower left), unitubular (upper left) and multitubular (right).

Granular propellants used in hunting, military and airbags applications usually have length and diameter dimensions in the range from 1 mm to 30 mm [4]. Rocket motor

applications often use longer sticks which can be several meters in length (the solid booster rockets of the space shuttle are an example of a very long propellant stick).

1.2 Propellant fire safety

Any combustible material constitutes a danger when used in an industrial setting. Since propellants are usually designed to burn quickly, they are especially dangerous fire hazards. As is the case with most commonly found combustible materials, such as wood and volatile fuels, the heat generated by the fire is an important safety factor [15]. This heat will contribute to two main consequences: propagating the fire through the ignition of surrounding materials and weakening structural elements of buildings and other constructions. When modelling fires involving common materials, only the heat contribution is used to calculate the convective gas flow properties [15]. There is thus no expectation of pressure differential. In the case of propellants, the speed at which this heat is liberated and the gas mass generated are such that it is not possible to ignore pressure effects. As will be seen next, the effect of pressure is so important for propellants that it is given a larger importance in many safety analyses.

There are numerous reported examples of propellant fire incidents that have occurred in the recent past around the world. The following list describes some of these events. Note that more exhaustive lists can be found in the literature.

(A) May 1969 (Valleyfield, Canada): detonation of 500 kg of propellant at a burning ground. No damage or injuries. [16]

(B) November 1975 (Pont-de-Buis, France): Deflagration and detonation of 12,000 kg of single base propellant. Buildings damaged and destroyed, 3 fatalities, 81 injured. [16]

(C) May 1978 (Valleyfield, Canada): Deflagration of propellant in a blending tower. Building destroyed, 1 injured. [16]

(D) August 1980 (Valleyfield, Canada): Deflagration of 3600 kg of single base propellant in a dryer. Building destroyed, 3 fatalities, 1 injured. [16]

(E) May 1983 (Muiden, Netherlands): Detonation of 250 kg of porous single base propellant which led to the subsequent detonation of nearby propellants in storage (1200 kg of porous single base and 1200 kg of triple base). Building destroyed, 3 fatalities. [16]

(F) October 1993 (Valleyfield, Canada): Deflagration of 3600 kg of single base propellant in a dryer. Building destroyed, 2 fatalities, 2 injured. [16]

(G) March 1994 (Vihtavuori, Finland): Deflagration of 70 kg of single base propellant in a pneumatic conduit leading to the open burning of 600 kg of propellant stored nearby. Building destroyed, no injury. [16]

(H) August 2000 (Taketoya, Japan): Deflagration and detonation of 7,700 kg of propellant (several types). 106 building destroyed, 1200 buildings damaged, 78 casualties. [16]

(I) October 2006 (Valleyfield, Canada). Deflagration of 2 kg of triple base propellant during conditioning in a laboratory refrigerator. Equipment destroyed, no injury. [16]

(J) January 2007 (Picatinny, USA): Deflagration of a small quantity of double base propellant in a laboratory. 1 injury. [16]

(K) August 2008 (Kirikkale, Turkey): Detonation of 2000 kg of double base propellant in a homogeneization barrel. Buildings destroyed, 2 fatalities, 22 injuries. [16]

(L) July 2009 (Valleyfield, Canada): Ignition of solvent vapor surrounding 500 kg of solvent wet single base propellant in a container with subsequent extinguishing by the sprinkler system. No damage, no injuries (near miss). [16]

When considering the consequences of a propellant fire, the conditions in which this fire occurs are important. If the combustible material is stored in a closed or partially closed environment, there is potential for pressure buildup. In such a case, an explosion could occur as the pressure generated inside the enclosure goes beyond safe limits and causes a sudden rupture in the building or equipment structure. Most of the above listed cases are good examples of this behavior. These examples show that there is considerable danger for what is inside the building. There is also a risk of material loss due to a structural failure of the building. Thirdly, the resulting explosion would create potentially harmful projections. In the previously given list of incidents, most of the negative consequences arose from pressure buildups and the subsequent explosions.

If the material is not enclosed, the size of the event and the location of surrounding structures or personnel must be considered. For example, items (D) and (F) of the above list are nearly equivalent to burning 3600 kg of propellant in an open air setup. In that case, the building provides no other protection than keeping the propellant free of the outside elements during normal operations (snow, rain, etc). Therefore, one must examine the radiant heat generated by such a fire and determine safe distances at which other buildings and roads should be located. The goal is to prevent the fire from spreading to other structures and anyone passing nearby to sustain dangerous burns due to their proximity from the potential fire.

1.3 Context of the study

Fire safety science is a well researched field. Numerous studies have been published on a variety of fundamental and applied topics. These publications cover a large amount of combustible materials, as shown by the following list:

- Wood (and other cellulosic materials) [17] [18]
- Polymers [19]
- Gases [20]
- Dusts [21]
- Solvents [22]
- Liquid fuels [22]
- High explosives [23]

In some of these examples, combustion takes the form of a fire plume. In others, the events are better described by an explosion (or at the limit, a detonation). At this point, it is useful to define three important terms used in the fire safety field [10]:

- Deflagration: combustion for which the flame front travels at a velocity which is below that of the sonic velocity.
- Detonation: combustion for which the flame front travels at a velocity which is at or above that of the sonic velocity. It is usually characterized by the presence of sharp pressure, temperature and density differentials known as shock waves.
- Explosion: sudden release of a high pressure into a lower pressure environment. The high pressure can be the product of a deflagration, detonation or the presence of a pressurized fluid.

Propellants can thus have a combustion behaviour spanning the two extremes (deflagration and detonation). Airbag propellants are often very slow burning in standard atmospheric conditions. Products used in small calibre hunting rifles burn very quickly and create conditions akin to explosions (case (K) in the previous list of accidents is a good example). In the right conditions, confined propellants can detonate with as much force as high explosives [24]. Using data gathered in the literature [25] [17] [18] [19] [20] [21], it was possible to plot the power generation as a function of the combustion velocity (both scaled by the area). Figure 1.2 shows the resulting plot for various combustible material fires. The red markers show the average power of various propellant fires. It is seen that propellant events spent a relatively large region of Figure 1.2. The fire safety of the propellant handling facility must thus consider a large array of possible behaviours. To ensure a safe design, limitations must be imposed on the operating conditions. These limitations must be variable and adapt to a maximum possible number of cases for efficiency purposes. Economic constraints impose restrictions on the possible size of a facility and lead to the need for efficient designs.

Whereas, as previously said, there are a multitude of studies on the topic of combustion related to various materials, a gap exists where propellants are concerned. The majority of studies that were published on the matter are from a period between 1950 and 1980. The work described in these publications also lacks the formal theoretical background which would make the results general. In many cases, only certain specific configurations are discussed and studied empirically. The type of work observed is consistent with an approach based on the need to solve a very specific problem with limited resources. Although not applicable in general situations, the published results do form a good background on which to build more general models.

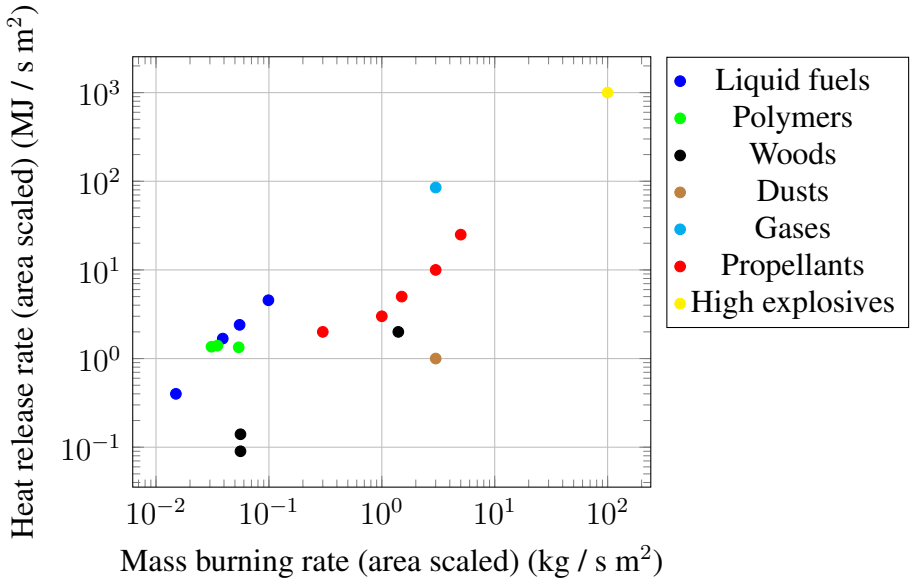

Figure 1.2: Relationship between the mass burning rate and heat release rate (both scaled by the area) of various fuels. Propellants (red markers) are shown to span an important region of the plot. This plot was produced from data obtained in the literature [25] [17] [18] [19] [20] [21].

1.4 Goals of this study

The goal of this thesis is to study the combustion of granular propellants in situations that would be found in accidental fires. In particular, these variables are studied:

(1) Radiant heat flux

(2) Pressure generated

(3) Size of the event

For each of these variables the answer to these fundamental questions are sought:

(1) What is the maximum value obtained?

(2) How long does it take to reach this maximum value?

(3) How does the event evolve qualitatively with time?

Although the answers to these questions are expected with respect to radiant heat flux, pressure and event size, an understanding of how fires propagate is necessary. It must be noted, however, that a fundamental description of propellant flame propagation is not required here. The extent to which that phenomenon is studied is limited to the requirements of the main topics described above.

1.5 Methodology

At the base of any study on propellant fire safety science, there should be an application of relevant previously determined relationships. It is important to discern the similarities between cases involving propellants and other materials. As Figure 1.2 shows, propellants span a space of the behaviors occupied by other materials. Similarly, one must recognize what makes propellant fires unique: an energetic granular solid undergoing a deflagration with a relatively high combustion rate. Note that the term ”deflagration” was used in the last sentence. Although propellants can detonate when properly confined, their expected, or desired, combustion behaviour is a deflagration. Propellant detonations behave very similarly to those involving high explosives (since the energetic ingredients used in propellants are often classified as high explosives). For this study, only the deflagration behaviour is described.

Based on the previous discussion, the methodology used to study each aspect of this work is as follows:

(1) Literature study of previous work performed with propellants and other materials. The goal at this stage is to obtain a general idea of possible subsequent models.

(2) Theoretical derivation of relations that would model the studied variables.

(3) Experimental work designed to determine unknown parameters and validate the designed models.

(4) Reduction of the models into a set of simple guidelines and their respective domain of validity.

Each of the studied variables are very different and relatively independent. The previously listed steps will therefore be covered in the chapter relevant to that variable. Breaking down the steps (for example, by covering the literature study of all variables in an initial chapter) would likely be confusing to the readers. After the three main variables are covered, a subsequent chapter will present a synthesis which integrates all the results and apply them to a case study. The thesis will conclude by discussing the contributions of the work to the field in general and possible future improvements.

1.6 Industrial context

Even if the current thesis represents an academic endeavor, the work was supported and partially funded by the industry. The problem studied has important implications on how propellant facilities can be designed and what operations can be allowed to take place. Therefore, it is important to be reminded that there is a limit to the required precision of a model applied in a setting where safety margins are subsequently added. Although much is learned about the fundamentals of propellant combustion science, the ultimate goals are the derived safety guidelines. Recognizing these two different goals is important when approaching such a study.

Chapter 2

Flame propagation

> "To understand a name you must be acquainted with the particular of which it is a name."
>
> Bertrand Russell - The Philosophy of Logical Atomism (1918)

2.1 Introduction

In essence, fire is a self-sustaining combustion reaction. To initiate the reaction, some fundamental conditions must be met. Given a fuel, an energy input in the presence of an oxidant (usually oxygen) is required. This is often explained using the concept of a fire triangle, as shown in Figure 2.1 [26]. As combustion releases a large quantity of energy, the three conditions thus continue to be fulfilled as long as there remains a fuel and oxidant. Figure 2.2 shows this concept of a reaction that sustains itself once initiated.

This self-sustenance property can be impaired if something is present to absorb the available energy. For example, if the fuel (propellant, wood or otherwise) contains a small concentration of some solvent, like water, part of the energy will be absorbed to vaporize the water. Additional energy is therefore necessary to overcome absorption by the solvent if the establishment of a self-sustaining reaction is desired. This principle is most useful in fire

Figure 2.1: The fire triangle

combat methods. Adding water to a building in flames usually helps in extinguishing the fire. Spraying water on the surrounding structures can help to prevent the fire propagation. These are not the only firefighting methods but these examples show that acting on one of the variables of the fire triangle can be beneficial.

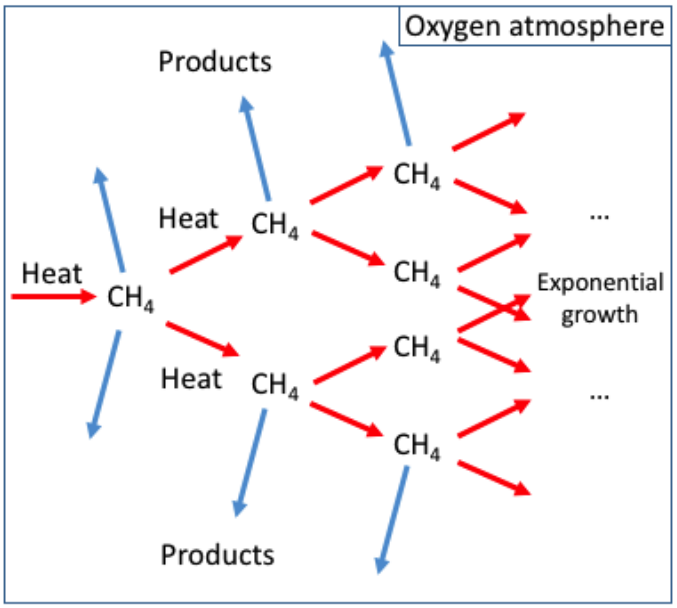

Figure 2.2: Schematic representation of a self-sustaining reaction for the example of methane combustion.

From the previous discussion, it can be inferred that an understanding of fire propagation requires a description of the ignition phenomenon. Indeed, combustion ignition can happen with many energy sources. Within this framework, fire propagation is imaged as

ignition through the energy liberated by already combusting material. A basic understanding of the ignition process is thus a good foundation on which to study flame propagation. Subsequently, the energy transfer (or heat transfer) modes from the burning material to the surroundings can help in categorizing and eventually quantifying flame propagation. This methodology is illustrated in Figure 2.3.

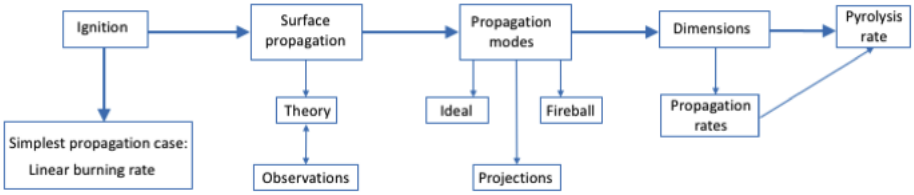

Figure 2.3: Diagram showing the methodology used to study flame propagation.

This analysis of propellant fires spread yields two important pieces of information:

- The maximum dimension of the event
- The propagation rates

From these two results, it is also possible to infer on the combustion rate of the burning material. The goal of this chapter is to apply the methodology of Figure 2.3 to characterize the dimensions of propellant fires. Through this analysis, approximations are also obtained for the propagation and combustion rates. As it will be seen in the subsequent chapters on radiant heat flux and pressure generation, some knowledge of these flame propagation parameters is important in the predictive models designed.

2.2 Ignition and propagation

2.2.1 Ignition

Any combustion reaction begins with the ignition of the material in question. In very simple terms, ignition is defined as “the process of starting the combustion process” [27].

The ignition point is the condition in which the exothermic decomposition reaction will continue without any further external energy input [28]. Although the present work is concerned with what occurs after ignition, many theoretical concepts developed for explaining combustion initiation are of interest.

The problem can be illustrated by imagining a block of propellant. Most of the ingredients often used in propellant formulations are not stable. If left on their own, they will slowly decompose. This decomposition is exothermic and thus produces heat, which is dissipated in the surrounding material [29]. If the propellant bloc configuration is such that the heat dissipates at a lesser rate than it is produced, the temperature will increase. Since decomposition rates are usually temperature dependent, the temperature increase will cause a higher decomposition rate. At a certain limit, this "self-heating" will continue until the energy needed for the combustion reaction is available [15]. At this point, the material will be said to ignite. The propellant bloc could thus spontaneously ignite on its own even if left at ambient temperature. It is seen that the global path to ignition is a competition between the heat input to the material (either from its own decomposition or from external sources) and how this heat can be transferred away from the material. Stabilizers are usually added to propellant formulations in order to slow these decomposition reactions and obtain longer shelf lives [3]. This is of special interest to the lifetime and storing capacities of energetic materials. Knowledge of the storing conditions of such substances is important in determining they are safe to store for additional time. There have been documented occurrences of fires with materials kept at temperatures well below their ignition point [29].

The often used concept of ignition temperature is thus not a precise description of the event and must be used carefully. When a substance is heated to its ignition temperature, self sustained combustion takes place [10]. As was shown above, there is a subtlety to this, as time is a non-negligible parameter. The ignition temperature assumes an "instantaneous" transition to self-sustained combustion. It was previously discussed that lower temperatures

can and will often lead to a self-sustained reaction if enough time is allowed to pass. At these lower temperatures, exothermic decomposition reactions still take place and can heat the substance to the point where a self-sustained regime will occur [29]. Under the ignition temperature, there could still eventually be self sustained combustion, even if the heat source is removed in time. A better term for the ignition temperature could therefore be the "instantaneous ignition temperature" as this adds the needed time component.

There are many possible types of ignition sources. As discussed previously, all that is required is a source of heat or energy. One can recall the previously mentioned "fire triangle" explanation which states that a combustible material, an oxidizer (most often oxygen), and a source of heat are required to start a fire [26]. Any source of energy which transforms into thermal energy can thus lead to combustion initiation.

(1) Thermal energy: direct contact with high temperature body or fluid, exothermic chemical reactions, radiant heat flux

(2) Mechanical energy: shock, friction

(3) Electrical energy: contact with an electrical arcs, resistive heating

Observation of these sources yields the constitution that heat transfer is very important in ignition. Most ignition models take for input a heat flux and the physical properties of the material in question. The heat flux is subdivided into three parts: convection, conduction and radiation. Which modes come into play depends on the case in question. The possible fire hazard of a material stored in a drum will involve air convection and conduction of the heat in the material themselves (neglecting the fact that the source of heat is radiation from the Sun). Determining the possibility of secondary initiation (ignition of something due to the combustion of nearby material) will be equivalent to a radiant heat flux problem.

Understanding the distribution inside the igniting material is of importance to modelling the process. Two cases have been proposed [15]:

(1) Thermally thin case: the material is considered as a "lump" with no temperature variation within its depth.

(2) Thermally thick case: there is a temperature variation within the material depth.

Selecting which case applies to a given situation will depend on the geometrical configuration in question, the heat conductivity of the material and the input heat flux. One dimensional heat conduction is described by the following form of the Fourier law [30]

$$q = k\frac{dT}{dx} \tag{2}$$

where q is the heat flux, k the thermal conductivity, T the temperature, and x the spatial dimension. Simplifying the spatial derivative as $\frac{\Delta T}{\Delta X}$ and solving for ΔX yields a relationship showing the required spatial dimension variation for a given temperature difference when the body is under a specific heat flux. To be thermally thin, a body is considered as a lump solid with the same temperature throughout its volume. The spatial variation should be less than the value required to produce the desired temperature difference. A thermally thin body thus requires that the following condition on its thickness, $d_t = \Delta X$, be followed [15]:

$$d_t \ll k\frac{(T_s - T_o)}{q_{in}} \tag{3}$$

where q_{in} the heat flux at the surface, T_s and T_o are the temperatures at the surface and maximum thickness of the body, respectively. When the above condition is not followed, the solid is considered as thermally thick. When constructing an ignition model using either of these cases, an energy balance is performed and a solution found for the ignition time, t_{ig}, by solving the resulting differential equation. In general, the following results are found [15]:

(1) Thermally thin case: $t_{ig} \sim \frac{(T_{ig} - T_{inf})}{q_{in}}$

(2) Thermally thick case: $t_{ig} \sim (\frac{(T_{ig}-T_{inf})}{q_{in}})^2$

where T_{ig} and T_{inf} are the ignition and surroundings temperatures, respectively. It is thus observed that the spatial variation of the temperature present in the thick case produces a quadratic evolution of the ignition time.

In the case of propellants, the thermal conductivity has been measured to be between 0.20 and 0.50 W/m K for most cases of interest [31]. Assuming an ignition temperature in the vicinity of $180°$C and a maximum thickness temperature at the room value of $21°$C, the previously stated condition can be applied. From existing data on propellant radiant heat flux, maximum values ranging from 1 to 20 W/cm^2 are observed for fires [32]. For the range of thermal conductivities and heat flux given, the conditions become

(1) Lowest value ($k = 0.20$ W/m K and $q_{in} = 20$ W/cm^2): $d_t \ll 0.2$ mm

(2) Highest value ($k = 0.50$ W/m K and $q_{in} = 1$ W/cm^2): $d_t \ll 9.0$ mm

It must be noted that during the fire growth, the heat flux will have lower values, yielding a larger thickness. However, in order for the condition (much smaller than) to be followed, thicknesses in the mm order and under will be required. Even in a laboratory setting, propellant samples of a few grams will have a thickness in the cm order. Granular propellant webs are usually in the range between 0.1 to 2.0 mm, hence the grains are often much larger, which already falls outside the condition. Stick propellants used in motors are even larger. It will thus be best to assume the thermally thick case when performing heat transfer calculations on cases involving propellant grains.

2.2.2 Linear burning rates

2.2.2.1 Previous work

Propellant formulations are characterized by their rate of combustion, usually known as their linear burning rate. The linear burning rate of a composition is defined as the recession

rate of the propellant surfaces [7]. The logarithm of this quantity usually has a linear relationship with the logarithm of pressure and is thus expressed as an exponential law known as Vielle's law [7]. Given the high pressures encountered in propellant applications and the pressure dependence of the burning rates, burning rate measurements are not usually made at near atmospheric pressures. Measurements have been made at pressures around 1 MPa on formulations designed for rocket applications [3] [33]. In most other applications, the operating pressures are usually between 30 and 700 MPa (thus up to 7000 atmospheres). Two main ways used to measure linear burning rates have traditionally been applied: reduction of closed vessel pressure data and direct measurement in a strand burner. These two methods have been considered for the present study.

As stated in its description, the closed vessel method yields the burning rate from a calculation and is thus indirect. The granular propellant sample is burned in a closed vessel and the generated pressure is measured using a piezoelectric transducer. From the knowledge of the geometry and thermodynamic properties of the sample, the pressure-time relationship is transformed to a gas generation rate and a linear burning rate [7]. Note that the thermodynamic properties of the combustion gases are computed using codes such as Cheetah [13] from the measured chemical composition of the formulation. Calculation routines which apply this method have been designed to aid designers [34], and the methodology has been standardized by the North Atlantic Treaty Organization (NATO) [35]. The disadvantage of this method compared to the former one is that the calculation rests on the assumption of the simultaneous ignition and burning of all surfaces [7], which is known to not hold in the majority of cases. It must be noted that this method is used for all high pressure applications, as it is easier to apply in these cases.

The strand burner technique consists in measuring the passage time of the flame front on a propellant strand ignited at one end. The sides of the strand are sometimes inhibited in order to confine the combustion on only one axis. Several methods have been used to

measure the flame front passage time at various points on the strand: embedding thermocouples or electrical wires at specific locations [36], filming the combustion with a known distance marker. A recent publication has proposed using infrared thermography to detect the combustion front [37]. It is important to note that the strand is usually contained in a sealed vessel which is pressurized to a desired measurement pressure prior to ignition. The advantage of this method is that it enables a direct measurement of the burning rate.

Little data has been published on near atmospheric pressure burning rates since applications usually make use of the pressure dependence of the combustion. Schoyer and Korting have studied sub atmospheric pressure burning rates for composite propellants [38]. Their experimental setup was based on a combination of the methods discussed above. The sample burned linearly (on one axis only) and the pressure rise was measured. The setup enabled control of the combustion area while providing a more precise distance measurement than standard strand burner techniques [38]. In the case of the present study, such a method would probably prove not to be the best choice in terms of costs, precision and ease of use.

2.2.2.2 Linear burning rate

Given that it is not practical to pressurize a vessel to values observed in larger pressure applications (up to 700 MPa), the strand burner is applied to cases with limited pressures. The standard strand burner methods would thus most likely be a logical choice here. Experiments have been made to determine the atmospheric pressure linear burning rates of single, double and triple base propellant formulations. As discussed previously, the strand burner technique was applied to cylindrical and rectangular samples. In order to get these samples the mixed propellant was extruded through cylindrical and rectangular dies (without any perforation). Each strand was then cut manually and left on a tray to dry until the residual solvent level reached values below 1.0% (measurement done using gas chromatography).

A summary of the protocol subsequently used to obtain these measurements is shown in the following list:

(1) Positioning of the sample vertically with a support at the base

(2) Positioning of the distance reference parallel to the sample

(3) Ignition at the top with a propane flame

(4) Visual recording of the combustion (Sony Cybershot camera at 30 frames per second)

(5) Measurement of the distances and times using frame by frame still images and an imaging software

Figure 2.4 shows two frames of recorded combustion tests made on the single base sample. It must be noted that the initial tests were performed without inhibiting the outer surface of the samples in order to observe the effect of surface flame propagation on the results. Visual recordings have shown that the flame propagation is faster on the edges than on the flat center of the strand. The combustion surface thus goes from a circular area to a steady state conical shape with all angles around 60°. This steady state shape is obtained after approximately 4.5 to 5.0 seconds and is shown on Figure 2.4-a. Prior to attaining its steady state, the combustion surface is that of a truncated cone. Velocities computed from the measured distances and times are summarized in the diagrams of Figure 2.5.

The velocity differences shown in Figure 2.5-a have been described as "edge effects" by Drysdale [39]. These effects have been studied for cases involving the combustion of polymers [9]. It is interesting to note that the 60° angle was also consistently observed by Sibulkin et al. in a study involving the combustion of various PMMA configurations (in that case, a value of 30° was reported since the samples were inhibited on one side) [40]. In that same study, the burning rate component normal to the edge was given to be [40]:

$$V_N = V_u \sin \phi \tag{4}$$

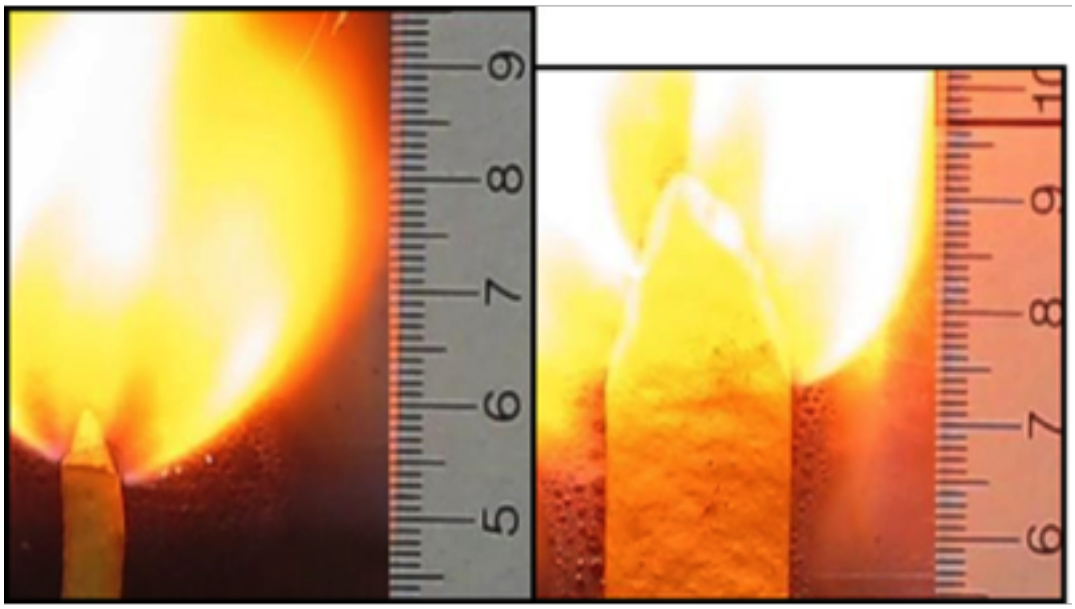

Figure 2.4: Sample recording stills of single base strand burning tests. Figure 2.4-a (left) shows the combustion of a cylindrical strand. Figure 2.4-b (right) shows the combustion of a rectangular strand.

where V_N, V_u and ϕ are the burning rate normal to the edge, the burning rate in the vertical direction and the edge half-angle, respectively [40]. Considering the average rate of 1.5 mm/s and a half-angle of 30° obtained in the present case, a value of 0.75 mm/s is calculated for V_N.

Similar tests have been done with the same batch of samples to verify the effect of inhibiting the outer surface. The propellant strands were immersed in water for 15 seconds prior to being placed on the combustion setup and ignited. The method proved to be less effective for taking measurements, as the samples tended to extinguish after a few seconds of normal combustion. However, some measurements were taken, and an average burning rate situated between 0.60 and 0.80 mm/s was obtained (rates between 0.37 and 1.14 mm/s were measured with the largest concentration of data points around 0.60 mm/s). Although

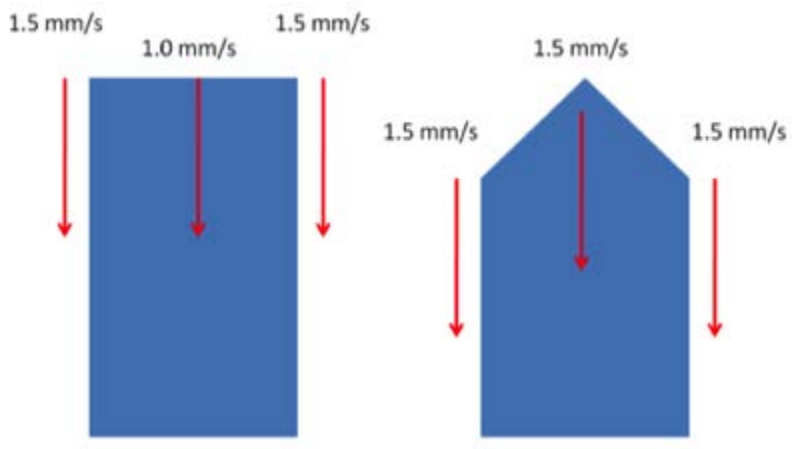

Figure 2.5: Summary of the velocity measurements for the single base propellant sample. Figure 2.5-a (left) shows the beginning of the combustion. Figure 2.5-b (right) shows the steady state.

the experiments with the inhibited samples did not yield results with the same quality as those from the pure propellant strands, it is observed that the predicted burning rate of 0.75 mm/s seems to be in the good region.

The previous considerations apply to the measurements made on double and triple base propellants as well. For reference, the measured burning rates of the tested samples are shown on Table 2.1. These samples are described in Tables 2.2 and 2.3 (although the grain diameters and bulk densities are not applicable here as the samples were extruded in larger strands). It is observed that changing the formulation makes a notable difference but that all values are in the mm/s order of magnitude.

Table 2.1: Linear burning rate of various propellants under standard temperature and pressure conditions.

Propellant	Linear burning rate (mm/s)
SB1	1.10
SB2	0.75
DB1	2.20
DB2	2.20
TB1	0.50

2.2.3 Surface flame propagation

2.2.3.1 Theory

The solid to gas transformation which occurs during propellant combustion is a rapid process. The speed at which the transformation takes place is of paramount importance in calculating the pressures generated. Most propellant combustion models have been tailored to specific applications and assume the simultaneous ignition and combustion of all surfaces of the propellant. When propellant fires occur, the ignition takes place in a very specific region of the propellant bed. The flames then spread until the entire stack is engulfed. Predicting the combustion rate of the propellant is beyond the scope of the present study as it involves a deep understanding of the reaction chemistry. Work has been performed by various researchers to predict these rates but the computing requirements are prohibitive [14].

A semi-empirical approach is instead proposed where the flame propagation rates are measured in a controlled laboratory setting. Subsequent calculations based on the physical configuration are made to compute the actual rates that would be observed for a given case. Three fundamental propagation rates can be measured for a given propellant:

- Linear burning rate, r: the rate at which the combustion front travels perpendicularly through the solid material. This rate is the most fundamental measurement about the

propellant combustion rate and is pressure and temperature dependent. Details about the linear burning rate were given in the previous section.

- Horizontal flame propagation rate, r_h: the rate at which the flame propagates horizontally at the surface of the propellant bed.

- Vertical flame propagation rate, r_v: the rate at which the flame front travels vertically through the propellant bed. This is a two-phase problem as the front is travelling in a granular solid (equivalent to a porous media).

As stated above, the linear burning rate is fundamental as it depends solely on the chemical composition and external conditions. The horizontal flame propagation depends heavily on the heat flux from the combusting material and will thus vary with a given configuration and during the evolution of the fire. This heat flux can take many forms depending on the configuration (conduction, convection and radiation). The vertical rate also depends on heat flux but the two-phase nature of the granular material arrangement complexifies the situation.

The horizontal flame spread problem can be broken down as follows:

(1) Ignition at a certain point or region at the surface of the propellant stack.

(2) Individual grain combustion governed by the linear burning rate and heat conduction.

(3) Surface spread rate ideally governed by the radiant heat flux of the combusting material.

(4) Growth of the flame with the associated increase in radiant heat flux and combustion gases velocity.

In each of these items, the three heat transfer modes are present but more or less negligible. Surface flame propagation rate has been studied in the past for various materials. As

is the case for ignition, two prevalent models can be used to describe the phenomena: the thermally thin and thick cases respectively. The criterion given previously as Eq. (3) has been used to show that the thermally thick case is most applicable for propellants. In the thermally thick case, the general form of the resulting relationship is:

$$v_p = \frac{4q_{in}^2\gamma_f}{\pi k\rho_{solid}c_p(T_{ig} - T_o)^2} \tag{5}$$

where γ_f is the effective heating length, ρ_{solid} is the propellant density and c_p is the heat capacity of the propellant. Unless the surface is in direct physical contact with the flames or combustion gases, radiant heat flux is the prevalent form of heat transfer in propellant fire events. It is thus ideally assumed that q_{in} is only from radiation. The other variables found in Eq. (5) are often similar for propellants. It is therefore the heat flux input that will drive the propagation rate. Since the heat flux at a certain point depends on the size of the event, larger fires will have larger surface propagation rates.

2.2.3.2 General observations on large scale fires

Propellant samples of known masses were disposed in circular stacks with measured diameters and heights. These stacks were located in an open air flat burning pan of negligible depth. The ignition was done at the top center of the stacks using an incandescent wire connected to a 48 V DC source. Samples with a larger grain dimension required a small amount of black powder in order to properly ignite but this amount was typically less than 0.1% of the charge burned (where 0.1% was for the smaller samples). A picture of a 10 kg propellant stack is shown on Figure 2.6. From the observation of Figure 2.6, it is seen that the stacks could not be made perfectly cylindrical due to the natural angle of the sides. It must, however, be noted that this angle remained constant for all configurations. These side effects were thus negligible for larger quantities.

The events were captured on a Casio Exilim camera at a rate of 256 frames per second.

Figure 2.6: Picture of a typical propellant circular stack (10 kg in this case).

Using distance markers placed around the fires, the flame dimensions were measured as a function of time. The footage captured for each fire was reviewed on a frame by frame basis using the Matlab Image Processing Toolbox. For the various dispositions used with the camera, resolutions varying from 0.7 cm per pixel for the smaller tests to 7 cm per pixel for the larger tests were obtained (representing approximately 0.1% to 5% of the distances measured). The width at the base and top of the fire and total height were noted. Any intermediate zone of smaller or larger width was also noted in the form of the maximum width and height of the zone. A summary of the tested configurations and measurement results is shown in Table 2.10.

Various propellants were tested, again for the model generality. In the present case, the assumed most important propellant combustion variable is the heat of explosion, E (in J/kg). The heats of explosions were measured in a standard calorimetric bomb under an inert nitrogen atmosphere [3]. The linear burning rate is also non-negligible, but does not take into account the geometry of a given configuration. The propellant samples used for the present study along with their characteristics are given on Tables 2.2 and 2.3. It can be seen that the samples were selected among practically available inventories to cover a wide range of energies and burning rates. Various geometrical propellant grain configurations were tested and webs going from 0.08 mm to 1.5 mm were used. In addition, care was taken to limit the propellant stack heights to 10 cm for the double base cases and 20 cm for the other cases.

Propellant fires have been compared to fireballs in making determinations about event times and dimensions. Video footage of propellant fires, however, showed these events to be more akin to pool fires. Figure 2.7 shows a comparison of the flame shapes for several

Table 2.2: Tested propellants chemical description. Although DB1 and DB2 have the same heat of explosion and composition, the dimensions of the propellant grains are different. Note that the abbreviations NC, NG and NQ stand for nitrocellulose, nitroglycerin and nitroguanidine, respectively.

Propellant	Heat of expl. (J/kg)	Composition
SB1	3603	NC: 97% / Inert: 3%
SB2	3499	NC: 85% / Inert: 15%
DB1	5392	NC: 60% / NG: 39% / Inert: 1%
DB2	5392	NC: 60% / NG: 39% / Inert: 1%
TB1	3553	NC: 21% / NG: 20% / NQ: 54% / Inert: 5%

Table 2.3: Tested propellants physical description.

Propellant	Geometry	Grain diameter (mm)	Abs. density (kg/m^3)	Bulk density (kg/m^3)
SB1	Unitubular	1.80	1560	970
SB2	Multitubular	6.71	1590	880
DB1	Disc	0.12 (thickness)	1600	550
DB2	Disc	0.08 (thickness)	1600	550
TB1	Multitubular	7.12	1680	920

proposed configurations and that of a typical fireball. The shape of the propellant fire flame has a cylindrical characteristic closer to that of pool examples. It can be seen that faster burning cases, such as the double base, exhibit a behaviour which seems between the two extremes.

Ignition plays an important role in the shape of the subsequent fire. The Figure 2.7 frames are for a top center ignition. When the ignition is located in an internal position, there is a piston effect where the propellant above the ignition is ejected prior to combustion. If the propellant is fast burning and has an aerodynamically favourable shape, it is possible to generate something similar to a dust cloud. This then causes a spherical fireball. In slower burning cases, there will be a projection of burning debris. These two internal ignition cases are shown as video frames in Figure 2.8. The propellant burning rate and geometry, along with the location of the ignition, are thus important in making a proper

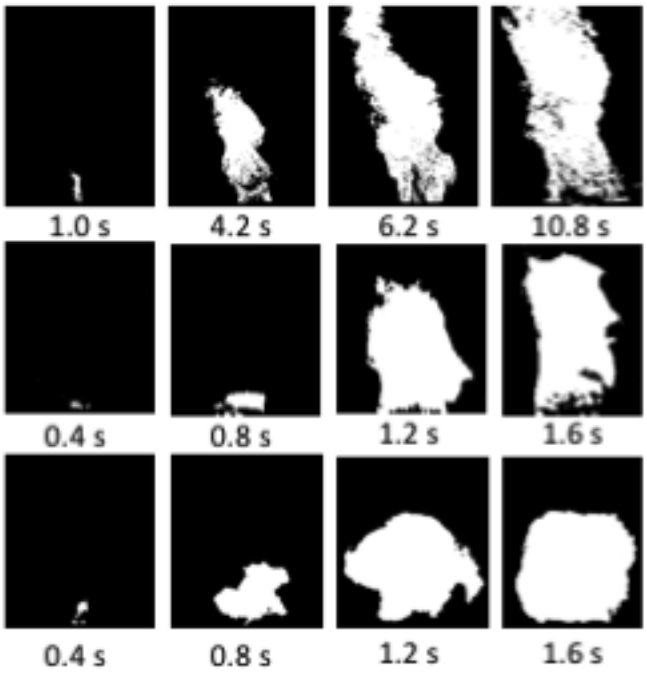

Figure 2.7: Video frames showing the evolution of the flames for various configurations. The top fames are for a fire involving SB2 propellant. The middle and bottom frames are for DB1 fires with increasing quantities. Note that the images have been treated such that the pixels containing flames are in black while the other pixels are white.

determination of the fire shape.

From the set of observations, it was possible to discern five main classes of behavior:

- Equal width throughout the height of the flame (cylindrical).
- Gradually increasing width with the height of the flame (inverted conical section).
- Gradually decreasing width with the height of the flame (conical section).
- Equal width everywhere except for part of the height where there is a quasi-spherical section of larger width (cylinder with intermediate sphere of larger radius.
- Quasi-spherical growth leading to a cylindrical profile.

The first and second cases were observed in the majority of events. The third case was seen at the end of some events as the intensity of the fire was decreasing. The fourth case

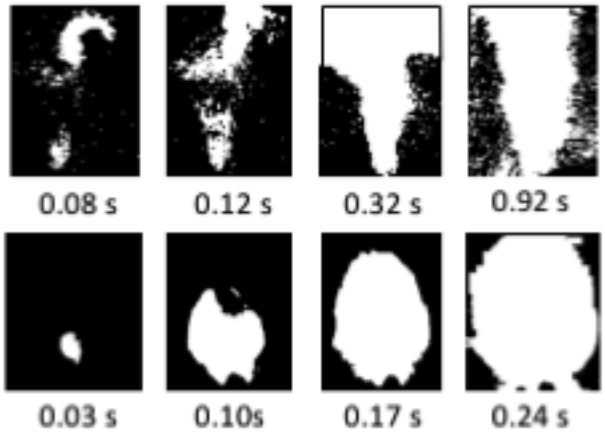

Figure 2.8: Video frames showing the evolution of the flames for various configurations with a bottom center ignition. The top and bottom frames involve fires with SB1 and DB1 propellant, respectively. Note that the images have been treated such that the pixels containing flames are in black while the other pixels are white.

was observed in the burning of slower propellants. This last spherical feature was dynamic as it could be observed to start at the base of the fire and rise up subsequently, in a way comparable to boiling liquid expanding vapor explosions fireballs (often referred to by the abbreviation BLEVE) [41]. The difference here is that these fireballs occurred amidst the rest of the flame. The fifth class was only observed for the fastest burning propellants.

It is useful to initially look at the measured evolution of the flames in a graphical manner. Figures 2.9 and 2.10 respectively show the flame base width and total height for multiple masses of tests involving SB1. In both the width and height cases, the following general phases are observed in the events:

(1) Steady increase of the width / height as the fire spreads on the surface of the propellant bed.

(2) Plateau at the maximum dimensions values.

(3) Decrease when the fuel is depleted.

In the case of slower burning propellants with a large stack diameter, the plateau region is never reached as the fuel depletes prior to the flame spreading on the entire surface (this

is seen for example in the 136.4 kg and 909.1 kg cases of Figure 2.9). It must be noted that although the propellant stack is ignited at its center, the fuel often depletes at the edges first. This is explained by the depth of the bed being lesser there due to the lack of any container or barrier to hold the propellant grains in place. Viewed in two dimensions, a cross section of such a stack has a trapezoidal shape instead of the ideal rectangular shape.

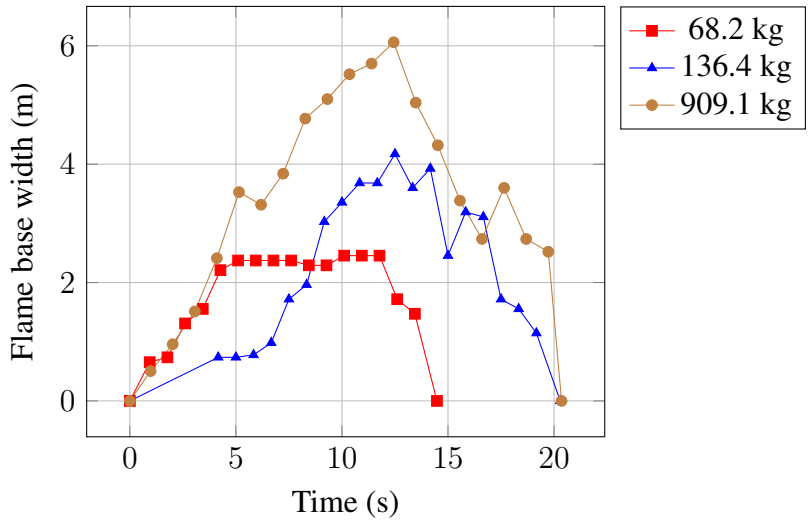

Figure 2.9: Horizontal propagation of the flame for various cases of SB1 fires.

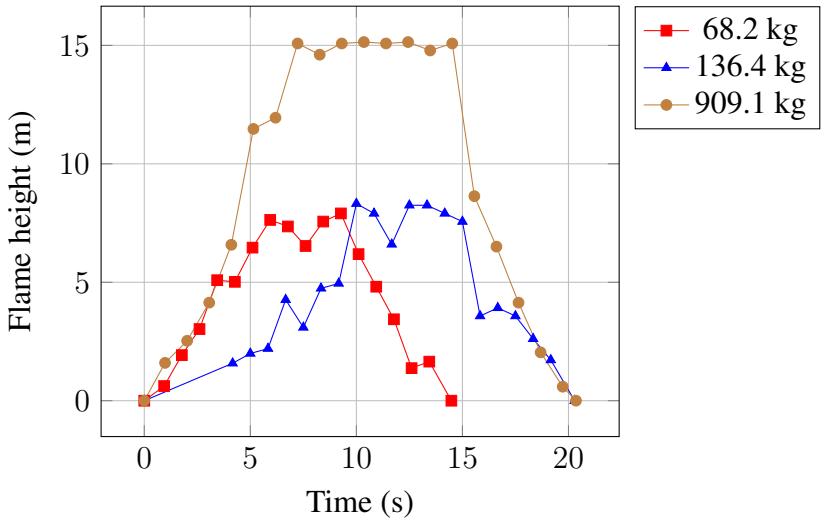

Figure 2.10: Height of the flame for various cases of SB1 fires.

2.2.3.3 Horizontal dimension of the fire

Table 2.4: Flame dimensions for large scale fires of various propellants.

Propellant	Mass (kg)	Initial width (m)	Max. base fire width (m)	Width ratio	Max. flame height (m)	Projections observed	Fireball observed
SB2	68.2	1.0	2.5	2.5	7.9	Yes	No
SB2	136.4	2.0	4.2	2.1	8.3	Yes	No
SB2	909.1	4.0	6.1	1.5	15.1	Yes	No
SB1	45.5	1.0	2.5	2.5	7.6	Yes	No
SB1	90.9	2.0	2.1	1.1	6.2	Yes	No
SB1	909.1	4.0	4.0	1.0	NA	Yes	No
DB1	15.9	0.7	2.5	3.6	4.5	Yes	Yes
DB1	47.7	1.0	2.9	2.9	5.0	Yes	Yes
DB1	477.3	4.0	3.1	0.8	6.9	Yes	Yes
TB1	45.5	1.0	1.2	1.2	3.5	No	No
TB1	454.5	3.0	3.5	1.2	17.5	No	No

A summary of the dimensional measurements obtained with the image analysis is shown on Table 2.4. When observing the initial and maximum base fire width, it is observed that the flame often extends to a lateral width greater than the original stack diameter. The ratio of both quantities can reach values of up to 360% in the double base case. Careful observation of the recorded video helps in determining what causes higher flame widths. Three main behaviors have been noted:

(1) Fireball generation and expansion: stack engulfed by the fireball (an example is shown on the bottom part of Figure 2.7).

(2) Steady growth with propellant grains projection: ignition by contact with projections (an example is shown on the top part of Figure 2.8).

(3) Steady growth: closer to ideal surface flame spread (an example is shown on the top part of Figure 2.7).

In the first case, the expanding fireball explains the larger values obtained. For the second case, the projected grains ultimately collect outside of the propellant stack, which result in a larger apparent diameter. The third case, only observed with the slow burning TB1, yields ratios close to unity. The burning velocity of the propellant can help in determining which case might apply to a given situation.

Having subdivided the space of possible behaviours into three possibilities, it is of interest to determine the following:

- When can each behavior be expected to occur?
- What is the expected diameter of the event in each case?

The first of these questions requires that these behaviours be explored in more detail. It will thus be treated in the following sections. The second question can be answered by analyzing Table 2.4. By observation, the data can first be splitted between the presence or absence of projections. Considering the observation couples (projection, fireball), the only combinations found are (Yes, No), (Yes, Yes) and (No, No). The absence of a (No, Yes) couple provides an argument for an initial split based on projections. The second split is thus based on the presence or absence of a fireball. A third split can be inferred to separate the cases where projections contribute in propagating the flame but do not significantly affect the total event diameter. This would be expected to differentiate between the projection of slower or faster burning grains. The proposed splitting scheme is illustrated in Figure 2.11.

The structure shown in Figure 2.11 forms a decision tree. The actual decision process pertains to the first question (When) and will be treated in the following sections. To answer the second interrogation (What), an event diameter can be assigned to each endpoint of the tree through the width ratio. From the data, the case that does not exhibit projections has an ”ideal” behaviour with a width ratio close to unity. The cases involving the fireball

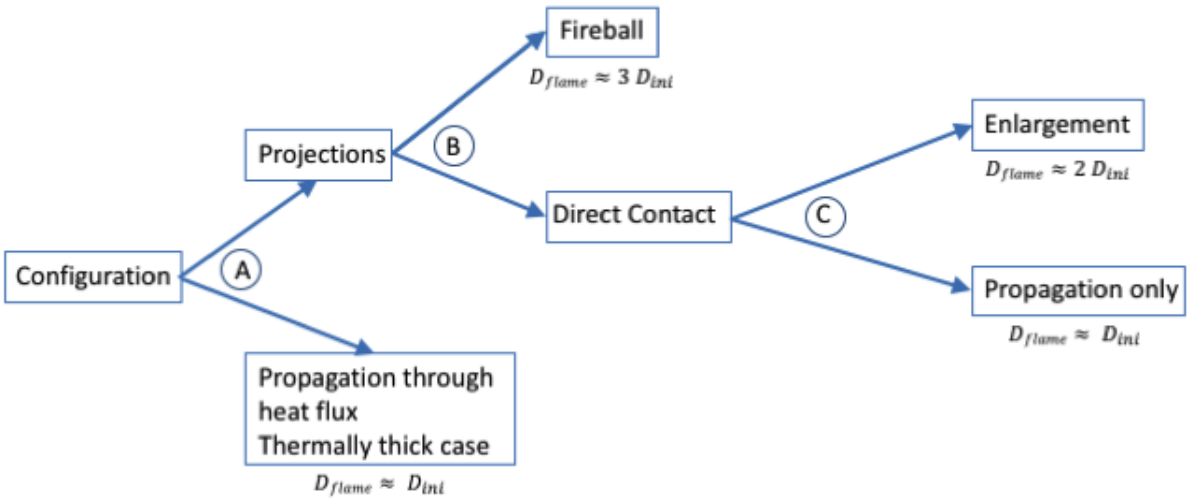

Figure 2.11: Decision tree for granular propellant fires propagation modes. Note that points A, B and C represent decision stages.

behaviour have a width ratio of approximately 3. The two remaining projections driven cases have width ratio values ranging from 1 to 2, depending on whether enlargement is applicable. The resulting width ratio are shown for each endpoint of Figure 2.11. It must be noted that for a larger set of conditions, a statistical classification method (logistic regression, tree building algorithm) could have been applied [42].

2.2.3.4 Flame height

Because of its importance in safety problems, flame height has been studied extensively. A study published in 1961 proposes the following general expression for the height of liquid pool fires [43]:

$$H = 1.7 D_{flame} \tag{6}$$

From a dimensional analysis standpoint, the last equation can be expressed as $H/D = 1.7$. In trying to obtain more general results, subsequent studies have used the power generation of the fires. One of the popular dimensionless scaling of the power generation was

developed by Zukowski and used in multiple studies [15] [39]:

$$\frac{H}{D_{flame}} = \gamma \left(\frac{\dot{Q}_m}{\rho_\infty c_p T_\infty g^{1/2} D^{5/2}} \right)^n \tag{7}$$

where n and γ vary depending on the type of material studied. More recent correlations have been proposed by Quintiere et al. [44] and Heskestad [45]. These last results use the chemical heat of combustion and Froude number to account for combustion efficiency, source geometry and air entrainment.

Using the recorded dimensional data for the test fires shown in Table 2.4, it is possible to verify if a correlation between the fire height and diameter can be found. The flame height and base diameter are compared in Figure 2.12 for all tested configurations. Note that Figure 2.12 contains all the data points from ignition to maximum for the test cases (as opposed to only the maximum values). Not including the points beyond the maximum base diameter is a logical choice, as the diameter will vary as the fuel exhausts and thus not yield reliable results. Two families of points can be observed in Figure 2.12. The main family contains the points corresponding to SB1, SB2 and TB1 tests. The second family contains only the DB1 tests points.

Linear regression lines are given for each family and show the slopes to be different. The main family cases have slopes varying from 2.41 to 2.71. The second family has a slope of 1.45. In order to properly analyze the data, it is important to visualize the main difference between the families. Other than differences in power generation, the second family (DB1 case) has one important particularity: it is the only one for which the measured base diameter is not necessarily the size of the propellant stack. This is a particularity of the fireball behavior, where the expanding combustion gases yield a visible flame larger then the fuel source diameter. For the other cases, the propellant stack diameter grows with time due to projections. In keeping with the methodology of previous studies, it is the actual fuel source diameter which should be considered when studying the flame height. In this

case, the dimension of the source is the propellant stack diameter.

Correcting the DB2 data to account for the initial propellant stack diameter yields what is shown on Figure 2.13. It can be observed that the diameter correction has the effect of merging the two families by increasing the DB1 slope from 1.45 to 2.86. By taking an average slope of 2.63, all of the tested cases can be described by a single flame height correlation:

$$\frac{H}{D_{fire}} = 2.63 \tag{8}$$

Given the fact that the test cases cover power generations relevant to most propellants used, it is thus not necessary to go any further in this analysis. The simple relationship found here is precise enough to describe relevant cases, provided that the correct base dimension is used.

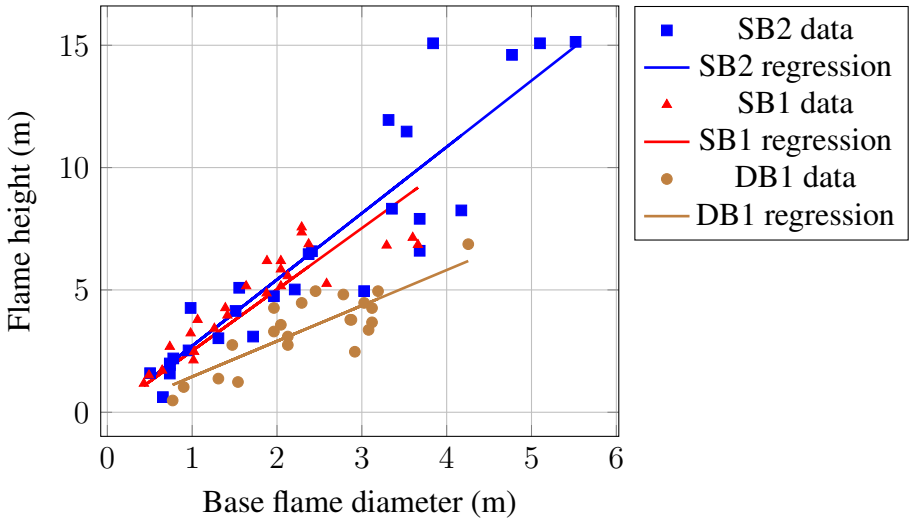

Figure 2.12: Comparison of the measured base flame diameter and total height. Note that the solid lines represent a linear regression through the corresponding data. The correlation coefficients, r^2, are 0.85, 0.96 and 0.95 for the SB2, SB1 and DB1 data respectively.

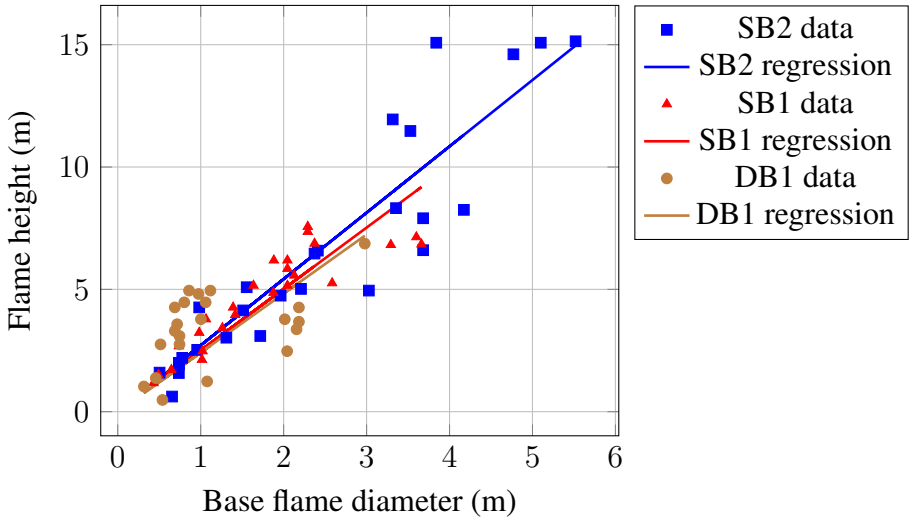

Figure 2.13: Comparison of the measured base flame diameter and total height. In this case, the DB1 flame base data is corrected to yield the actual source base. Note that the solid lines represent a linear regression through the corresponding data. The correlation coefficients, r^2, are 0.85, 0.96 and 0.78 for the SB2, SB1 and DB1 data respectively.

2.2.3.5 Fireball radius

The evolution of the flame surface and volume are interesting parameters to consider as they synthesize the entire dataset into a single measurement. Previous studies have even considered the equivalent radius of a sphere with the same volume for modeling purpose. This last parameter is denoted as the fireball radius [46] [47]. In all cases, the goal is to quantify the size of the flames in a parameter which is practical for the design of safety guidelines.

Two main components are of importance when considering the fire dimension: the maximum dimension and the time required to reach that same maximum. Table 2.4 shows the measured value of these components for the performed tests. It must be noted that the maximum fireball radius values found in Table 2.5 are calculated using the above described cylinder to sphere volume equivalence. It is first interesting to verify if the relationship between the sample mass, m, and fireball radius, R_{fire}, is similar to published values.

Table 2.5: Maximum fireball radii computed for the tested configurations.

Propellant	Mass (kg)	Max. fire surface (m^2)	Max. fireball radius (m)
SB2	68.2	31.7	3.2
SB2	136.4	42.4	3.7
SB2	909.1	115.7	6.1
SB1	45.5	22.2	2.7
SB1	90.9	17.9	2.4
SB1	909.1	NA	NA
DB1	15.9	8.9	1.9
DB1	47.7	17.8	2.4
DB1	477.3	15.0	2.6
TB1	45.5	3.9	1.1
TB1	454.5	61.0	4.5

Using regression analysis, the following result is obtained (r^2 of 0.67):

$$R_{fire} = 0.61 m^{0.29} \tag{9}$$

This last relationship is similar to what has been reported in the literature. Exponential laws with exponents around 0.33 have been reported by various sources [46] [47]. This verification constitutes a validation of the quality of the data. The interpretation of this parameter must however be done carefully. It will be shown here that the maximum fireball radius expression can be derived from fundamental principles.

Starting from the assumption of a cylindrical fire plume, the volume of the flame is given as:

$$V_{cyl} = \pi R_{flame}^2 H \tag{10}$$

Taking this volume as that of a sphere, an equivalent radius can be calculated as:

$$R_{sphere} = \left(3/4\pi^2 R_{flame}^2 H\right)^{1/3} \tag{11}$$

It has been previously determined that the height of the fire is proportional to its radius. Substituting this relationship and simplifying yields:

$$R_{sphere} = \left(3/4\pi^2\alpha_1\right)^{1/3} R_{flame} \tag{12}$$

In the subsequent analysis of the radiant heat flux, it will noted that there exist a relation between the mass and radius for the tested configurations. This relationship is shown on Figure 3.8 and can be expressed as follows using regression analysis:

$$R = \alpha_2 m^{0.39} \tag{13}$$

Substituting in the spherical radius expression yields:

$$R_{sphere} = \left(3/4\pi^2\alpha_1\right)^{1/3} \alpha_2 m^{0.39} = \alpha_3 m^{0.39} \tag{14}$$

The last result has the same functional form as that discussed in previous studies and obtained here as Eq. (9). In fact, after replacing the two constants by their numerical values ($\alpha_1 = 2.5$ and $\alpha_2 = 0.24$), the following result ensues:

$$R_{sphere} = 0.69 m^{0.39} \tag{15}$$

which is quite similar to Eq. (9). This is, however, by no means a general result, as it relies on the colinearity between two independent test variables. The most general result would be that given as Eq. (12). The radius could be replaced by the propellant mass through the knowledge of the height and bulk density. There is no advantage in making the transformation, as the horizontal dimensions of the sample are usually known precisely.

2.2.4 Propagation modes

2.2.4.1 Fireball expansion

The present case refers to situations when the gas generation rate is high enough such that natural convection of the high energy gas cannot prevent a pressure buildup. This results in the formation of a pressurized pocket of these gases which then expands freely, as there is no confinement. Surrounding propellant is engulfed by the lateral expansion of the fireball. For these cases, propagation does not solely depend on the absorption of the radiant heat flux emitted by the flame, as the propellant is in direct contact with high temperature gases.

As pointed out previously, the present situation requires the gas generation rate to be above a certain level. A high energy gas generation rate can be summarized by the power released by the event. The power emission is approximated by the following equation:

$$\dot{Q}_m = \frac{Em}{t_{tot}} \tag{16}$$

where E is the propellant heat of explosion (in J/kg), m is the mass of the configuration and t_{tot} is the duration of the event. Measured event times and calculated average power emitted are shown on Table 2.6 for all tested cases. It can be observed that there is no sharp division between the power level of a configuration which produces an expanding fireball. If however the average power is scaled by dividing with the configuration mass, a notable difference appears. Given the available data, it may be concluded that for power with a mass scaled power emission below 0.50 MW/kg, there will be no generation of fireball. Therefore, decision stage B of Figure 2.11 can be stated as follows:

- If $\bar{Q} \leq 0.50$ MW/kg then the propagation mode will be fireball driven.
- If $\bar{Q} > 0.50$ MW/kg then the propagation mode will be projections driven.

Table 2.6: Average power emitted by the tested cases.

Propellant	Mass (kg)	Event duration (s)	Average Power (MW)	Scaled Power (MW/kg)	Fireball observed	Projections observed
SB2	68.2	14.5	16.5	0.25	No	Yes
SB2	136.4	20.3	23.5	0.17	No	Yes
SB2	909.1	20.3	156.7	0.17	No	Yes
SB1	45.5	12.8	12.8	0.28	No	Yes
SB1	90.9	16.5	19.9	0.22	No	Yes
SB1	909.1	21.3	153.8	0.17	No	Yes
DB1	15.9	5.5	15.6	0.98	Yes	Yes
DB1	47.7	7.6	33.9	0.71	Yes	Yes
DB1	477.3	6.7	384.1	0.81	Yes	Yes
TB1	45.5	35.0	4.6	0.10	No	No
TB1	454.5	45.0	35.8	0.08	No	No

To determine if a certain configuration can produce a fireball, one must thus be able to predict the event time in order to compute the average emitted power. A previous study by Lucotte proposes the following relation to predict the event time [46]:

$$t_{tot} = 3.225m^{0.126} \tag{17}$$

The last equation assumes that the duration depends solely on the configuration mass. This does not seem likely, as two cases with the same mass involving a fast and slow burning propellant would yield different times. As an example, the cases involving 45.5 kg of SB1 and 47.7 kg of DB1 yield durations of 12.8 s and 7.6 s, respectively. An event duration prediction equation must thus take into account the burning rate of the propellant. The total burning time will depend on the horizontal and vertical burning rates along with the dimensions of the propellant stack. This problem can be simplified by decomposing the propagation rate into the horizontal and vertical physical dimensions.

$$t_{burnx} = \frac{R_{ini}}{r_x} \tag{18}$$

$$t_{burny} = \frac{H_{stack}}{r_y} \tag{19}$$

The ratio of these two individual burning times yields the following result:

$$\frac{t_{burnx}}{t_{burny}} = \frac{R_{ini}/r_x}{H_{stack}/r_y} = \frac{R_{ini}}{H_{stack}}\frac{r_y}{r_x} \tag{20}$$

Given the value of this ratio, there are cases when one particular burning time is much greater than the other, which means that the smaller value may be neglected. The total burning time is thus represented as follows:

$$t_{burn} \approx t_{burnx},\ if\ \frac{R_{ini}}{H_{stack}}\frac{r_y}{r_x} \geq 2.0 \tag{21}$$

$$t_{burn} \approx t_{burny},\ if\ \frac{R_{ini}}{H_{stack}}\frac{r_y}{r_x} \leq 0.1 \tag{22}$$

$$t_{burn} \approx t_{burnx} + t_{burny},\ if\ 0.5 \leq \frac{R_{ini}}{H_{stack}}\frac{r_y}{r_x} \geq 2.0 \tag{23}$$

From the previous considerations, the event can be divided in two phases:

(1) Induction time (defined here as t_{ind})

(2) Steady state burning (defined previously as t_{burn})

The total burning time computed represents the time for which the second of these phases occurs. The first phase represents the time when the fire is growing to its steady state values. In that aspect, the third burning time condition given represents a case where the induction time and steady state time are comparable. Larger error is thus expected for that case, assuming an average behavior will not represent the highly transient nature of the event.

By applying the methodology shown previously, the total burning times were calculated for the tested examples. The results are shown in Table 2.7 along with the measured values.

Table 2.7: Comparison of the predicted and measured total event times.

Propellant	Mass (kg)	Measured event duration (s)	Predicted event duration (s)	$\frac{R_{ini}}{H_{stack}}\frac{r_y}{r_x}$ (dimensionless)	Predicted Power (MW)
SB2	68.2	14.5	20.0	0.05	11.9
SB2	136.4	20.3	22.0	0.10	21.7
SB2	909.1	20.3	24.0	0.20	132.5
SB1	45.5	12.8	11.0	0.10	14.9
SB1	90.9	16.5	12.0	0.20	27.3
SB1	909.1	21.3	12.0	0.20	273.0
DB1	15.9	5.5	4.0	0.06	21.4
DB1	47.7	7.6	4.0	0.08	64.3
DB1	477.3	6.7	5.0	0.25	514.7

2.2.4.2 Projections

Grain projections are often observed during granular propellant fires. In the fires observed here, it was possible to observe projections even with the limited resolution of the camera. The higher resolution, smaller tests were useful in quantifying this behavior with greater precision for a given propellant. In all cases, the presence of projection was a yes-no decision based on the direct observation of the available video footage. The variety of propellants used showed that this methodology was sufficient in making proper determinations and could even provide with additional details pertaining to the general amount of projected grains.

Tests performed on laboratory samples (a few grams) or individual grains have shown that grains generally do not self-propel. This last statement is, however, not true for very energetic compositions such as double bases. The large amount of projections observed here with less energetic single base is thus attributed to grains being entrained in the gas flow. Figure 2.14 shows the effect of these projections. Assuming that the grains are travelling at the combustion gases velocities given in Table 2.9 and an angle of $45°$ from the ground (worst case), the horizontal travel and flight time can be computed. The situation

is illustrated in Figure 2.15. The total base fire width would then be the original stack diameter and twice the grain travel distance. This would result in the maximum base fire width being approximately 2.4 m larger than the starting diameter.

Observation of Table 2.6 shows that projections are observed only in fires of sufficient power. Lower power fires simply do not generate the sufficient conditions (in terms of gas flow and turbulence) to entrain grains away. From the set of data, a limiting condition for the presence of projections can be established as $\bar{Q} = 0.10$ MW/kg. This condition does not differentiate between cases where the fire can increase in size due to projections. To make this further separation, a condition based on the combustion dynamics of individual grains is required. Decision stage A of Figure 2.11 can thus be described as follows:

- If $\bar{Q} \leq 0.10$ MW/kg, then the propagation mode will be driven by the radiant heat flux (ideal).
- If $\bar{Q} > 0.10$ MW/kg, then the propagation mode will be projections driven.

An important point to consider when dealing with the projection of grains is the time required to burn a propellant grain. If the grains completely burn prior to reaching the calculated distance, the result will not be valid. Using the all burnt point as half the web size of the grains and the burning rates measured on each propellant, the burning times are calculated and shown in Table 2.8. When taking the ratio of the total travel time on the burning time, some important differences can be observed. These differences are important in determining the main flame propagation mode.

Projections also have another important consequence: igniting surrounding material. Even if a propellant might have a time ratio which would not affect the total diameter of the event, projected grains can still have a major role in flame propagation. All of the SB1 and SB2 tests show that it is indeed through direct contact with projected combusting grains that the flame propagates. An example is shown in Figure 2.16. It is therefore not radiant heat flux which plays the dominant role in such cases.

Figure 2.14: The effect of propellant grains projection on the fire width. On the left, projections are seen in the early part of a fire involving 136.4 kg of SB2. On the right, the same fire 15 seconds later. On both images, the horizontal line at the bottom represents the width of the propellant stack.

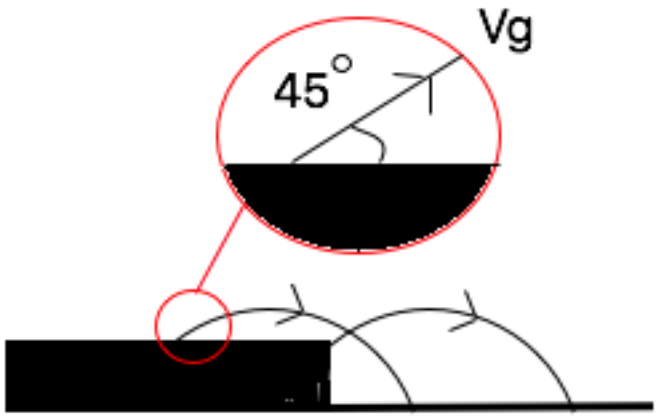

Figure 2.15: Schematic representation of the propellant grain projection fire propagation mode.

Based on the grain combustion and flight time, a ratio can be used to characterize if a fire will grow in size. Indeed, the ratio of flight time over the combustion time can be taken as a measure of the growth potential of the fire. In this case, the limit is naturally set at unity. Decision stage C of the Figure 2.11 decision tree is thus governed by the following:

- If $\bar{\tau} \leq 1.0$, then the projections will propagate the flame without enlarging the event diameter.
- If $\bar{\tau} > 1.0$, then the projections will propagate the flame and enlarge the event diameter.

Table 2.8: The projection of propellant grains during fire events.

Propellant	Mass (kg)	Grain burn time (s)	Flight time (s)	Time ratio (unitless)	Characteristic flight distance (m)	Distance ratio (unitless)
SB2	68.2	0.8	0.11	7.1	0.06	0.06
SB2	136.4	0.8	0.06	14.1	0.02	0.01
SB2	909.1	0.8	0.18	4.5	0.20	0.04
SB1	45.5	0.4	0.08	4.7	0.04	0.04
SB1	90.9	0.4	0.18	2.1	0.18	0.09
SB1	909.1	0.4	0.40	1.0	0.80	0.20
DB1	15.1	0.05	0.88	0.1	3.92	5.61
DB1	47.7	0.05	0.93	0.1	4.45	4.45
DB1	477.3	0.05	0.66	0.1	2.23	0.56
TB1	45.5	1.2	0.13	9.0	0.09	0.09
TB1	454.5	1.2	0.12	9.8	0.08	0.03

The effect of projections can seem diminished as the initial diameter is increased. This can be explained by the decreasing weight of the grain flight distance over the propellant stack initial diameter. Larger propellant stacks will thus have a maximum flame diameter close to that of the original stack.

A flame propagation model for cases involving ignition by projected grains could thus be deduced from these few simplifying assumptions:

- Entire surface covered with projected grains instantaneously at ignition.
- Instantaneous ignition of material in contact with projected grains.
- Surface flame spread on ignited grain over a characteristic length $\bar{L}$ at the measured horizontal propagation rate r_x.

From these considerations, the characteristic length would be the largest linear dimension of the grains (either their length or diameter). The propagation rate r_x would be that measured in the laboratory scale test conditions. An induction time can thus be defined as the period during which the fire will grow to its steady state maximum diameter and height.

Figure 2.16: Example of flame propagation due to projected SB1 grains.

The induction time is thus:

$$t_{ind} = \frac{\bar{L}}{r_x} \tag{24}$$

In reality, some cases will feature a more gradual growth. Projections will travel only part of the total available surface, ignite the material, which will in turn project grains further until the entire sample is covered.

2.2.5 Flame growth rate

An important observation to make while observing Figures 2.9 and 2.10 is that the growth rate of both the width and height of the fire seems independent of the sample mass. To verify and quantify the last statement, the slope of the rising part of each curve can be computed using the least square technique. The computed growth rates are shown on Table 2.9 for all tested samples and configurations. From the previous calculations, the rates are indeed seen to be mostly dependent on the propellant type. This lateral spread behavior is predictable, as the horizontal flame propagation has been shown to be dependent on the radiant heat flux, ignition temperature and sample thermal properties when assuming

either a thermally thin or thick solid [15]. In the case of vertical rise, the nature and rate of production of the combustion gases, both dependent only on the nature of the tested sample, would most likely affect the growth rate.

The gas velocity can be estimated using the fire power and stack dimensions. If the fire power and the gas energy flow rate are equated, the following is obtained [39]:

$$\dot{Q}_m = \rho_{gas} U E A_{base} \tag{25}$$

Noting that $A_{base} = \pi D^2/4$ and solving for the gas velocity, U, yields the relation:

$$U = \frac{\dot{Q}_m}{\rho_{gas} E(\pi D^2_{flame}/4)} \tag{26}$$

Here, the combustion gas density, ρ_{gas}, can be estimated from thermodynamic codes. The calculated gas velocities are shown on Table 2.9. There is no expected match between the flame vertical growth rate and the vertical gas velocity, as they are two different quantities. The former expresses the growth rate of the luminous flame while the latter gives the combustion gases velocity at the surface of the burning propellant.

Table 2.9: Flame propagation velocities of various propellants for large scale fires.

Propellant	Mass (kg)	Horizontal propagation velocity (m/s)	Flame vertical growth rate (m/s)	Vertical gas velocity (m/s)
SB2	68.2	0.5	1.3	0.8
SB2	136.4	0.6	1.1	0.4
SB2	909.1	0.5	1.5	1.3
SB1	45.5	0.6	1.6	0.6
SB1	90.9	0.4	1.3	1.3
SB1	909.1	0.9	1.8	2.8
DB1	15.9	1.3	2.6	6.2
DB1	47.7	1.4	2.8	6.7
DB1	477.3	2.0	3.3	4.7
TB1	45.5	0.1	0.8	0.9
TB1	454.5	0.2	0.7	0.9

2.3 Case study: small scale surface propagation

The dependence of the horizontal flame propagation rate to the width of the flame front was examined for a single propellant using linear configurations of various widths. Samples disposed in a 2 m long line with widths varying from 2.5 to 56 cm were ignited at one end using a nichrome hot wire. The events were captured on a Casio Exilim camera at a rate of 256 frames per second. Using a distance marker placed in front of the linear sample, the flame front traveled distance was measured as a function of time. Figure 2.17 shows a still image of the setup during a test. The slope of the linear relationship obtained is the desired propagation velocity. Table 2.10 shows the various configurations tested and their resulting propagation velocity. Plotting the horizontal propagation velocity as a function of the width yields what is shown on Figure 2.18. It is seen that the propagation rate increases by almost a tenfold factor compared to the width increase.

A variation of the propagation rate is expected as the event dimensions are changed. From an ideal standpoint, a larger flame front yields larger heat fluxes. From Eq. (5), a heat flux increase has a direct effect on the propagation rate. In the present case, however, the

Figure 2.17: The 2 m horizontal propagation test. Note that the width would go into the paper. The flame length is the distance between the left and right endpoint of the luminous flame againt the bottom reference.

Table 2.10: Measured surface propagation velocities and flame zone lengths for SB1 samples of various widths.

Width (cm)	Height (rough estimate) (cm)	Propagation velocity (cm/s)	Flame length (cm)
2.5	1	2.1	15
12.7	3	5.6	40
17.8	8	12.5	90
30.5	8	11.5	110
55.9	8	11.5	100

propellant generates a fair amount of projections. These burning projectiles are responsible for spreading the fire. It was previously shown that these projections have velocities which depend on the power generation of the fire. A more detailed analysis of these parameters can thus be helpful.

Table 2.10 also features another important measurement, the length of the flame, l_f. This length is defined as the distance between igniting and completely combusted material (measured by estimating the left and right endpoints of the flame against the fixed reference). It is observed to remain fairly constant throughout a test and correlates with the height of the propellant bed. Using the additional measurements along with the flame front width, it is possible to calculate the burning surface area and volume. With the further application of the propellant bulk density and heat of explosion, the average combusting mass

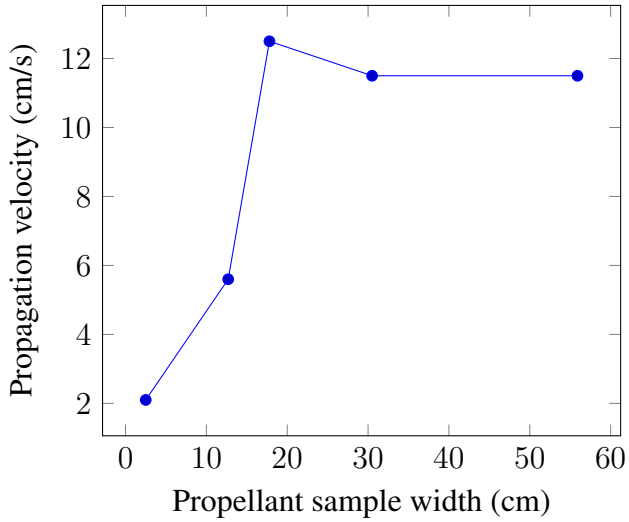

Figure 2.18: Dependance of the surface propagation velocity on the sample width.

and power generation can be obtained. These parameters are shown on Table 2.11 along with the calculated scaled powers and gas rise velocities. The scaled power results oscillate between 0.38 and 0.50 MW/kg, which supports the propagation by projection scheme.

Table 2.11: Calculated area, mass, power generation, and gas rise velocity for the tests described in Table 2.10.

Width (cm)	Surface area (m^2)	Avg. burning mass (kg)	Power generation (MW)	Scaled power (MW/kg)	Gas velocity (m/s)
2.5	0.0037	0.037	0.018	0.49	1.1
12.7	0.051	2.03	1.02	0.44	4.6
17.8	0.16	12.8	6.41	0.50	9.3
30.5	0.34	26.8	10.10	0.38	6.9
55.9	0.56	44.7	18.52	0.41	7.64

A key observation is that the resulting gas velocities follow the same relationship as the propagation rate with respect to the width (as shown in Figure 2.19). Further observation shows that the same relationship is followed by the flame length and the propellant bed height. Comparing the width of a configuration to the test value will yield the flame length and thus the burning height. Scaling factors for the burning propellant height and volume can than be defined as $\bar{h} = h_i/h_{test}$ and $\bar{V} = V_i/V_{test}$, respectively. Here, h_i and h_{test} refer

to the burning propellant height for the estimation and test configurations (the same logic applies for the volumes). These scaling factors can be used to estimate the fire power and propagation velocity for a larger scale case.

The reported variation of the propagation velocity is thus mostly due to the change in the propellant bed height. From this, it is seen that one can obtain satisfactory estimates of the propagation rate velocities at all widths using the results of the smallest scale case (i.e., the 2.5 cm configuration). The last conclusion is of importance as it is relatively easy to perform the 2 m linear propagation test on such a small width. Although each problem will inevitably contain its own particularities, the general quantities derived here are simply applied within the specific context.

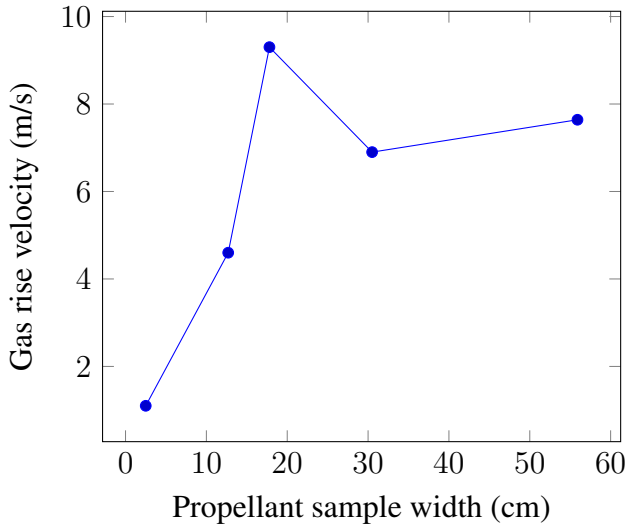

Figure 2.19: Dependance of the gas rise velocity on the sample width.

The horizontal flame propagation velocities of various propellants were measured by applying the same method. The width of propellant in the setup was approximately 2.5 cm throughout the linear length. The measured propagation velocities are given in Table 2.12.

Table 2.12: Horizontal flame propagation velocities of various propellants for a width of 25 mm.

Propellant	Horizontal propagation velocity (cm/s)
Single base 1	5
Single base 2	2
Double base 1	16
Double base 2	14
Triple base 1	0.5

2.4 Summary

The solid to gas transformation which occurs during propellant combustion is a rapid process. The speed at which the transformation takes place is of paramount importance in calculating the pressures and heat fluxes generated. Most propellant combustion models have been tailored to specific applications and assume the simultaneous ignition and combustion of all surfaces of the propellant. When propellant fires occur, the ignition takes place in a very specific region of the propellant bed. The flames then spread until the entire stack is engulfed. Predicting the combustion rate of the propellant is beyond the scope of the present study, as it involves a deep understanding of the reaction chemistry. Work has been performed by various researchers to predict these rates, but the computing requirements are prohibitive. The present effort, instead, attempted to obtain meaningful information about how propellant fires spread and what their final dimensions might be. The study of this topic has shown to provide somewhat of a synthesis of the fire safety issue. Propagation is driven by some form of heat flux and the nature of this heat flux indicates what the maximum dimensions of the event will be. Pressure generation in closed or semi-closed systems is dependent on the size of the event. Secondary behaviors that have not been studied here, such has flame jetting from openings, are also very dependent on dimensions and spread rates. Flame propagation is thus indeed at the crux of fire safety.

Three fundamental propagation modes have been observed for propellant fires: radiant

heat flux (ideal), projections and fireballs. A semi empirical approach is proposed where the flame propagation rates are measured in a controlled laboratory setting. Subsequent calculations based on the physical configuration are made to compute the actual maximum dimensions that would be observed for a given case. It is thus possible to build a flame spread model for a given case using the propellant stack dimensions and combustion properties. The model is a decision tree and is shown as Figure 2.20. Starting from the top of Figure 2.20, one is able to move downward and approximate the maximum fire diameter and height. In performing the analysis, one is also able to estimate the time required to reach these maximum values through a comparison of individual grain burning and projection travel times. In its current form, it is important to note that the model is not applicable when the grains become too large and can travel larger distances. Such would be the case with stick propellants used in rocket motors. In these cases, a sort of self propulsion criterion would be required to further the analysis.

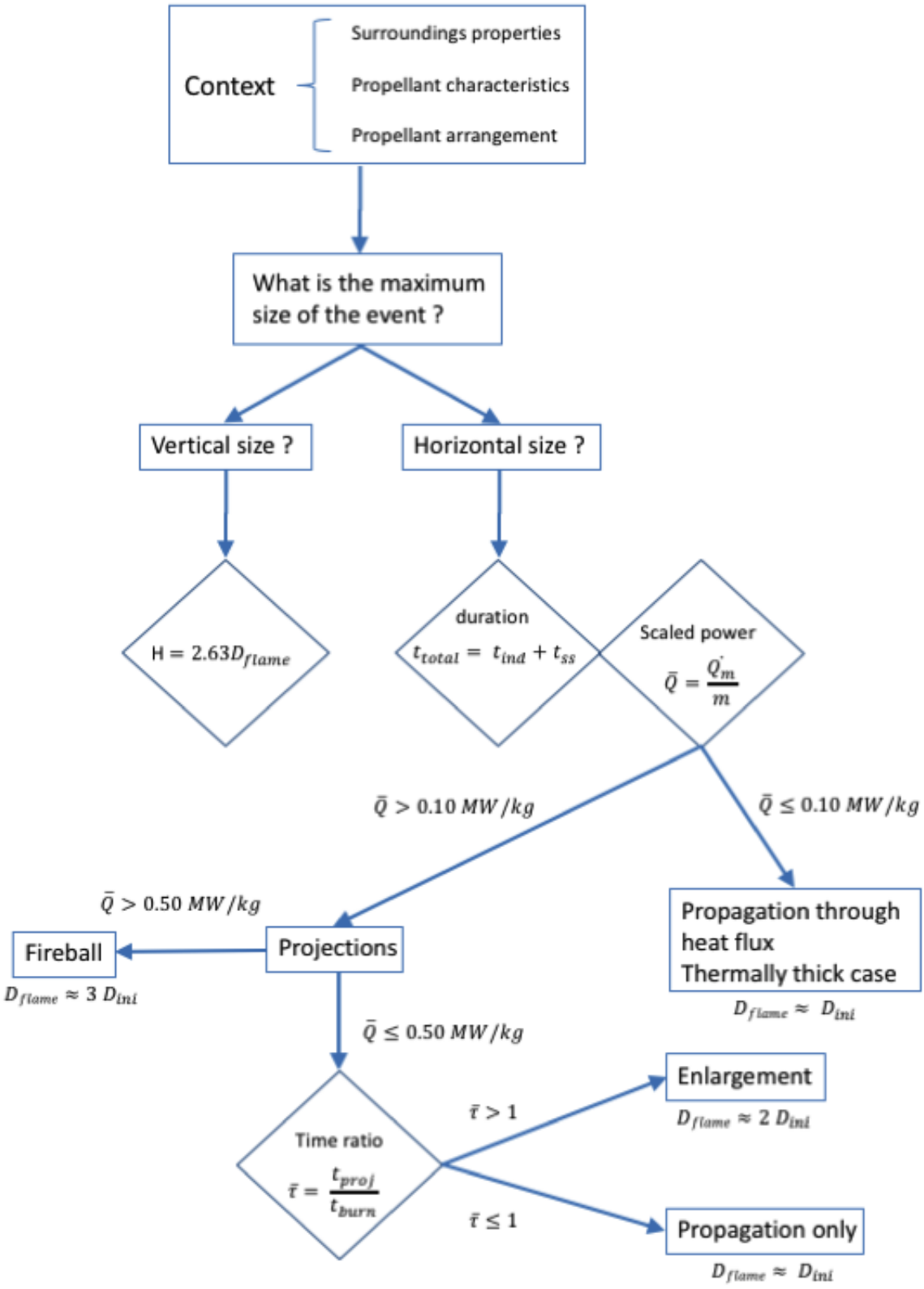

Figure 2.20: Decision tree to select the proper flame propagation mode.

Chapter 3

Design of a predictive propellant fire radiant heat flux model

> "The principles of the theory are derived, as are those of rational mechanics, from a very small number of primary facts, the causes of which are not considered by geometers, but which they admit as the results of common observations confirmed by all experiment."
>
> Jean-Baptiste Joseph Fourier - The Analytical Theory of Heat (1878)

3.1 Introduction

Fire has always been associated with the release of heat. A large portion of the world's population uses fire as a source of heat. For all its benefits, heat can also be a source of danger. Someone sitting too close to a campfire can readily observe its adverse effects. At the extreme limit, the heat associated with the initial flash of a nuclear explosion can vaporize many known substances. From the fire safety standpoint, heat transfer from the fire to the surroundings is probably the most important aspect to consider for most materials.

Two situations cover most of the applied cases:

- Engulfment in the flames: this is the worst possible case. In this situation, heat is transferred through all three modes. There is convection as high temperature gases are moved from the source to the engulfed object. Since there is a direct contact between the solid and combustion gases, conduction would also happen. Finally, the surrounding high-energy gases radiate heat which can be absorbed by the object.

- Object away from the flames: in that case, only radiation is pertinent. There can be an amount of natural convection as the heated air closer to the fire diffuses toward the cooler external air. This last transfer is, however, often of a lesser magnitude than the radiation transfer [15].

The first situation is clearly unwanted and depends on the size of the event. It can therefore be avoided by simply ensuring that the object is located beyond the estimated maximum dimension of the fire. The second case requires some knowledge about how the heat radiates from the flames.

The campfire analogy is interesting as some of the important variables can be estimated through a simple thought experiment. It was already noted previously that the distance at which one sits from the fire is of importance. The amount of heat radiated per unit area, or heat flux, decreases with increasing distances. Another situation is when the fire suddenly changes in dimension. For example, when a log breaks into pieces that roll away and ignite the surrounding unburned wood. When this happens, it is often necessary to quickly move away from the fire, due to the increase in heat. There is thus a relationship between the radiated heat and the size of the fire. A larger fire emits more radiant heat. Finally, although this occurs less often, it is sometimes observed that a change in fuel can generate more heat.

From this simple example, three basic variables have been identified:

- Distance from the fire

- Size of the fire
- Nature of the fuel

As will be shown, these variables are indeed fundamental in obtaining a radiant heat flux model for propellant fires. The next section will review previous work on the subject performed with various fuels. This review is helpful in the subsequent analysis of propellant fire experiments.

3.2 Theoretical considerations and previous work

3.2.1 Radiation heat transfer theory

Flames are a zone of high temperature gases usually rising above a fuel undergoing combustion [10]. Because of their high temperature, the gases are in various excited electronic states and thus emit electromagnetic waves [48]. The intensity of these emissions has been described by Boltzmann using classical thermodynamics [49]. A description of the wavelengths associated with these electromagnetic waves proved to be more challenging. Ultimately, an accurate picture was drawn by Planck using arguments which founded the field of quantum mechanics [48]. Both of these aspects, intensity and wavelength, are of interest when considering the radiant heat flux at a point.

For any problem involving radiation heat transfer, the heat flux at a given distance depends on five parameters [30]:

(1) The total surface of the source.

As heat flux is defined as the heat per unit surface, an emitting surface shall emit more heat if its surface is larger (assuming constant conditions on the entire surface). In the case of a fire, this surface is located at the edge of the flame or fireball and is a dynamic parameter. Determining the surface area of the flames thus involves

looking at the flame propagation in the material. It is reasonable to expect that the total surface would be dependent on the diameter of the propellant stack.

(2) The surface emissive power of the source.

The surface emissive power parameter defines the quantity of heat per unit surface emitted by the fire. This quantity is usually calculated using the Stefan-Boltzmann law [30]:

$$\dot{Q}_S = \epsilon \sigma T^4 \tag{27}$$

where ϵ and T are the emittance and temperature of the gases respectively and σ is the Stefan-Boltzmann constant. Since a fire plume is composed of high temperature gases and solid particles (such as soot), it is possible to predict the radiative emission of the flame through the knowledge of the chemical and thermodynamical properties of the gases. Empirical correlations have been developed to simplify this process but these are for specific cases with properties that are difficult to measure in a fire [30] [50]. Given a set of surface emissive power or radiant heat flux measurements, it should be possible to obtain a correlation applicable to a given material.

(3) The distance from the source.

A diffuse source of light is one that emits equally in all directions [51]. As a receiving surface gets further away from a source, the light intensity will decrease. This follows from the fact that a surface with all points equidistant from a central region will have an area which increases with distance. Two cases are often used in applications: the point and line sources. These cases are both shown on Figure 3.1.

The point source has an attenuation which follows an inverse square law (area of the

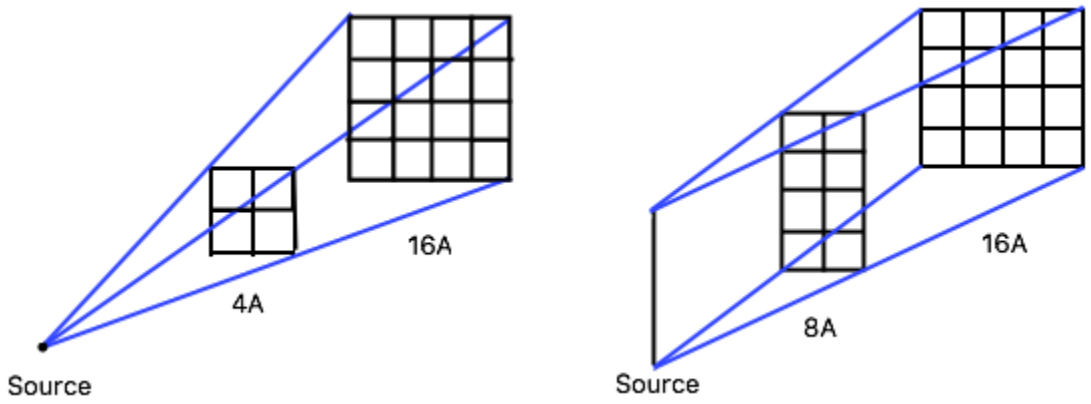

Figure 3.1: Diagram showing a comparison of the point and line source approximation on the area of surfaces away from the source at distances d and $2d$ respectively.

sphere).

$$\frac{I_2}{I_1} = \frac{\pi R_2^2}{\pi R_1^2} = \left(\frac{R_2}{R_1}\right)^2 \tag{28}$$

The case of the line source follows an inverse law.

$$\frac{I_2}{I_1} = \frac{2\pi R_2 H}{2\pi R_1 H} = \frac{R_2}{R_1} \tag{29}$$

More complicated cases follow more complex relations which require integration and sometimes numerical results [50].

(4) The relative angle between the source and receiving surface.

The relative angle and distance between the emitting and receiving surfaces are often treated using the concept of view factors (also denoted as configuration factors in the literature). The view factor between surfaces 1 and 2, denoted as F_{1-2}, is defined as the fraction of energy leaving 1 reaching 2. View factors have been computed for a large number of configurations and can be found tabulated in the literature [50]. The previous considerations result in the heat flux at a certain surface away from the fire to be given by:

$$R = F_{1-2}\dot{Q}_S = \epsilon\sigma F_{1-2}T^4 \tag{30}$$

where the emission of the receiving surface (due to its own temperature) has been neglected [30]. In the case where the receiving surface temperature cannot be neglected the last equation becomes:

$$R = \epsilon\sigma F_{1-2}(T^4 – T_s^4) \tag{31}$$

where both surfaces are taken as grey bodies with equal emittance. For typical propellant flames and receiving surface, where the temperatures are in the 3,000K and 300K ranges respectively [52], the fourth power law implies that the fire contributes 10,000 times more to the total flux.

(5) The transmittance of the medium separating the source and receiving surface.

The previous discussion on the propagation of electromagnetic waves assumed no losses in the propagation medium (i.e. the case of vacuum). As soon as the medium is lossy, additional attenuation is observed. This loss is usually modelled by a parameter denoted as the transmittance, T_{OD} [51]. Although often treated as a constant in a given problem, the transmittance is dependent on the nature of the medium and wavelength of the radiation. An example of this relationship is in the Beer-Lambert Law [51]:

$$T_{OD} = e^{-\tau_{OD}} = e^{-\sum_{i=1}^{N}\tau_{OD}^i} \tag{32}$$

where τ_{OD} is the optical depth of the medium and τ_{OD}^i is the optical depth of the ith component making up the medium. The concept of optical depth is defined as the logarithm of the ratio between the incident and transmitted radiation in a medium [51]. Other such relations exist and describe the transmission of electromagnetic

waves in detail. It is notable that this phenomenon and the models describing it are largely applied in the field of spectroscopy [14].

It can thus be observed that the radiant heat flux is generally described by an expression of the following form:

$$\dot{q}'' = f(d, A, \theta)\ g(E, r) \tag{33}$$

where $g(E_f, r)$ is a function describing the energy radiated by the fire and $f(d, A, \theta)$ is a function describing the energy which ultimately reached the receiving surface (thus equivalent to the view factor F_{1-2}). In Eq. (33), the function f depends on the distance from the flames, d, the area of the flame, A, and the angle between the emitting and receiving surfaces, θ. The function g in turn depends on the combustion rate of the substance, r, and the energy content (or heat of explosion) of the substance, E.

3.2.2 Previous work

Because a heat emitted by fire is of great importance to fire safety, it has been studied extensively. Experimental measurements were performed on various materials arranged in a stackwise or pool (for liquids) fashion. Radiative heat fluxes and flame dimensions were recorded to obtain a subsequent model with the help of theoretical principles.

One of the simplest such models is that obtained by Modak [22]:

$$\dot{q}'' = \frac{\dot{Q}_r \cos\theta}{4\pi r_{fire}^2} \tag{34}$$

Where $\dot{Q}_r$ is the total radiant energy output of the fire, r_{fire} is the distance from the fire and θ is the elevation of the receiver with respect to the source. Given its inverse square relationship, this is a point source model. Figure 3.2 illustrates this configuration.

Given the finite height of flames, the point source is usually located halfway between

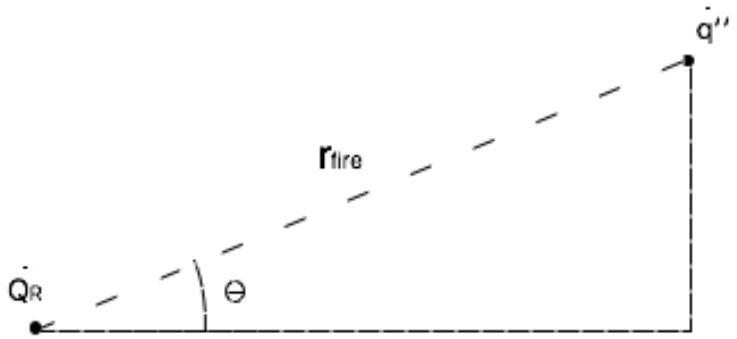

Figure 3.2: Diagram showing the Modak model as a point source approximation.

the top and bottom of the fire. The total radiant energy is usually computed as a fraction of the total energy of the fire. The value of this fraction depends on the fuel.

The Modak point source model is a simplification, as fires usually have a finite width, depth and height. However, as the receiver moves further away from the fire, its dimensions become negligible. A point approximation thus becomes fairly precise (see Figure 3.3). It is estimated that the point source approximation works well when $r_{fire}/D_{flame} > 2.5$ (error within 5%) [53].

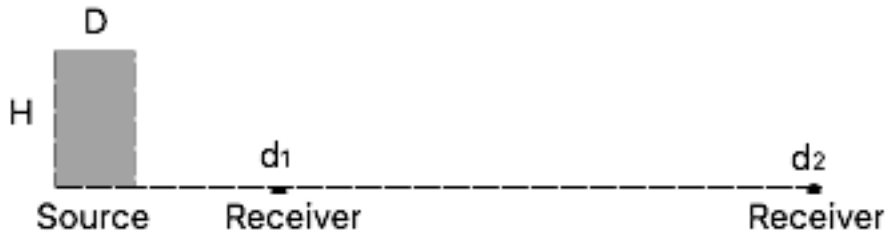

Figure 3.3: Comparison of the validity of the point and line source models. For Receiver 1, the ratios $d_1/H \approx 1$ and $d_1/D \approx 1$ and the dimensions of the source cannot be neglected. For Receiver 2, the ratios $d_2/H \gg 1$ and $d_2/D \gg 1$ and the dimensions of the source cannot be neglected.

When further precision is required, the model must take into account the shape of the fire. This is actually done by assuming either a rectangular or cylindrical shape. When a shape is established, configuration factors may be computed.

A popular such model is that of Dayan and Tien, which uses a cylindrical approximation [54]. This is a flexible model as it considers the receiver as a differential surface, dA, with no normal vector $\hat{n} = u\hat{i} + v\hat{j} + w\hat{k}$. Figure 3.4 illustrates this model. An important parameter of the model is the angle, θ, which is the angle between the vertical direction and a line going from dA to the center top of the cylinder. The factors corresponding to each component of $\hat{n}$ are given as:

$$F_1 = \frac{u}{4\pi}\left(\frac{r_{flame}}{r_{fire}}\right)^2(\pi - 2\theta + \sin 2\theta) \tag{35}$$

$$F_2 = \frac{v}{2\pi}\left(\frac{r_{flame}}{r_{fire}}\right)(\pi - 2\theta + \sin 2\theta) \tag{36}$$

$$F_3 = \frac{w}{\pi}\left(\frac{r_{flame}}{r_{fire}}\right)\cos^2\theta \tag{37}$$

From this, the radiative heat flux is computed from:

$$\dot{q}'' = \sigma\epsilon T_f^4(F_1 + F_2 + F_3) \tag{38}$$

For a receiving surface aligned perpendicular to the normal from the fire surface, only the F_2 component is nonzero. The heat flux then simplifies to the following:

$$\dot{q}'' = \frac{\dot{Q}_r r_{flame}}{2\pi r_{fire}}(\pi - 2\theta + \sin 2\theta) \tag{39}$$

In this case, an inverse distance relationship is obtained. This results in a line source approximation. Here, there is an additional dependence on the radius, r_{flame}, of the fire. The Dayan and Tien model has been found to be relatively precise for $r_{fire}/D_{flame} > 1.5$ [54]. Another slightly more complex model is that of Shokri and Beyler [53]. For all

practical purposes, precision for cases involving $r_{fire}/D_{flame} > 1.5$ is acceptable since $r_{fire}/D_{flame} \leq 1$ is considered inside the fire itself.

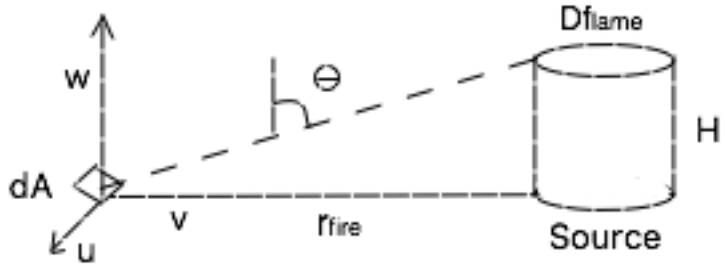

Figure 3.4: Diagram showing the Dayan and Tien model as a line source approximation.

Many other studies have applied similar models to verify empirical results. For example, Orloff used a point source expression to model polymer pool fires [41]. Other published examples can be found, but are beyond the scope of this study.

Previous studies on the subject applied to propellant fires have produced models which are currently used in the industry. The most known model was published by the French S.N.P.E. (Société Nationale des Poudres et des Explosifs) in 1982 [46]. Their conclusion was the following relationship for the maximum radiant heat flux, $\dot{q}''$, based on the propellant heat of explosion, E, the mass burning rate, dm/dt and the distance from the fire, r_{fire}:

$$\dot{q}'' = \frac{c_\tau E}{4\pi r_{fire}^2} \frac{dm}{dt} \tag{40}$$

where c_τ are constants related to the fraction of energy radiated and transmitted through a given medium. For fires involving propellant quantities of less than 800 kg, c_τ is equal to $1/3$ [46]. The mass burning rate is computed using the known propellant properties and geometrical parameters. Estimating $\frac{dm}{dt}$ can be a source of error, as this is a dynamic parameter which depends on flame propagation. Finally, this law assumes an inverse square relationship for the distance, which is equivalent to a point source of heat flux [30]. Given that propellant fire usually consists of a cylindrical or triangular plume of some height, the

point source estimate is disputable.

A recent study by Merrifield and Wharton [47] tested a large array of pyrotechnic products, including propellants. In that case, the surface emissive power, S, of the event rather than the heat flux at a specific distance was measured. The result was a set of relations of the form:

$$\dot{Q}_S = am^b \tag{41}$$

where a and b are constants which depend on the type of propellant. The main drawback from this last type of model is that the constants must be determined empirically for each new propellant tested. Furthermore, additional calculations are required to obtain the radiant heat flux at any point away from the fire.

Other empirical work has also been performed on specific cases without yielding any model [32] [55]. Variations in the methodologies of previous studies results in differences in what is reported concerning the tested configurations. It is thus necessary to perform additional tests to properly design a model. There is a need for a predictive expression which uses variables that can be measured in a laboratory environment using standard methods.

3.2.3 Synthesis

Given the form of Eq. (33), a set of variables is first assumed as containing the necessary information in order to describe the maximum radiant heat flux, $\dot{q}''$ (in W/cm^2), emitted during the combustion of propellants. These variables are the following:

- Propellant stack diameter, D_{ini}, in meters.
- Propellant mass, m, in kg.
- Propellant heat of explosion, E, in J/kg.
- Propellant linear burning rate, r, in m/s.

- Distance from the fire, r_{fire}, in meters.

These variables are such that the energy emitted by the fire can be represented by the heat of explosion, mass and burning rate while the physical dimensions are represented by the other quantities listed. The goal is then to express the previously discussed functions as:

$$\dot{q}'' = f(r_{fire}, D_{ini}, m)g(E, r) \tag{42}$$

Given the previous results obtained through work with different substances (especially the Modak point source, Dayan and Tien line source and S.N.P.E relations), a general form can be inferred for radiant heat flux models. The resulting general form is similar to Eq. (42) and given as follows:

$$\dot{q}'' = k\ r_{fire}^{a_1}\ D_{ini}^{a_2}\ E^{a_3}\ m^{a_4}\ r^{a_5} \tag{43}$$

where k, a_1, a_2, a_3, a_4 and a_5 are constants. The set of experiments performed was thus designed to increase the efficiency of the process. Given the number of variables to study, a statistical analysis on a limited number of trials can yield meaningful models. This is important as the resources required to perform large scale propellant fires are non-negligible.

3.3 Experimental work

The goal of the present study is to obtain a general model applicable to as many cases as possible. A test setup was thus designed to minimize any feature which would have constrained the subsequent analysis. The circular propellant stacks used in the previous chapter to characterize the flame propagation and event dimensions were used to perform irradiance

measurements (the configurations, propellants chemical characteristics and physical properties are described in Tables 2.4, 2.2 and 2.3, respectively).

The radiant heat flux was measured using three water cooled Gardon gauge radiometers of model TG9000 manufactured by Vatell Corporation. These sensors are designed with a 300 W/cm^2 full range, but were precisely calibrated in the 0 to 18 W/cm^2 range. The calibration of the gauges was performed by the manufacturer before and after the tests to verify their precision and no significant variation was observed. Each radiometer was located at a specific distance from the edge of the propellant stack and was aligned to face its center. Given the symmetry of the setup, it was not expected that the angular position of the sensors would have an impact on the results. A previous study has shown that average flux values measured at an angle of 90° are fairly similar [47]. Although maximum values can have larger differences, these variations are largely due to the transient shape of the flames, and therefore more erratic. Each radiometer was thus disposed so as not to interfere with the field of view of the others. Figure 3.6 illustrates the setup and the tested configurations are given in Table 3.1. Masses ranging from 0.1 kg to 954 kg were thus tested, a range covering four orders of magnitude. Because of the mass variation, the tested distances spanned three orders of magnitude (0.1 m to 20 m).

The small voltages produced by the radiometers were amplified using a set of differential instrumentation amplifiers. Signal acquisition was made at a rate of 10 samples per second using a 16 bit analog-to-digital conversion process. The results of each test came in the form of radiant heat fluxes versus time data points, which were subsequently analyzed using a computer. Examples of such radiant heat flux curves are shown on Figure 3.7. The measured maximum radiant heat flux of each of the tested configurations are shown on Table 3.2. For reference, Appendix B contains all radiant heat flux traces obtained.

Given the magnitude and cost of the performed tests, it was not possible to duplicate all of them. Some repetitions were, however, made in order to assess the error of the heat flux

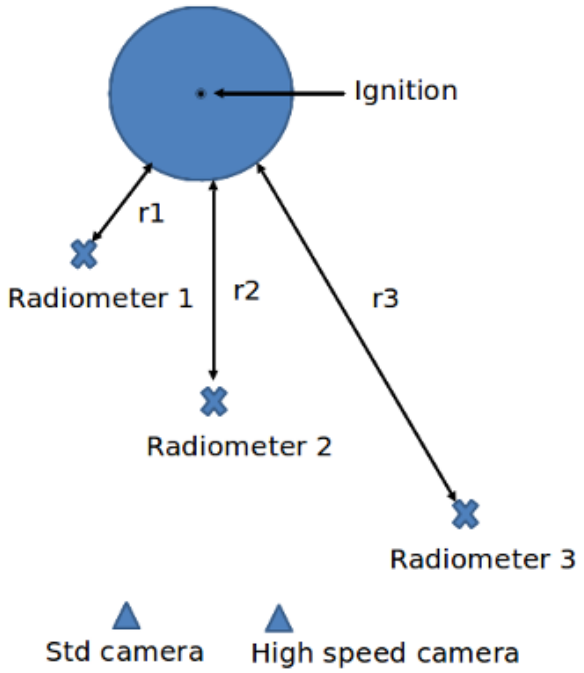

Figure 3.5: Configuration used for the large scale radiance measurements. Note that propellant stacks of various masses and diameters were used. The measurement distances were adjusted accordingly.

measurements. Two cases were used to look at the duplication statistics: 45.4 kg of SB1 and 15.9 kg of DB1. The results are shown on Table 3.3. It must be noted that although two configurations were used, each fire implied measurements at several distances, thus multiplying the number of cases. In error analysis, the measurement error is often approximated as the standard deviation of a series of repeated measurements [56]. Table 3.3 thus shows that a relative error of 10 to 15% can be expected in each measurement. The error can also be estimated by considering each contributing factor: radiometer precision, data acquisition system precision, propellant configuration measurement (mass, diameter, radiometer distance) and variations in atmospheric conditions. The effect of the last two contributions on the radiant heat flux emitted is difficult to predict prior to having a model giving insight on the importance of each of the variables. An error estimate based on the measurement standard deviation is thus satisfactory at this point. Any model derived from the measured data

Figure 3.6: Picture of the test setup for configuration A2.

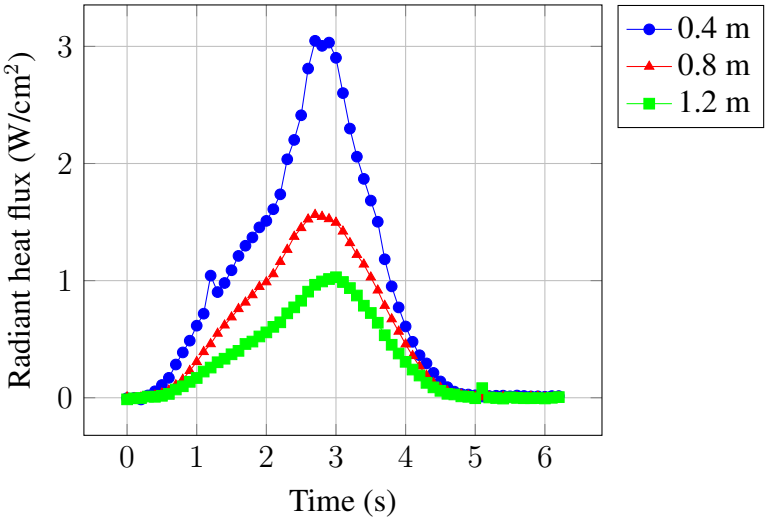

Figure 3.7: Typical radiant heat flux curves obtained during testing. The case shown involves 0.1 kg of SB1 with measurements performed at the three distances given in the legend.

will have a precision limited by the previously discussed error. Given that configurations spanning several orders of magnitude in masses and distances were tested, the observed error range is not of concern here.

Table 3.1: Tested configurations.

Config.	Propellant	Mass (kg)	Diameter (m)	Dist. 1 (m)	Dist. 2 (m)	Dist. 3 (m)
A1	SB1	0.1	0.1	0.4	0.8	1.2
A2	SB1	1.0	0.2	0.4	0.8	1.2
A3	SB1	10.0	0.5	1.0	2.0	3.0
A4	SB1	90.9	1.1	3.0	6.0	9.0
A5	SB1	909.1	3.0	6.0	12.0	18.0
B1	SB2	0.1	0.1	0.4	0.8	1.2
B2	SB2	1.0	0.2	0.4	0.8	1.2
B3	SB2	10.0	0.5	1.0	2.0	3.0
B4	SB2	136.4	1.1	3.0	6.0	9.0
B5	SB2	954.5	2.1	6.0	12.0	18.0
C1	DB1	15.9	0.7	1.0	2.0	3.0
C2	DB1	15.9	0.8	2.0	4.0	6.0
C3	DB1	47.7	2.0	4.0	6.0	8.0
C4	DB1	525.0	3.6	8.0	16.0	20.0
D1	DB2	27.3	1.0	2.0	4.0	6.0
D2	DB2	190.9	3.0	4.0	8.0	12.0

Table 3.2: Measured maximum radiant heat fluxes for the configurations described in Table 3.1. Note that all given results are in units of W/cm^2.

Config.	Dist. 1	Dist. 2	Dist. 3	Config.	Dist. 1	Dist. 2	Dist. 3
A1	3.05	1.56	1.03	B1	3.63	1.21	0.74
A2	9.69	4.68	3.11	B2	7.92	5.96	3.15
A3	8.54	4.82	4.71	B3	10.77	6.89	5.21
A4	10.33	6.45	2.32	B4	15.89	10.82	4.09
A5	10.67	6.56	4.69	B5	15.67	7.37	6.09
C1	18.90	17.73	6.03	C2	20.58	10.94	3.81
C3	11.84	9.57	5.49	C4	21.78	11.02	4.63
D1	22.75	13.86	5.14	D2	15.70	10.82	4.78

Table 3.3: Results and standard deviations obtained in three cases of repetitive testing.

Propellant	Mass (kg)	Distance (m)	Average max. radiant heat flux (W/cm^2)	Rel. standard deviation (%)	Number of tests
SB1	45.4	6.0	2.33	9.3	4
DB1	15.9	2.0	20.58	15.9	4
DB1	15.9	4.0	10.94	11.4	3

3.4 Results analysis

3.4.1 Statistical analysis of the empirical variables

It is important to recognize if some of the variables are not important in the analysis or are collinear in the tested range. Care must be taken in interpreting a limited experimental set of data. The statistical analysis results must be viewed in light of known physical facts. Collinearity between independent variables is an important issue as it can render the model very dependent on small variations in the inputs [57]. In the present dataset, two such relations may be inferred:

- Dependence of the burning rate on the heat of explosion.
- Dependence of the stack diameter on the total propellant mass.

There is generally no clear relationship between the energy and burning rate of a formulation [52]. Higher energy formulations are, however, often used in applications requiring a larger burning rate. As a result, observing these two variables for standard propellants can tend to exhibit a relationship. Only one of these two variables is thus required for a model. Since the heat of explosion measurement is a simpler task than the strand burning method for burning rates, the former was selected. In addition, it would make physical sense to expect that the energy emitted by a fire depends on the energy contained in the burning substance.

The set of trials performed required scattering the propellant samples on the ground in a circular fashion with a stack height no higher than 25 cm. There was a definite possibility of observing a relation between the stack diameter and the sample's mass. Figure 3.8 shows the tested data points and reveals a weak exponential relationship. It is important to note that from a physical standpoint, the flame diameter shall grow until the stack diameter is reached. Since the total radiant flux received is composed of radiation from the entire plume

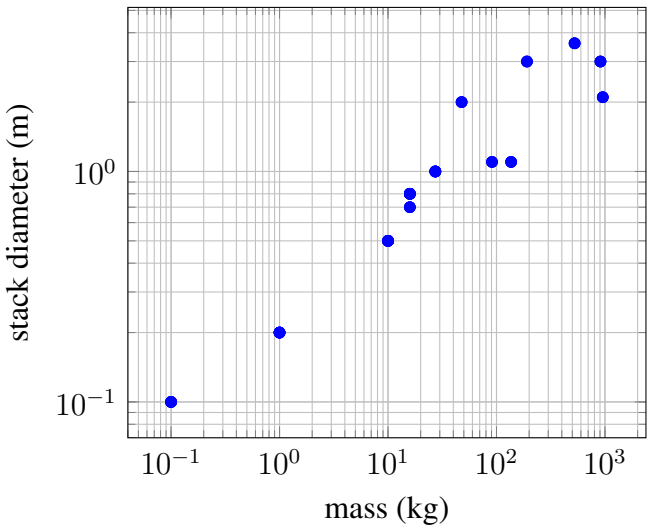

Figure 3.8: Relation between the measured propellant masses and stack diameters for the samples under study.

surface, the flux is expected to depend more on the diameter than on the mass. The extreme case would be the example of a propellant container ignited from the top. Although there might be a large mass of propellant inside the container, only a small portion of the total mass is burning at any given time. The maximum flux thus depends on the size of the fire plume, which is in turn related to the container diameter. The other extreme is that of a thin layer of propellant for which a steady state is not reached (diameter still increasing while the fuel is expanded at the center). These considerations would tend to favor selecting the stack diameter as a model variable.

3.4.2 Empirical model fitting

In the current case, statistical tools provide ways to obtain a model with an empirical dataset. A multivariate statistical analysis of the independent variables in the dataset can be performed to efficiently find the best regression relationship. This task is accomplished using the method of multiple linear regressions [42]. The goal is to remove any redundant information and minimize the number of independent variables. It is often found that only a

fraction of the components are necessary to account for the majority of the variance, which reduces the number of parameters to consider in any subsequent analysis [57].

The general model form obtained through theoretical considerations, given as Eq. (43), is helpful in going forward in optimizing the model. This form and the previous conclusions indicate that the new model should look as follows:

$$\dot{q}'' = k\, r_{fire}^{a_1}\, D_{ini}^{a_2}\, E^{a_3} \tag{44}$$

By taking the logarithm on both sides of Eq. (44) and simplifying, a linear relationship with the unknown constants is obtained.

$$\log \dot{q}'' = \log k + a_1 \log r_{fire} + a_2 \log D_{ini} + a_3 \log E \tag{45}$$

Solving for the unknowns in the last equation is possible using the method of multiple linear regressions and linear algebra [57]. Suppose that the vectors **Q** and **B** represent the maximum radiant heat fluxes and the unknowns parameters respectively. Matrix **X** has columns composed of the independent variables r_{fire}, D_{ini} and E. A solution for vector **B** can be found using [57]:

$$\mathbf{B = (X'\ X)\ X'\ Q} \tag{46}$$

The application of this method was performed using the R statistical code [58] through the R-Studio interface. Applying this methodology with the current set of large scale testing data yields:

(1) When considering the following variables: distance, fire diameter and heat of explosion:

$$\dot{q}'' = 10^{0.48} r_{fire}^{-1.03} D_{ini}^{1.25} E^{0.76} \tag{47}$$

The regression line fits the data with a correlation coefficient $r^2 = 0.76$.

(2) When considering the following variables: distance, mass and heat of explosion:

$$\dot{q}'' = 10^{-9.00} r_{fire}^{-1.11} m^{0.50} E^{2.07} \tag{48}$$

The regression line fits the data with a correlation coefficient $r^2 = 0.88$.

The previously derived equations have some interesting characteristics. The maximum radiant heat flux follows an inverse relationship (the exponent of r_{fire} can be viewed as $0.98 \approx 1$). This points toward the line source approximation [30], a reasonable result given the shape of the observed flames. In the first case, the radiance is also strongly dependent on the propellant stack diameter and less dependent on the heat of explosion. For the second case, the heat of explosion has the larger contribution. In these last cases, the exponents are not rounded numbers but show the dependences clearly. Again, the advantage of Eq. (47) lies in the fact that only the heat of explosion, E, must be measured or calculated (both methods of obtaining E are easy to implement and fairly precise [52]). As the mass based model is the most precise, the general model form thus becomes:

$$\dot{q}'' = \frac{k m^{1/2} E^2}{r_{fire}} \tag{49}$$

where $k = 2.75\ X\ 10^{-9}$ kg$^{1/2}$s/m^3 is a constant parameter. It must be noted that k was optimized using a least square regression in order to fit the exponents found in Eq. (49). It, however, does remain fairly close to the value shown in Eq. (48).

3.4.3 Empirical model validation

Any empirical model should first be compared to the experimental data used for its derivation. The analysis of residuals is often applied for this purpose. For each data point,

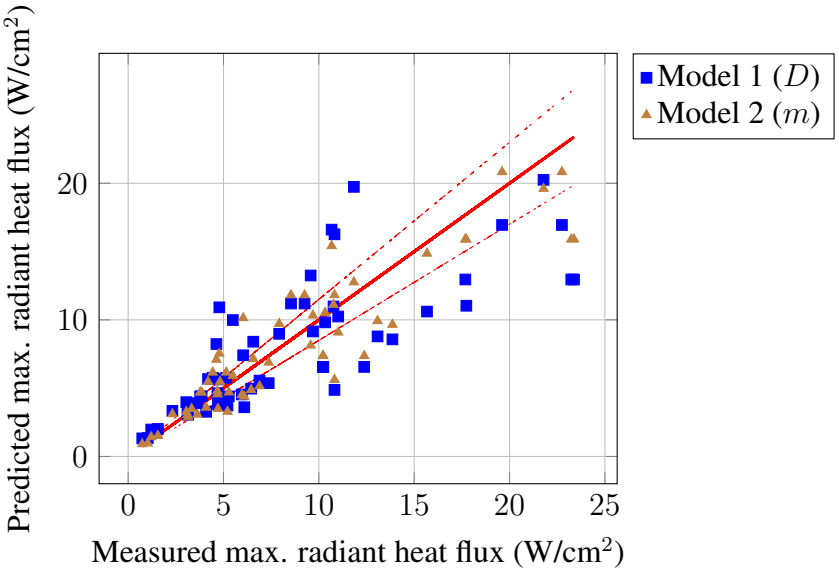

Figure 3.9: Comparison of the measured and predicted maximum radiant heat fluxes calculated using the two regression models. Note that the solid line has the desired unity slope and that the dashed lines represent the measurement error boundaries.

the residual is the difference between a measurement and model result under the same conditions [42]. This is equivalent to plotting the measured values against their respective predicted counterparts and expecting a linear relationship with unity slope. The residuals are usually standardized by subtracting the average residual and dividing by the standard deviation [42]. The result is then observed using bar graphs. When observing a residuals plot, a Gauss bell-curve shape tightly centered around 0 on the x-axis (number of standard deviations) is desired. The proposed equation produces a model which better fits the experimental data, as shown in the residuals plot of Figure 3.10. This distribution is centered around 0 and has a near Gaussian shape without any occurrence above 3 standard deviations.

The model developed in this study should improve on what is currently available to predict the maximum radiant heat flux of a propellant fire. In this respect, the best available model is that developed by the French S.N.P.E. in 1982 and previously given as Eq. (40) [46]. In this last model, one must calculate the combustion rate, $\frac{dm}{dt}$. For a given fire, the

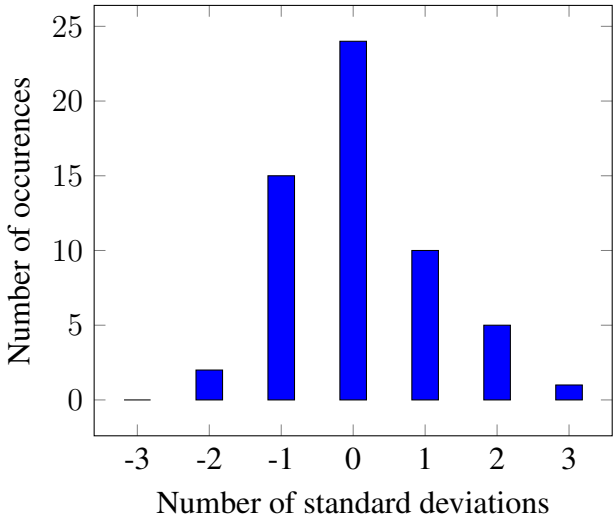

Figure 3.10: Residuals plot of the regression model given as Eq. (47).

average combustion rate can be approximated as:

$$\frac{dm}{dt} \approx \frac{m}{t_{tot}} \tag{50}$$

where t_{tot}, the total duration of the fire, is obtained from the following empirical relation [46]:

$$t_{tot} \approx 3.225 m^{0.126} \tag{51}$$

For bulk product, as is the case studied here, the c_τ factor found in Eq. (40) equals $\frac{1}{3}$ [46]. After substitution and simplification, the final equation used thus becomes:

$$\dot{q}'' = \frac{0.026}{\pi} E\, m^{0.874}\, r_{fire}^{-2} \tag{52}$$

A comparison of the predicted heat flux as a function of the measured value is shown on Figure 3.11 for both the S.N.P.E. and presently proposed models. From Figure 3.11, one can observe that the S.N.P.E. model generally underestimates the measured value and yields a larger spread around the true value. The relation proposed here produces a tighter

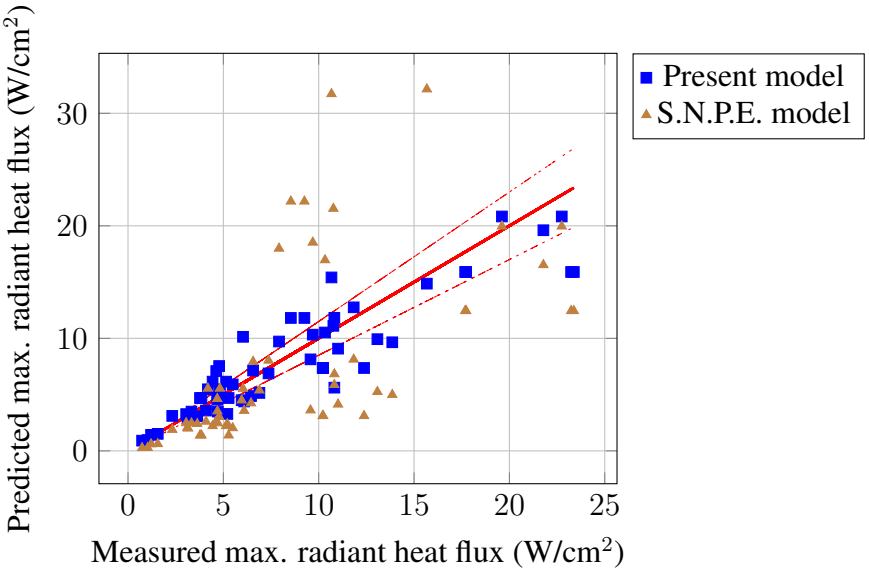

Figure 3.11: Comparison of the measured and predicted maximum radiant heat fluxes calculated using the presently proposed and S.N.P.E. models. Note that the solid line has the desired unity slope.

fit centered on the true values. The last observations can be confirmed by looking at a plot of the residuals for each of the cases, as shown on Figure 3.12. In addition, Figure 3.12 plots the residuals as a function of the distance from the fire. It can be seen that the S.N.P.E. model is less precise at smaller distances. This last observation can be explained from the use of an inverse square relationship in Eq. (40). Such a relationship implies a point source of radiant heat. The model proposed here uses an inverse relationship, which represents a line source. Given that propellant fires have a cylindrical shape, the use of a line source approximation would seem more appropriate. As the distance from the fire increases, the line source can be reduced to a point source without much loss in precision.

It is important to remember that the empirical radiant heat flux law was developed for maximum (thus steady state) conditions. The previous combustion rate equation must be viewed as a steady state value as well. A certain initial time will be required for the flames to reach their maximum dimensions. This initial time is what has been referred as the induction time.

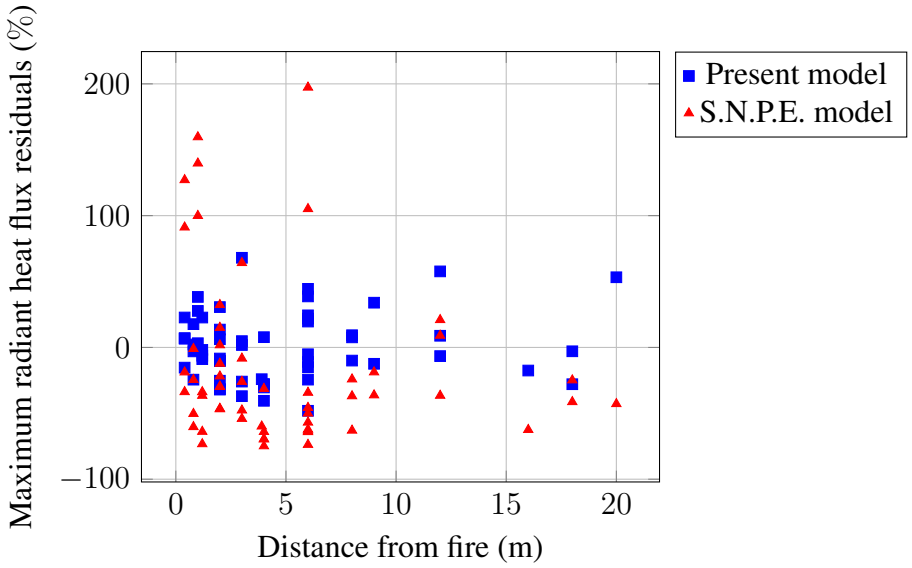

Figure 3.12: Relation between the predicted heat fluxes residuals and the distance from the fire for the compared models.

The resulting empirical law, Eq. (49) has a direct inverse relationship with distance. The result is thus similar to the model derived by Dayan and Tien [54] and shown as Eq. (39). A comparison of the fluxes calculated with the Dayan and Tien scheme and the measured values is shown in Figure 3.13. The quality of the fit is not as good as with the statistical model but the present case can be expected to hold more generally. The drawback of the Dayan and Tien model shown here is that it is sensitive to the error in estimating the combustion rate, $\dot{m}$.

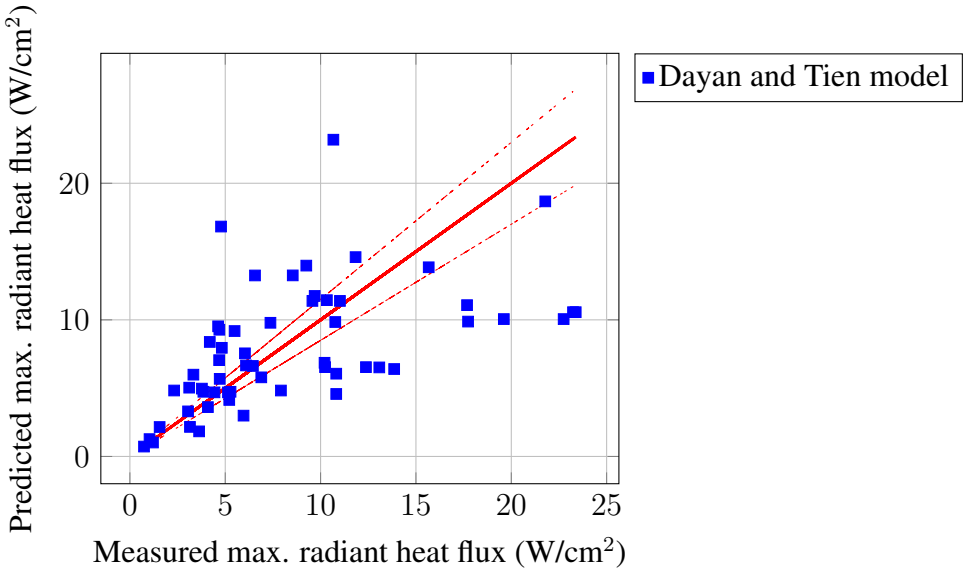

Figure 3.13: Comparison of the measured and predicted maximum radiant heat fluxes calculated using the Dayan and Tien model. Note that the solid line has the desired unity slope.

3.5 Summary

Using theoretical considerations and multivariate statistical methods, it was possible to design a general radiant heat flux level prediction model. The resulting expression is relatively simple to use and its derivation was instructive in understanding the important parameters to consider. Upon observing the proposed expression for the model, several important characteristics can be noted and compared to previous attempts. The new model yields a result in which the radiance decreases inversely with increasing distance. The S.N.P.E. model [46] favors an inverse square relationship. In all test cases, the flames were of a relatively cylindrical shape, where their maximum height was two to five times greater than their width. Such a cylindrical configuration is closer to the ideal line source than it is from a point source model. In the line source case, the radiant heat flux decreases inversely with distance, which is the case observed here.

The final result is able to predict the maximum radiant heat flux emitted during a propellant fire using only the propellant stack diameter and the heat of explosion standardly measured in a calorimeter or calculated using available thermochemical codes [52]. The burning velocity is not required here. If the stack diameter, D, becomes large enough or if the propellant bed thickness is too small, there could be cases where the fuel at the center consumes completely prior to the flame spreading over the entire surface. This last eventuality could potentially yield a maximum radiant heat flux which deviates from the proposed model. The model is thus valid for fires involving a stack diameter of up to 4 m (masses going from 1 kg to over a metric ton of propellant). Although the relationship could be expected to hold for fires involving larger samples, it was not possible to perform tests of these magnitudes. Typical stacks of propellants found in industrial settings, however, seldom have a diameter larger then 4 to 6 m. Larger quantities can be found in the form of arrays of containers, with each array being of the size discussed previously.

The comparisons are satisfactory as they show the proposed model to improve on previously published results. As a direct next step, it shall be important to look at the radiant heat flux rise times. This last information, coupled with the present conclusion, is essential to the design of effective evacuation and fire fighting procedures. In order to study the rise times, a better understanding of flame spread at the surface of various propellant configurations is necessary. This spread is mainly affected by heating through the heat flux of already burning material [15]. The proposed radiant heat emission model shall therefore be of use in that aspect as well.

Chapter 4

Pressure generation

"In fact, a sense of essence is, in essence, the essence of sense, in effect."

Douglas Hofstadter - Metamagical Themas (1985)

4.1 Introduction

In most facilities around the world, propellants are handled inside buildings. The main reason for this is to protect the products from the outside elements (rain, snow, dust, moisture, temperature variations, sunlight exposure, etc). As a result, propellant fires are most often enclosure fires. For the purpose of performing the various process manipulations inside these buildings, propellants are quite frequently further confined by equipments. As an example, most products are tumbled in a rotating barrel as a way to coat their surface with graphite powder [8]. In such cases, quantities as large as 1000 kg are enclosed in an equipment with moving parts. The operation described in this example is usually performed at a distance, since fires can often lead to disastrous detonations.

The previous discussion highlights a few important observations concerning propellant

fires pressure generation. The concept of confinement is seen as important in the pressure generation potential. By confinement, it is meant to enclose a quantity of product in a closed volume, with or without an opening. The sentence contains three main components of the problem:

- Closed volume
- Quantity (mass)
- Opening (area)

The first two components relate to the pressure generation potential of the configuration. The third component is a measure of the overpressure ventilation effectiveness. In addition to these components, a fourth important property can be inferred as the propellant combustion characteristics (burning rate, combustion gases properties). This fourth component will act both on the pressure generation and release potential of the configuration. In a mathematical fashion, the pressure generated by a propellant fire can be expected to take the following form:

$$P = f(V, m, A, \Omega) \tag{53}$$

where Ω is a thermodynamic state function representing the combustion properties of the fuel. Such a representation is compatible with what has been found with other types of fuels.

In the present chapter, the nature of the function shown as Eq. (53) is studied. As various gas dynamic modelling schemes are possible, the thermodynamic aspect of the problem is initially treated. From these basic considerations, a theoretical model is derived. The model is based on a fundamental differential equation and specific solutions applicable to the problem. A numerical solution scheme is also presented, as the methodology is useful in inferring some of the thermodynamic properties of the combustion gases. The results of small and medium scale experimental tests are then presented. Statistical methods are

used to analyze the results and link them to the theoretical model. Comparisons are also performed between the theoretical, numerical and empirical methods in order to validate the results.

4.2 Previous work

Propellants are designed to provide mechanical energy through the action of the pressure generated by the transformation of solid grains to a high temperature gas. For that same reason, an unwanted combustion will generate pressures that can have disastrous consequences for the environment surrounding the fire. Propellants at very low densities (small mass in a large volume) can easily generate pressures that far exceed what standard walls can resist. When there is some confinement of the propellant, pressures in excess of 70 kPa can easily be generated at 12 m from the event [59].

There are very few publications of pressure measurements made with propellant fires in open areas. Test results related to storage areas and naval vessel compartments have been published, but often do not include a theoretical analysis, or cover only certain limited cases [60] [61]. A paper by Polcyn and Mullin examined the pressure generation during airbag propellant fires in a 5.3 m^3 vented enclosure [62]. An electric detonator located at the bottom of the samples was used to ignite the propellants. Such a configuration can be problematic, as it would generate a large amount of projections and thus yield potentially erratic results. An attempt at modelling explosion pressure venting was made by Graham in cases involving the slow burning of high explosives (such as RDX and Composition B) [63]. The model involved building a pressure-time derivative equation by taking the difference between a pressure rise and pressure decay term. Each term was determined from basic thermodynamics and gas flow dynamics principles. The resulting equation was as follows:

$$\frac{dP}{dt} = \left[RT_B \frac{\rho}{M} \frac{\alpha}{(A - BT_o)} S_B - A_V C_D a^* \right] \frac{P}{V} \tag{54}$$

From this last result, a critical vent area ratio was defined as the solution yielding a pressure-time derivative of zero. At this point, the pressure generation and decay are equal, and the critical ratio is found to be:

$$\frac{A_v}{S_B} = \frac{RT_B \rho \alpha}{MC_D A^* (A - BT_o)} \tag{55}$$

where the vent area, A_v (area of the opening), is divided by the burning surface area, S_B. Comparisons with a limited number of tests performed shows the merit of the analysis. Even if the substances used and combustion modes are different when comparing explosives and propellants, it is the general modelling methodology used that is interesting, as it would be applicable to a large amount of cases.

Modelling these types of events was also attempted by Porterie et al. through the use of a fully numerical methodology where the Navier-Stokes equations are solved [64]. The model applies thermodynamical and chemical considerations of the combustion to calculate the gas temperature, pressure, velocity and composition in a room. Although it would eventually constitute the most complete approach, it remains complex to use in an industrial setting, given the limited knowledge often available about the propellant combustion characteristics.

Some studies have been made by the industry about the critical height of propellants for detonation in which generated pressures were recorded [59] [65] [66]. These results have not often been published. The pressure data was used to determine if a shock wave was created by the combustion (as a criterion to discern between deflagration and detonation) [59]. A study by Merrifield and Myatt explored the effect of a black powder type propellant fire with quantities and containers comparable to those that could be manipulated by a

hunter in his house [67]. Although the core of the study focused on the flight of container fragments, the results show various levels of overpressures generated at a given distance from the combustion of a sample [67]. In these previous cases, no attempt is made to derive a prediction model for the observed pressures. Many of these studies also focus on cases where the burning sample is initially confined and thus generates pressure waves upon the sudden rupture of the container. The analysis is therefore more akin to that of detonating substances, such as explosives, than it is to that of fire science. A good example is that of the study related to the venting of explosion initiated by fragment impact on cased ammunition [63]. Comparisons with explosive effects have been made in the measurement methods used and application of the TNT (trinitrotoluene) equivalence concept [62] [68].

Although propellant fire venting has not been studied rigorously, the explosion venting problem has seen much research performed in the context of various other applications. Combustible gas, vapor and dust mixtures can ignite and generate violent explosions. Oil refineries [69] and coal mines [26] are examples that show that such events can indeed occur in industrial settings and have terrible consequences. As a result of these unfortunate events and through the application of research results, explosion venting guidelines have been published. One of the most known set of guidelines is NFPA 68 by the National Fire Protection Association (NFPA) [70]. Although the NFPA 68 goes at length in covering various vent panel masses and building geometries, a very fundamental result is given for the vent sizing of gas explosions:

$$A_v = C A_s P_{red}^{-1/2} \tag{56}$$

The maximum vented pressure, P_{red} (often denoted as the reduced explosion pressure in the literature), is thus inversely proportional to the square of the vent area, A_v. Note that C is a constant which depends on the fuel used. In the case of dust explosions, a similar relationship is proposed [70] [71]:

$$A_v = 10^{-4} K_{st} V^{0.75} \left(\frac{P_{max}}{P_{red}} \right)^{1/2} \tag{57}$$

where K_{st} is known as the deflagration index (rate of pressure rise of a dust as measured in a standard test) and P_{max} is the maximum unvented explosion pressure. An interesting analysis of dust explosion pressures has been presented by Ural where the two limiting cases of low and high pressure asymptotes are discussed [71]. When comparing unvented and vented maximum pressure, an asymptotic behavior is observed when varying the vent area. At one extreme, the vented pressure tends to get closer to the unvented case when the area decreases. On the other end, the pressure goes toward zero (or atmospheric value) as the area is increased. Using this concept, the maximum vented pressure can be calculated as follows for the low pressure asymptote [71]:

$$P_{red}^{LP} = 0.5 \rho V [(\gamma - 1) S_u]^2 \left[\frac{A_f}{C_D A_V} \right]^2 \tag{58}$$

Here again, the maximum pressure is inversely proportional to the square of the vent area. In addition, the maximum pressure is proportional to the square of the flame velocity and surface area. Other published models also point toward the same type of relationships between pressure, burning velocity and flame area [72] [73].

Even if the mechanisms at play differ in each application, there are some similarities in the mathematical formulation of such problems. Gas and dust explosions both involve a volume filled with a mixture of fuel and oxydant in which a combustion front is travelling. High explosives and confined propellants generate a spatially localized pressure wave which will also travel in the enclosure. Unconfined propellant fires can be compared to having a high pressure tank emptying in the room after opening a valve. In this last analogy, the period between ignition and maximum fire dimension (flame propagation) is equivalent to the valve opening. Albeit their intrinsic differences, all these cases ultimately

involve a mixture of pressurized gases flowing through a constriction to an infinite medium at atmospheric pressure. It should thus be expected that the maximum pressure solution follows a form similar to the previously described equations.

4.3 Theoretical considerations

4.3.1 General considerations

By design, propellant is manufactured to eventually be used by applications requiring large impulses. The mechanical energy required for these impulses comes from the rapid transformation of solid propellant to gaseous products during combustion. For example, it is known that an ideal gas will be at standard temperature and pressure (STP, or ambient conditions) when each mole of gas occupies 22.4 L. The average molecular weight of propellant combustion gases is in the 20 to 30 g/mol range and quantities in the kilogram range are most often handled. It is thus observed that small amounts of propellants can generate important pressures in a closed space. Published data of closed vessel combustion tests have shown that it is possible to generate pressures in excess of 500 bar (or 50 MPa) with a 10 g sample in a 200 mL volume.

An important concept used in determining the thermodynamic behaviour of the propellant gases is that of the equation of state. Such an equation is used to relate the thermodynamic variables such as pressure, P, volume, V, and temperature, T, for a given substance. The often cited ideal gas law, $PV = NRT$, is an example and perhaps the simplest equation of state. In the ideal gas law, the three cited thermodynamic variables are related through the gas quantity, N, and the ideal gas constant, $R = 8.314$ kJ/kg K. In the case of propellant combustion, the Nobel-Abel equation is usually applied in calculations.

This last relationship is expressed as:

$$P(V - b) = NRT \tag{59}$$

where b is known as the covolume of the combustion gases. The covolume accounts for the departure from an ideal gas behaviour due to the non-negligible interaction between molecules, an effect here modelled as a loss in volume. Typical propellants have covolume values around 1 mL/g. For a 200 ml closed vessel containing 10g of propellant, this represents a volume loss of 10 mL, or 5$\%$ of the total available volume. In the case of a 1000 kg sample in a 1000 m^3 room, the volume loss is 1000 L, or 0.001$\%$ of the total volume. It can thus be observed that the effect of the covolume is negligible for cases involving small mass to volume ratios (denoted as the charge density, c). With a covolume of 1 cc/g, the volume loss over total volume ratio is indeed equal to the charge density. Assuming that a volume loss of less than 1% is negligible implies that cases where the charge density is less then 0.01 g/mL can be treated using the ideal gas law. Alternatively, for propellants with a covolume differing from 1 mL/g, a dimensionless quantity defined as the ratio of the charge density over the covolume can be computed:

$$X = cb \tag{60}$$

The use of the Nobel-Abel equation of state is thus warranted when $X \gg 0.01$. The ideal gas law can be used for all other cases.

To correctly model the dynamic pressure behaviour in a given situation, it is necessary to determine if spatial variations are expected within a domain. In most cases, a domain shall be defined as the volume of an enclosure. As gases are generated at the location of the fire, the surrounding air shall be compressed and subsequently mixed with the combustion products. The compression wave will travel through the enclosure volume at the sound

velocity corresponding to the air conditions. Depending on the gas generation rate, the magnitude of the compression wave will vary. In addition, a higher magnitude wave will reflect on the enclosure boundaries and generate dynamic effects. At the limit, for a slow enough event and large enough enclosure, the time required for the small compression wave to travel through the enclosure shall be negligible compared to the event time scale. In such a case, it will be advantageous to consider the entire enclosure volume as a lump with conditions that do not depend on spatial dimensions. This last situation is known as a lumped parameter problem and mathematical conditions must be determined to define the applicability of this case.

Considering a symmetrical enclosure with characteristic distance d (for example, in a cubical enclosure, d would be equal to half the size of any side) filled with mass m_a of air at STP conditions. A gas source located at the base center of the enclosure generates combustion products at a rate $\dot{m}$ in kg/s. The goal is to compare both the compression wave travel time to the enclosure dimension, and the generated gas quantity to the "potential" of the enclosure. By arranging the relevant variables together, a dimensionless expression containing ratios describing the previously discussed relationships can be formed. The following dimensionless quantity is thus defined as follows:

$$\chi = \frac{m_{air} c_{air}}{\dot{m}_{gen} d} \tag{61}$$

Computation of χ with several typical cases is shown on Table 4.1. It can be concluded that the lumped parameter methodology can be safely used when $\chi \gg 1$, as closed vessel modelling has been shown to be fairly precise [4]. This represents most of the cases covered in the present work. The present dimensionless quantity is similar to the often used Biot Number in heat and mass transfer problems (the Biot number gives a measure of the capacity of a body conduct heat / mass within itself when heat / mass is being convected at its surface).

Table 4.1: Estimated χ values for a variety of cases.

Case	χ (dimensionless)
0.7 L closed vessel with a fast burning propellant	0.9
0.7 L closed vessel with a slow burning propellant	5.6
60 L tank with a fast burning propellant	420
1800 L enclosure with a fast burning propellant	561
10^6 L enclosure with a fast burning propellant	675

The evolution of pressure inside an unvented enclosure due to a propellant fire can thus be computed using the ideal gas law in a lumped parameter setting with a gas generation model which fits the event in question. If venting is added into the picture, a mass loss term must be added into the equations to account for the vented gas. The determination of the mass loss can be performed either with or without the assumption of incompressible flow. The choice of assuming compressibility is made using the known criterion for these cases. The criterion is based on knowledge of the Mach number (ratio of the gas velocity over the sound velocity in the medium) for the flow in question. The Mach number can be calculated using the known pressure ratio between the interior and exterior of the enclosure [74]. In the presently discussed isochoric conditions, flows with a velocity below Mach 0.30 can be simplified as incompressible and the Bernoulli equation applied:

$$v = \left(\frac{2P}{\rho_{gas}} \right)^{1/2} \tag{62}$$

For Mach numbers above 0.30, compressibility must be taken into account through the use of isentropic relationships [74].

4.3.2 Pressure evolution model

In order to devise a pressure evolution model, mass conservation is used. Performing a mass balance on the enclosure volume yields:

$$\dot{m}_e = \dot{m}_{gen} - \dot{m}_{vent} \tag{63}$$

As discussed previously, the vented mass flow rate can be obtained by applying the Bernoulli equation to compute the gas flow velocity. The vented mass flow rate is thus:

$$\dot{m}_{vent} = C_D \rho_{gas} v A = C_D A (2\rho_{gas} P)^{1/2} \tag{64}$$

where C_D is the discharge coefficient. Using the ideal gas law, the pressure factor can be replaced by a mass dependent factor:

$$\dot{m}_{vent} = C_D A \left(\frac{2\rho_{gas} m_e RT}{M_w V} \right)^{1/2} \tag{65}$$

Substituting in the mass balance relation and rearranging the equation yields the following result:

$$\dot{m}_e + C_D A \left(\frac{2\rho_{gas} RT}{M_w V} \right)^{1/2} m_e^{1/2} - \dot{m}_{gen} = 0 \tag{66}$$

Assuming that the combustion rate, temperature and density are constant, this is a nonlinear first order ordinary differential equation. This assumption is only necessary in finding analytical solutions to the problem. In the case of numerical solutions, these parameters can be updated as the calculation evolves. Given the finite amount of propellant burning, the $\dot{m}_{gen}$ term will be nonzero when $0 \leq t \leq t_{burn}$. Two cases are thus possible:

$$\dot{m}_e + C_D A \left(\frac{2\rho_{gas} RT}{M_w V} \right)^{1/2} m_e^{1/2} - \dot{m}_{gen} = 0 \qquad when 0 \leq t \leq t_{burn} \tag{67}$$

$$\dot{m}_e + C_D A \left(\frac{2\rho_{gas} RT}{M_w V} \right)^{1/2} m_e^{1/2} = 0 \qquad when\ t > t_{burn} \tag{68}$$

The solution for the first case is difficult, as it requires using the Lambert special function. It is, however, possible to use the differential equation to determine the maximum pressure and the largest rate of pressure change. This analysis will be performed in the next sections.

For the second case, the problem reduces to solving a separable linear first order differential equation. Solving for $\dot{m}_e$ and integrating on both sides yield:

$$m_e = \left(k_2 - 1/2 k_1 (t - t_{burn}) \right)^2 \qquad when\ t > t_{burn} \tag{69}$$

where $k_1^2 = 2\rho_{gas} C_D^2 A^2 \left(\frac{RT}{M_w V} \right)$ and k_2 is determined by applying an initial value condition. For the present case, the initial value condition is that $m_e = m_{max}$ when $t = t_{burn}$, yielding $k_2 = m_{max}^{1/2}$.

By taking a closer look at the expression for k_1^2, one can observe that the term in parentheses can be simplified using the ideal gas law and a known pressure and mass point. Taking the point at which the pressure is at its maximum, one obtains:

$$k_1^2 = 2\rho_{gas} C_D^2 A^2 \frac{P_{max}^2}{m_{max}^2} \tag{70}$$

where m_{max} is the maximum mass of the gases in the enclosure. There is thus a dependency of k_1 on the maximum pressure. There is also an expected dependence on the venting area and sample mass. This last dependence could, however, be more difficult to observe, as the sample masses are modulated with the opening area to keep the maximum pressures in a safe range. The advantage of Eq. (70) is that it is in a form which makes for an easier comparison with empirically calculated values. It also only uses two factors which must be estimated: ρ, the combustion gases density, and C_D, the discharge coefficient.

It must be noted that this solution is valid until $m_e(t)$ reaches a minimum at $m_e(t) = 0$. Setting the first derivative equal to zero yields $t = \frac{2k_2}{k_1}$. The pressure decay solution is thus

valid in the interval $t_{burn} \leq t \leq t_{burn} + \frac{2k_2}{k_1}$. When $t \geq t_{burn} + \frac{2k_2}{k_1}$, the pressure is zero (which is the atmospheric value here). The evaluation of the maximum mass (and pressure) is carried out next.

4.3.2.1 Maximum pressure

From the previous differential equation, the maximum pressure can be determined by setting $\dot{m}_e = 0$ and solving for m_e. After some algebra, this yields the following:

$$m_e = \frac{\dot{m}_{gen}^2 M_w V}{2C_D^2 \rho_{gas} RT A^2} \tag{71}$$

Using the ideal gas law, the maximum pressure is calculated as:

$$P_{max} = \frac{\dot{m}_{gen}^2}{2C_D^2 \rho_{gas} A^2} \tag{72}$$

This constitutes the most general form of the solution for the maximum pressure inside a vented enclosure with the assumptions made. Any further simplification would involve finding an appropriate model for the factor $\dot{m}_{gen}$. One must, however, be careful in choosing an approximation for $\dot{m}_{gen}$, as the model choice will be highly dependent on the case configuration. The following general result is thus obtained:

$$P_{max} = f\left(\frac{\dot{m}_{gen}^2}{A^2}\right) \tag{73}$$

A result that is similar to the general form of models found in the literature and discussed previously:

$$P_m = f\left(\frac{r^2 S^2}{A^2}\right) \tag{74}$$

Here, the difference is seen to be strictly in the numerator of the two expressions. These expressions become nearly identical if, for example, it is assumed that the gas generation

rate is simplified as $\dot{m}_{gen} \approx Sr\rho_{bulk}$, where ρ_{bulk} is the bulk density of the propellant. Such a mass combustion model would be akin to the case of a propellant in a container with surface area S, burning from the top down. One can observe here that this last statement contains several assumptions: top ignition, constant surface area, laminar vertical propagation through the propellant bed. The problem is that propellant combustion is seldom that ideal. The most general solution therefore remains the best start point for further analysis.

4.3.2.2 Maximum rate of pressure rise

Starting with Eq. (67), the maximum value of the mass rate of change derivative can be obtained by differentiating the equation and setting the second mass derivative equal to zero as follows:

$$\ddot{m}_e = \frac{1}{2} C_D A \left(\frac{2\rho_{gas} RT}{M_w V} \right)^{1/2} m_e^{-1/2} \dot{m}_e = 0 \tag{75}$$

It can be seen that the maximum occurs when $m(t) = 0$, which is at $t = 0$ in this case. The maximum rate of change of the mass is thus:

$$\dot{m}_{max} = \dot{m}_{gen} \tag{76}$$

Transforming the last result to the pressure equivalent yields:

$$\dot{P}_{max} = \frac{\dot{m}_{gen} R \Delta T}{M_w V} \tag{77}$$

Here again, a proper flame propagation model is important in obtaining a precise value for $\dot{P}_{max}$. The considerations of Chapter 2 are seen to be imperative in making this determination. The other variables can be calculated using standard thermodynamic methods.

4.4 Experimental work

4.4.1 Test setup

In order to study the effect that varying the propellant configuration has on the pressure during a fire, tests were performed in vented enclosures. Enclosure volumes varying from 60 L to 1800 L were used in this study to check the geometrical scale effect. Two sizes of combustion chambers were used:

- Cylindrical 60-L steel reservoir previously used for airbag deployment simulations (cylinder with a radius of 40 cm and a length of 50 cm). A fixed circular opening with a diameter of 1.1 cm (thus an area of 0.0001 m^2) was part of this setup.
- Cubical 1800-L steel plated wooden box (cube with a side length of 122 cm). Openings of various sizes up to 0.40 m^2 could be used on one face of the enclosure.

All pressure measurements were made using Omega pressure transducers (PX309 series). These transducers were located at the centre of every lateral face of the rectangular chambers and on top of the cylindrical enclosure. Measured maximum pressures varying between 15 and 200 kPa, depending on the specific model, could be obtained with these sensors. The measurement range was selected based on the results of preliminary tests in a closed vessel in order to maximize the precision. A 12V DC source was used to power the transducer and the output signals were recorded on a Measurement Computing PMD-1608F data acquisition card, at a rate of 1 kHz. The acquisition was controlled by a laptop through the MCCDAQ software which generated ASCII files containing the pressure measurements.

Various propellant types were used and their summary description can be found in Tables 4.2 and 4.3. It must be noted that single base propellants use nitrocellulose as the only energetic component while double bases use a combination of nitrocellulose and

Table 4.2: Description of the propellants used in the 60-L and 1800-L tests. Note that the abbreviation NC and NG stand for nitrocellulose and nitroglycerin, respectively.

Propellant	Geometry	Heat of explosion (J/kg)	Composition
SB1	3871	NC: 98% / Inert: 2%	
SB2	3135	NC: 90% / Inert: 10%	
DB1	5392	NC: 60% / NG: 39% / Inert: 1%	
DB2	4490	NC: 73% / NG: 25% / Inert: 2%	

Table 4.3: Tested propellants physical description.

Propellant	Geometry	Grain diameter (mm)	Abs. density (kg/m^3)	Bulk density (kg/m^3)
SB1	Unitubular	0.89	1550	950
SB2	Unitubular	1.17	1590	810
DB1	Disc	0.12 (thickness)	1600	550
DB2	Unitubular	1.16	1590	970

nitroglycerin. The heats of explosion shown in Table 4.2 were measured with a bomb calorimeter.

For all cases, the granular propellant sample was placed in a small container at the centre of the enclosure base. Ignition of the propellant was done using a nichrome hot wire connected to a 25V DC battery. Since contact with the hot wire was enough to ignite the tested propellants, the wire was always laid on the top centre of the sample. For safety reasons, the ignition circuit contained an interlocking mechanism enabling the person in charge to disable its operation during manipulations. The general procedure used during all tests was as follows:

(1) Installation of the setup.

(2) Closing all necessary roads and sending a radio announcement about the testing.

(3) Disabling the ignition circuit.

(4) Installing the propellant sample.

(5) Closing the enclosure with the proper vent opening.

(6) Starting the data acquisition.

(7) Moving to a safe distance.

(8) Enabling the ignition circuit.

(9) Igniting the material and waiting for the end of the event (typically 20-30 s).

(10) Stopping the data acquisition and saving the created datafile.

(11) Opening the enclosure (in the case of a mis-fire, a waiting time of 5 min was observed prior investigating the source of the problem).

(12) Extinguishing any remaining cinders in the setup using a small amount of water.

(13) Repeating steps 3 - 12 for the number of tests required.

(14) Reopening the roads and sending a radio announcement about the end of testing.

(15) Cleaning and storing all equipments.

For any experimental measurement, it is important to have an idea of the uncertainty of the readings. This can be done by performing repetitive trials and looking at the standard deviation of the results [56]. For the types of tests involved in the present work, it would have been difficult to perform repetitive trials on every configuration tested due to economical and time constraints. Repetitions were, however, performed on a single typical case to get an estimate of this uncertainty. The test case was a configuration using 1000 g of small web double base (DB1) in the 1800-L enclosure with an opening of 0.093 m^2. Table 4.4 contains a summary of the results for the six repetitions performed. The pressure - time curves are shown in Figure 4.1. The data shows that a fairly important variation is obtained between seemingly identical tests. For example, the maximum pressure varies from 2.16

to 4.66 kPa, yielding a 33% relative standard deviation. One must thus expect a certain amount of variation in the data when looking for trends.

Table 4.4: Results of six repetitions involving 1000 g of small web double base in the 1800-L enclosure with a venting area of 0.093 m^2.

Repetition	Max. pressure (kPa)	Ind. time (s)	Max. time (s)
1	4.66	0.15	0.37
2	3.74	0.29	0.48
3	5.65	0.35	0.50
4	2.81	0.32	0.57
5	2.91	0.14	0.52
6	2.16	0.26	0.57
Average	3.77	0.25	0.52
Abs. standard deviation	1.23	0.09	0.09
Rel. standard deviation	33%	35%	17%

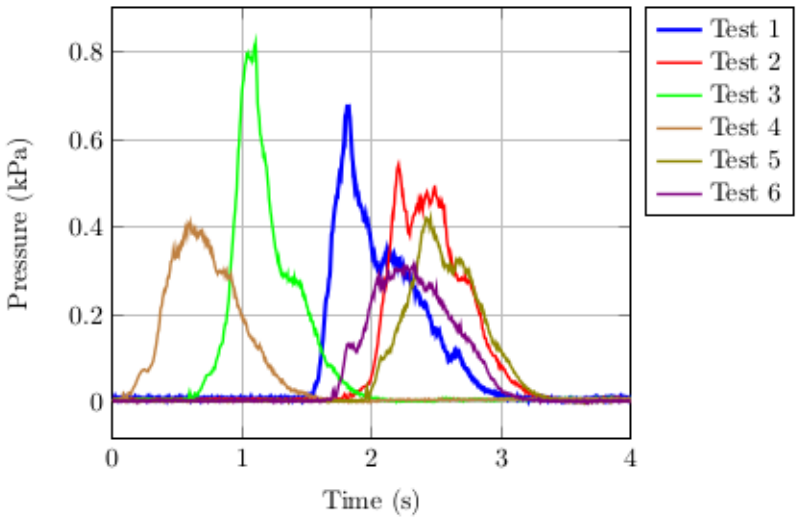

Figure 4.1: Pressure curves corresponding to the result shown in Table 4.4.

4.4.2 Flame propagation in enclosure tests

Using the pressure data obtained in vented enclosure tests, it is possible to extract the type of flame propagation behaviour that occurs during the fires. There are two main possibilities:

- Laminar burning of the propellant bed in the horizontal and vertical direction.
- Simultaneous combustion of all the propellant grains.

The first case was well documented in a previous section and requires using orthogonal flame propagation rate components (horizontal and vertical). For example, cylindrical containers of equal diameters and height h_1 and $h_2 = 2h_1$ would contain masses of m_1 and $2m_1$, respectively, but yield the same mass generation rate as that rate would only depend on the surface area. In this instance, a top ignition is required. As discussed previously, the steady state portion of the combustion will either be in the horizontal or vertical direction. The time required to reach steady state is defined as the induction time.

There are a few configurations available within the dataset which behave in a manner similar to the previous example. Configurations A2, A4 and C4 (in the 1800-L enclosure) were tests done in a smaller diameter container. It is observed that the maximum pressures obtained in these instances were all lower than those obtained with the same configuration in the larger container. For these three occurrences, the mass generation rate and induction time would differ. Given the larger height of the samples compared to their width, the main propagation mode is the vertical velocity, r_y.

The second case is more complex as there will still be a non-negligible time required for the flame to propagate in the entire charge. Again, this initial time will be defined as the induction time. Following the induction time, the combustion will be driven by the propellant linear burning rate and the grain geometry. In this eventuality, a larger sample mass will imply a larger gaseous mass generation rate and the sample diameter will not be

an important factor. This case could be observed with top, bottom or internal ignition. It must be noted that since the entire charge will be burning, it is quite likely that propellant grains shall be projected due to their presence in the convective flow.

A set of common pressure - time traces are shown in Figure 4.2 for fires involving three masses of double base propellant (DB1) in the 1800-L enclosure. From these pressure curves, the events can be decomposed into the following stages:

(1) Flames spread until a steady state is reached. This is defined here as an induction time and is apparent by the non-linear section found between 0.0 and 0.3 seconds in Figure 4.2.

(2) Steady state gas generation and venting (gas generation more important). Once either the edge or bottom center of the stack has been reached by the flames (depending on the stack dimensions), the gas generation rate stays constant. This is thus equivalent to the linear section comprised between 0.3 and 0.5 seconds in Figure 4.2.

(3) Steady state gas generation and venting (gas generation and venting in the same order). In that region the pressure is such that the vented gases rate becomes similar to the generated gases rate. It is not a true steady state since the combined effect of the source and vent yields an oscillatory behavior. In Figure 4.2, this section occurs between times of 0.5 and 0.8 seconds.

(4) At the end of the combustion, the gases vent outside, returning the pressure to the atmospheric value. When all the propellant has been consumed, the gas generation rate decreases to zero and enables the venting to reduce the pressure. This pressure drop can be found after 0.8 seconds in Figure 4.2.

Although the aforementioned sequence applies to all cases, it is important to note that depending on the configuration, some stages might not apply. For example, a stack with

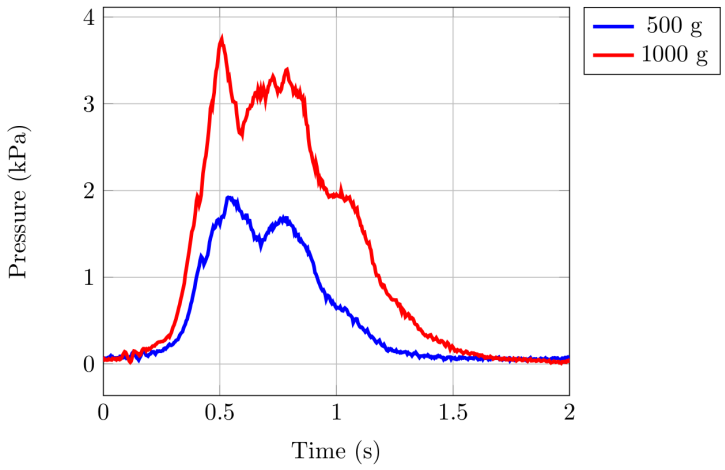

Figure 4.2: Pressure rise in a vented 1800-L enclosure.

dimensions and flame propagation velocities such that the edges and bottom are reached by the flames simultaneously would not exhibit as much of a steady state period (stages 2 and 3). Another example is that of a sample arranged such that the steady state gas generation is large enough to overcome the venting effect. This last case would not exhibit stage 3 and an example is shown in Figure 4.3. The abrupt pressure drop exhibited in Figure 4.3 can also occur when a vent panel is used, or if the enclosure suffers any kind of mechanical failure.

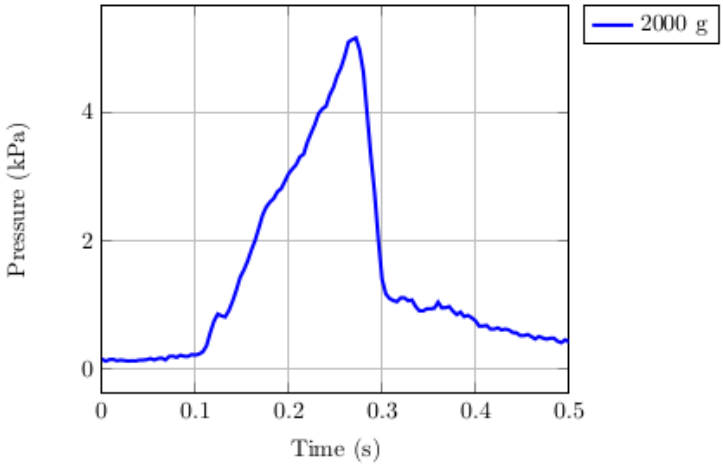

Figure 4.3: Pressure rise in a vented 1800-L enclosure without the 'stage 3' steady state.

An interesting part of the interpretation given above is that one can define a quantity equal to the time required to complete stage 1. This quantity was previously called the induction time and informs about the time required for the flames to propagate such that a steady state is reached. For example, propellant kept in an open container would ignite and the flames would quickly spread on the surface. Once the entire surface is burning, the gas generation is governed by the vertical propagation rate and a linear behavior is observed. Propellants with similar horizontal and vertical propagation rates or stacks of negligible height would not feature an important linear pressure rise section.

In the current case, the measured induction times are nevertheless shown in Tables 4.5 and 4.7 for the 60-L and 1800-L configurations. From Table 4.7, one can observe that configurations A2 and A4 have a noticeably smaller and similar induction time. This is expected as these two configurations have a smaller diameter (smaller container). The following general conclusions can thus be drawn from the available data:

- The induction time depends on the propellant bed diameter.
- The induction time depends on the propellant type (or burning rate).
- If the previous two properties are held constant, the induction time remains constant.

The previous conclusions can be observed graphically by plotting the induction time measured for each test, as shown in Figure 4.4. The tests performed in the 60-L tank show an evolution of the induction time with each type of propellant tested. The 1800-L induction times are all fairly similar (with the exception of the two smaller diameter cases discussed previously).

4.4.3 Maximum pressures

The 60-L configurations and maximum pressures obtained are given in Table 4.5. A description of all tested 1800-L configurations along with the maximum pressures obtained

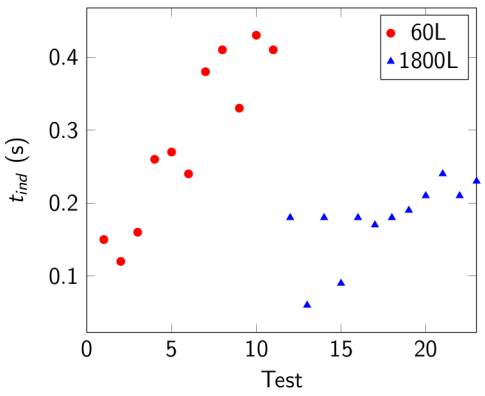

Figure 4.4: Distribution of measured t_{ind} for all tests.

are shown in Tables 4.6 and 4.7 respectively. For reference, Appendix A contains all 1800-L pressure-time traces obtained. The next step is to fit the data with a proper model.

Table 4.5: Configurations and results summary of the 60-L enclosure tested configurations. This enclosure has a single venting opening area of 0.0007 m^2.

Config.	Propellant	Mass (g)	Max. pressure (kPa)	Ind. time (s)	Max. time (s)
A1	DB1	2.5	9.6	0.15	0.39
A2	DB1	5.0	17.1	0.12	0.41
A3	DB1	10.0	58.7	0.16	0.35
B1	DB2	2.5	8.2	0.26	0.58
B2	DB2	5.0	21.9	0.27	0.59
B3	DB2	10.0	66.7	0.24	0.55
C1	SB1	10.0	9.6	0.38	0.64
C2	SB1	20.0	27.1	0.41	0.77
C3	SB1	30.0	47.0	0.33	0.99
D1	SB2	10.0	2.7	NA	NA
D2	SB2	20.0	23.8	0.43	0.85
D3	SB2	30.0	46.6	0.41	0.85

It is instructive to notice that there is a relationship between the propellant masses and maximum pressures obtained. This relationship is shown in Figures 4.5 and 4.6 for the 60-L and 1800-L cases, respectively. In the 1800-L case, the plot shows several opening areas while the 60-L plot shows four propellant types (since the 60-L vent opening size could not be modified). In both cases, a linear trend can be observed between the maximum pressures

Table 4.6: Description of the 1800-L enclosure tested configurations. Note that the stack heights are estimated values from measured diameters and bulk densities.

Config.	Mass (g)	Opening area (m^2)	Stack diameter (m)	Stack height (mm)
A1	50	0.016	0.30	2
A2	50	0.016	0.15	4
A3	100	0.016	0.30	4
A4	100	0.016	0.15	8
A5	150	0.016	0.30	6
B1	150	0.041	0.30	6
B2	177	0.041	0.30	7
B3	250	0.041	0.30	10
C1	250	0.093	0.30	10
C2	500	0.093	0.30	20
C3	1000	0.093	0.30	40
C4	1000	0.093	0.15	80

and masses. Linear regression equations have been computed for the data and are shown as the solid lines in Figures 4.5 and 4.6. The regression equations are also given in Table 4.8. These equations are all of the form:

$$P_{max} = k_i m \tag{78}$$

where k_i is the slope of the maximum pressure with respect to the mass of a given propellant i. Furthermore, a relationship between the slopes, k_i, and the vent area can be observed, as shown in Figure 4.7. From the analysis performed, the maximum pressure is estimated as

$$P_{max} = \frac{470m}{A} \tag{79}$$

for the DB1 cases. This empirical law is not satisfactory as its validity beyond the test conditions cannot be ensured. Such a simple relationship can, however, provide a way to compare with the following more complex analysis.

The general model form obtained through theoretical considerations, given as (72), is

Table 4.7: Results summary of the 1800-L enclosure tested configurations.

Config.	Max. pressure (kPa)	Ind. time (s)	Max. time (s)
A1	3.34	0.18	0.54
A2	2.78	0.06	0.40
A3	7.03	0.18	0.48
A4	3.07	0.09	0.40
A5	6.28	0.18	0.42
B1	2.34	0.17	0.53
B2	2.66	0.18	0.42
B3	4.13	0.19	0.43
C1	1.13	0.21	0.31
C2	3.14	0.24	0.50
C3	4.47	0.21	0.65
C4	3.38	0.23	0.49

Table 4.8: Linear regression equations of the data shown on Figures 4.5 and 4.6.

Propellant	Volume (m^3)	Area (m^2)	Regression equation
SB1 and SB2	60 L	0.0007 m^2	$P_{max} = 1870m$
DB1 and DB2	60 L	0.0007 m^2	$P_{max} = 6970m$
DB1	1800 L	0.016 m^2	$P_{max} = 29.4m$
DB1	1800 L	0.041 m^2	$P_{max} = 18.5m$
DB1	1800 L	0.093 m^2	$P_{max} = 4.2m$

helpful in going forward in optimizing the model. This form and the previous conclusions indicate that the new model should look as follows:

$$P_{max} = k\ m^{a_1}\ A^{a_2} \tag{80}$$

where the empirical constant k would be expressed in units of Pa/kg^{a_1}m^{2a_2}. By taking the logarithm on both sides of Eq. (80) and simplifying, a linear relationship with the unknown constants is obtained.

$$\log P_{max} = \log k + a_1 \log m + a_2 \log A \tag{81}$$

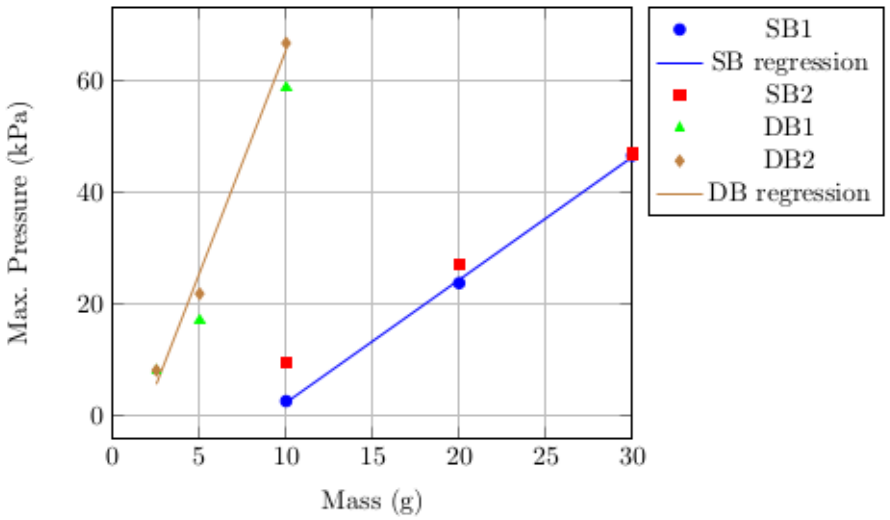

Figure 4.5: Maximum pressure as a function of the sample mass in the 60-L enclosure. The correlation coefficients, r^2, are 0.95 and 0.98 for the SB and DB data respectively.

The method of multiple linear regressions was applied on the data using the R statistical code through the R-Studio interface [58]. The following regression model was obtained:

- When considering the following variables for DB1: mass and venting area:

$$P_{max} = \frac{194.6 m^{0.97}}{A^{1.34}} \tag{82}$$

The regression line fits the data with a correlation coefficient $r^2 = 0.91$.

The interpretation of this last result must, however, be made carefully. Eq. (82) is seen to not follow the expected inverse square relationship for the area. If the inverse square relationship is forced in the regression, the fits are unacceptable. Two important observations must be made about the situation:

- The group of points (shown in Figure 4.8) is mostly within the uncertainty region between the error limits.

- The range of areas tested is relatively small (there is a factor of 6 between the extreme

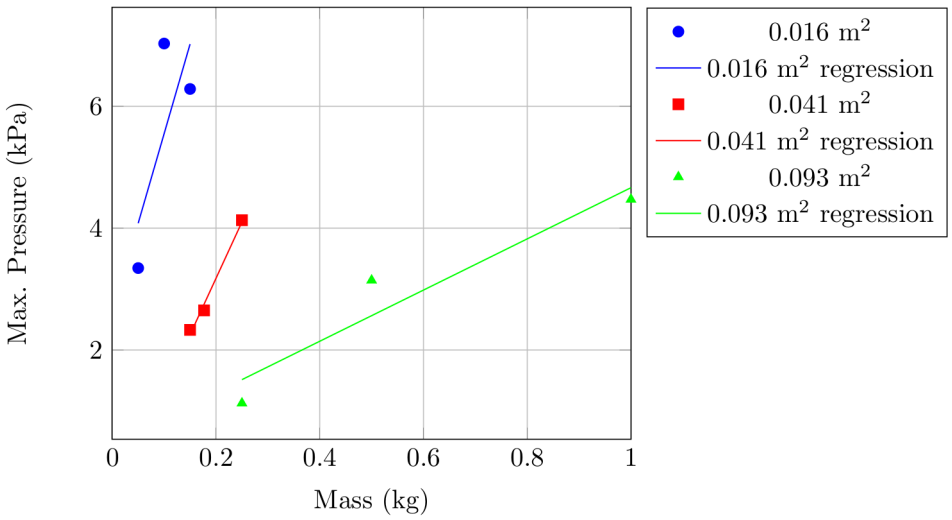

Figure 4.6: Maximum pressure as a function of the sample mass in the 1800-L enclosure. The correlation coefficients, r^2, are 0.60, 0.99 and 0.91 for the 0.016, 0.041 and 0.093 m^2 data respectively.

values in the 1800-L enclosure). Over such a small range, an inverse square relationship can be simplified as a direct inverse. Testing with larger areas is not practical as pressures become very low. Extending to smaller areas becomes problematic as pressures would rise to dangerously high levels (unless impractically small masses were used). The tested range was thus in the right location with respect to the intended application.

- The resulting expression does not take into account any change in the thermodynamic variables and discharge coefficient.

This is a classic issue when performing a statistical regression on experimental data. The best regression model does not necessarily reflect the ultimate best model. What can be said is the following: the best regression model, Eq. (82), represents the best fit for these variables in their tested range.

The inverse square area model has a theoretical background and is used in other cases. It should be expected to better predict the pressure in applications of various scales. By

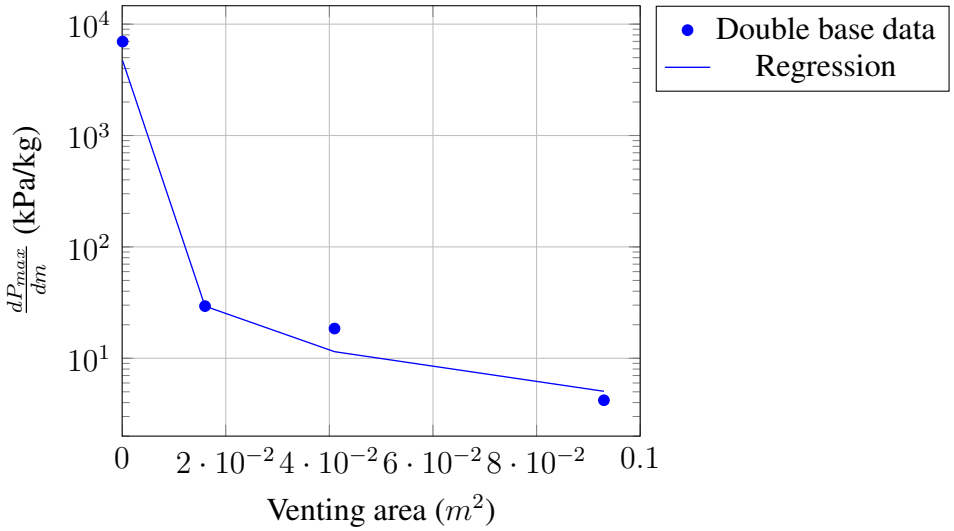

Figure 4.7: Maximum pressure rate of change with respect to mass as a function of the venting area for DB1. The correlation coefficient, r^2, is 0.99 for this data.

comparing the two models, it is possible to estimate the variation of the discharge coefficient with the venting area. The non-ideal behavior of fluid flow through restriction is such that the mass flow rate is smaller by a fraction equal to the discharge coefficient [75]. This flow reduction can be modelled by considering an ideal flow through a smaller area. Furthermore, since the discharge coefficient is used directly in the mass flow rate expression (i.e., not raised by any power), it should have the same effect on the area. The area relationship can thus be seen as follows:

$$\frac{1}{(C_D A)^{1.34}} \approx \frac{1}{A^2} \tag{83}$$

Here, $C_D = f(A)$ and thus varies such that its effect results in the desired inverse square relationship. Solving for the discharge coefficient yields the simple result:

$$C_D \approx A^{1/2} \tag{84}$$

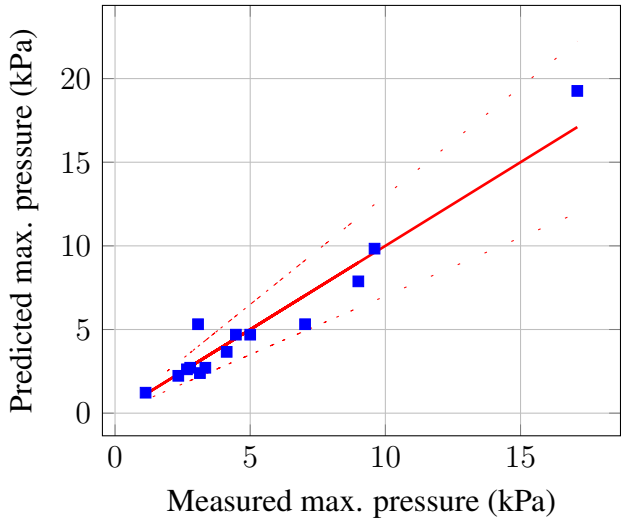

Figure 4.8: Comparison of the measured and predicted maximum pressures calculated using the best statistical model. Note that the solid line has the desired unity slope.

The previous result must, however, be used carefully as C_D usually takes values between 0 and 1. It can be seen that for the largest area tested (0.093 m^2), a resulting $C_D = 0.31$ is obtained. As the area is increased above 1 m^2, the predicted discharge coefficient would go above unity. In reality, it is expected that C_D will increase to an asymptotic maximum value located between 0.70 and 0.90 [75]. It can be concluded that the obtained model does follow the inverse square law as long as the variable nature of the state variables and discharge coefficient is recognized. If the pressure generation is modelled numerically, a further adjustment would be necessary to decouple the effect of the thermodynamic state variables and that of the discharge coefficient. This last conclusion is discussed further next, along with the issue of scale change, through the aid of a numerical tool.

4.4.4 Numerical solution of the pressure evolution equation

Although the solution of the derived pressure differential equation is difficult to find analytically, a simple numerical solution can be derived. In the previous introduction of

the pressure evolution model, it was shown that a lumped parameter approximation is sufficient. Therefore, one only needs to use Eq. (66) with a finite time interval, Δt, to obtain a numerical solution. A time evolution of the pressure is obtained by iterating the solution back as part of the inputs.

In all of the previous derivations, most thermodynamic parameters, such as temperature and density, were assumed to be constant. This assumption simplifies the calculation of the maximum pressure. In a numerical solution, these thermodynamic parameters can, however, be taken as variables. The solution for these new variables is obtained through an energy balance relation and the application of a proper equation of state. In the present case, the energy balance consists of two terms: an energy input due to the heat of combustion (heat of explosion) and an energy output due to the kinetic energy and enthalpy of the gases escaping from the vent opening. The energy balance equation is thus as follows:

$$\Delta T = \frac{\dot{m}_{gen} E \Delta t - C_v \dot{m}_{vent} T \Delta t}{C_v (m_{air} + \rho_{gas} V)} \tag{85}$$

where the energy output term, second term of the numerator, accounts for the kinetic energy and enthalpy of the exhausting gases. The energy balance equation yields a temperature difference at every time step. The gas density can then be computed from the ideal gas equation of state as follows:

$$\rho_{gas} = \frac{P M_w}{RT} \tag{86}$$

Starting from the standard conditions with a known combustion rate relationship, it is possible to increment the pressure, temperature and density at each step. These new results are iterated in the equations for the next time step and the process is repeated. Calculations can stop when the correct fuel mass has burned and the pressure is back at atmospheric

value. For reference, Appendix C contains a Matlab script of the designed lumped parameter numerical code.

For any numerical solution, the stability of the solution is important. In this case, selecting the right time step, Δt, is imperative in ensuring this stability. If the time increment is chosen too large, there is a possibility that more gas is vented than generated by the combustion during a single time step. This does not make sense physically as the pressure would decrease. If the time step is too small, the calculation time becomes long and inefficient as a viable solution method. An adaptive time step algorithm was used to determine an optimal increment size for each calculation step. This algorithm checks the effect of changing the time step size on the solution and selects the largest increment that keeps the solution stable within a certain defined error bound. Each time step of the solution is thus different, depending on the dynamic conditions of the system. The proper convergence of the integration scheme used is demonstrated in Table 4.9.

Table 4.9: Effect of the time step on the integration scheme solution of case A3.

Time step (s)	Max. Pressure (kPa)	Calculation time (s)
0.01	5.74	< 1
0.001	5.62	< 1
0.0001	5.60	≈ 1
0.00001	5.60	≈ 4

With the use of the previously presented experimental data, the values of some variables can be determined. In particular, the discharge coefficient, gas density and temperature are of interest. The goal is to determine which level of these variables could best represent the available data if they are subsequently kept constant in a simpler model equation. The results are shown tabularly and graphically in Table 4.10 and Figure 4.9 respectively. The resulting average minimum density and maximum temperature is thus 0.48 kg/m^3 and 823 K respectively.

To obtain these results, determining the combustion rate, $\dot{m}_{gen}$, is an important consideration. The following relation was applied to compute these mass generation rates:

$$\dot{m}_{gen} = \frac{m}{t_{max} - t_{ind}} \tag{87}$$

The idea is that the mass majoritarily burns when the fire has reached its maximum steady state dimensions (after the induction time). This works well in cases where the horizontal surface propagation can be assumed to completely take place before the steady state regime. It is thus observed that the determination of the combustion rate is not always straightforward and must be considered very carefully.

Table 4.10: Results and calculations summary of the 1800-L enclosure tested configurations.

Config.	Max. pressure measured (kPa)	Max. Pressures calculated (kPa)	Min. density calculated (kg/m^3)	Max. temperature calculated (K)
A1	3.34	1.83	0.81	396
A3	7.03	5.60	0.66	499
A5	6.28	10.98	0.57	601
B1	2.34	1.30	0.54	588
B2	2.66	1.95	0.50	640
B3	4.13	4.56	0.41	776
C1	1.13	0.18	0.41	775
C2	3.14	1.10	0.26	1206
C3	4.47	6.78	0.16	1925

4.4.5 Scale considerations

From the previous numerical results, it is obvious that a change of application scale results in a change in the state variable values. A further step can be taken by considering the case of a 100 m^3 room containing 50 kg of double bass propellant (DB1). Although this case was not the subject of an experimental test, its analysis using the numerical tool

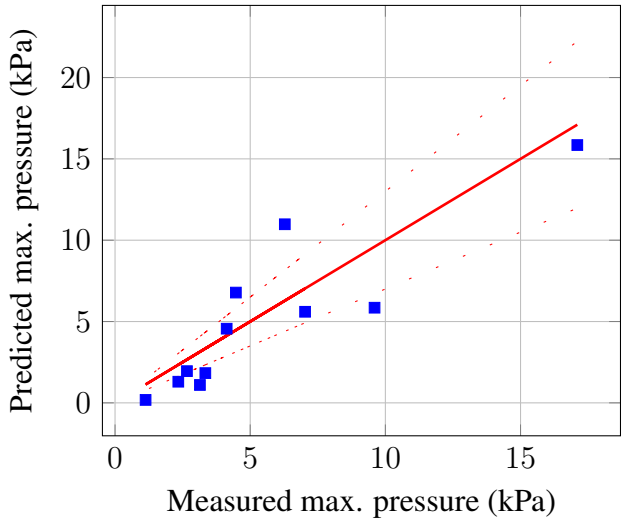

Figure 4.9: Comparison of the measured and predicted maximum pressures calculated using numerical solutions of the pressure evolution equation. Note that the solid line has the desired unity slope.

is instructive. Interestingly, similar quantities were studied in the irradiance analysis section. These tests showed a steady state time of around 4-5 s, thus yielding a combustion rate $\dot{m}_{gen} \approx 20$ kg/s. Applying these values, along with a 0.5 m^2 vent opening, yields a maximum pressure of 2.7 kPa. The resulting densities and temperatures of all tested scales are shown in Table 4.11.

Table 4.11: Summary of the calculated average minimum densities and maximum temperatures.

Volume (m^3)	Min. density (kg/m^3)	Max. Temperature (K)	Mass ratio (s^{-1})
0.06	0.74	452	0.2
1.8	0.48	823	0.5
100	0.18	1798	0.2

Interestingly, regression analysis yields the following expression for density with the DB1 cases (with a correlation coefficient, r^2, of 0.97):

$$\rho_{gas} = 0.47V^{-0.19} \tag{88}$$

Substituting in the theoretical expression for maximum pressure and simplifying yields:

$$P_{max} = \frac{1.06\dot{m}^2 V^{0.19}}{C_D^2 A^2} \tag{89}$$

where the discharge coefficient value derived previously, $C_D = A^{1/2}$, cannot be applied as the variation in density is part of this equation. By regression, one can find that the optimal discharge coefficient would here be $C_D = A^{1/3}$. The resulting equation thus becomes:

$$P_{max} = \frac{1.06\dot{m}^2 V^{0.19}}{A^{2.66}} \tag{90}$$

This expression is therefore valid for cases with a venting area below 0.5 m^2, as long as the pressure remains within the tested range of 0 to 10 kPa. For larger scale configurations involving venting area above 0.5 m^2, a constant discharge coefficient of 0.80 is assumed and the following is applied:

$$P_{max} = \frac{1.66\dot{m}^2 V^{0.19}}{A^2} \tag{91}$$

The previous three equations are valid for the DB1 case. A change in propellant type would be reflected on the combustion rate and the constant factor. As was done previously, the numerical code could be used to calculate the constant factors of other propellants (that calculation would take into consideration the changes in thermodynamical variables and heat release rate). A graphical comparison of DB1 measured and predicted values is shown in Figure 4.10. As expected, the fit is not as optimal as a statistical inverse area model (Eq. (82)) but the present expression is the more general version.

With the previous analysis in mind, it is worthwhile to analyse further the variation of the thermodynamic variables with scale. The problem must be viewed as the influx of high energy combustion gases in a given volume containing air at standard conditions. The combustion gases mix with the available air. A mixture with some intermediate conditions,

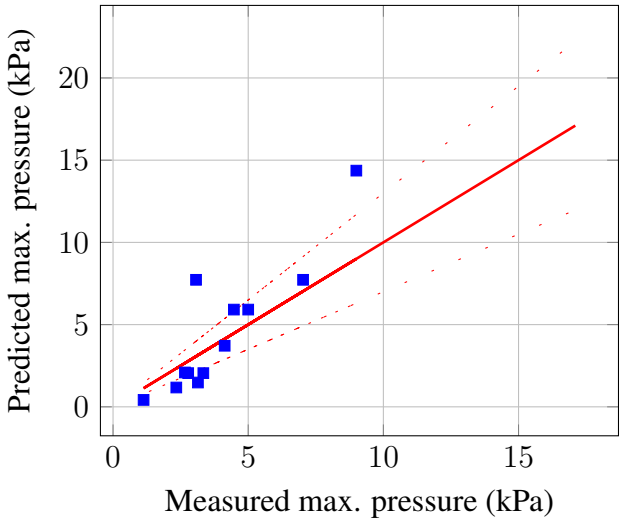

Figure 4.10: Comparison of the measured and predicted maximum pressures calculated using the scale dependant model. Note that the solid line has the desired unity slope.

between the flame and standard values, is obtained. The conditions of the mixture varies as gases are generated. The situation can be described by the following ratio:

$$\bar{m} = \frac{\dot{m}}{m_{air}} = \frac{\dot{m}}{\rho_{air} V} \tag{92}$$

This ratio expresses the quantity of combustion gases available for mixing with respect to the total air mass at any time within the volume. The values of the mass ratio, $\bar{m}$, are shown in Table 4.11. From the calculated mixture ratios, it is clear that as the volume diminishes, the fraction of potential mixing gases increases. An increase in the proportion of combustion gases will drive the conditions towards the flame values (i.e. flame temperature and lower density). This explains the data found in Table 4.11 and shows the behaviour to occur because of the increasing weight of $\bar{m}$ on the air quantity as V decreases. At the limit, $\bar{m}$ becomes so large in proportion to the air mass that flame conditions are assumed. This limit is used in the standard analysis of closed vessel propellant combustion tests.

4.4.6 Pressure rise time

In any enclosure fire, the rate at which the pressure will rise is of special importance to designers. Most facilities are equipped with explosion mitigation systems that have a specific response behavior. These systems range from various types of sprinklers, weaker walls or venting panels. In addition, it is important for those operating the facility to know how much time there would be to safely evacuate in case of a fire. Given that a model for the estimation of the maximum pressure has been derived previously, one only needs to know the time required to reach that maximum. The ratio of the maximum pressure and rise time yields an average rate of pressure rise.

The pressure rise times for both the 60-L and 1800-L tests are tabulated in Tables 4.5 and 4.7. All measured maximum times have been plotted in Figure 4.11. An interesting feature of the data is that the general shape of the plots for the maximum and induction (Figure 4.4) times are similar. One must remember that the maximum time is composed of both the induction time and the linear section that follows (stages 1 and 2 discussed previously). If the induction time is subtracted from the maximum time, what remains could very well be constant for all tests. This is indeed the case and is shown in Figure 4.12. Although there is some variation that could possibly be attributed to the standard deviations shown in Table 4.4, the linear part of the pressure rise (stage 2) is observed to lie around 0.30 seconds.

The seemingly constant nature of $t_{max} - t_{ind}$ can be explained by observing that the horizontal flame propagation occurs on samples of the same propellant and surface area. From the conclusions of the present section, an estimate of the maximum rate of pressure rise can be expressed as:

$$\left(\frac{dP}{dt}\right)_{max} = \frac{P_{max}}{t_{max} - t_{ind}} \tag{93}$$

It can be noted that the last expression assumes that the pressure is negligible at the end

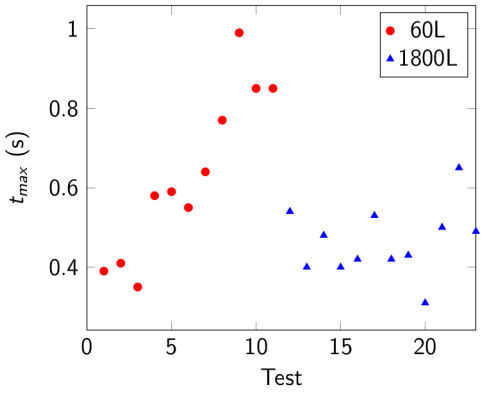

Figure 4.11: Distribution of measured t_{max} for all tests.

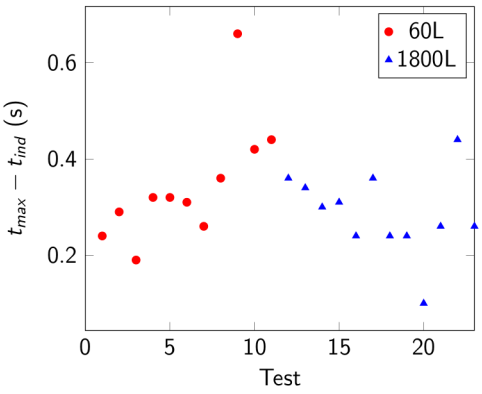

Figure 4.12: Distribution of measured $t_{max} - t_{ind}$ for all tests.

of the induction time. The result is thus a larger rate of pressure rise, which is acceptable in the context of a worst-case scenario. By using $t_{max} - t_{ind} \approx 0.30$ s, the following is obtained for the DB1 case:

$$\left(\frac{dP}{dt}\right)_{max} = \frac{3.53\dot{m}^2 V^{0.19}}{A^{2.66}} \tag{94}$$

A comparison of the calculated maximum rate of pressure increase and corresponding measured values is shown on Figure 4.13. The fit obtained is fairly good for most cases but some deviation is observed for a few occurrences. These deviations follow from the fact that these points also exhibited some variance in the pressure calculation shown in Figure 4.10. The deviation is amplified here because of the division by a small time interval.

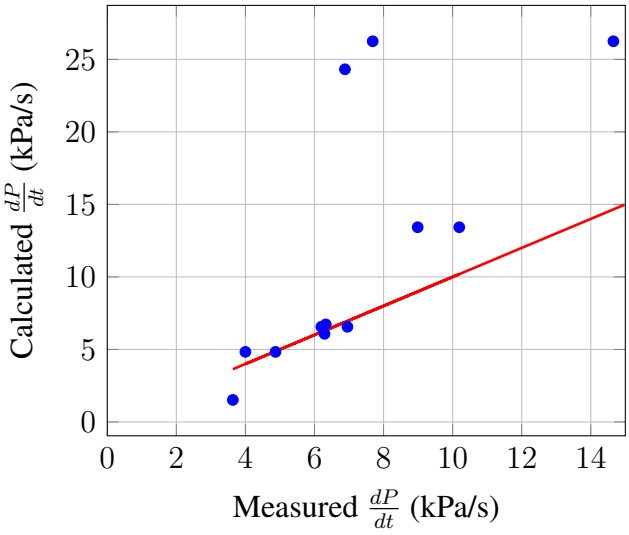

Figure 4.13: Comparison of the calculated and measured maximum rate of pressure rise for the 1800-L tests.

4.5 Summary

This study focuses on the analysis of a series of tests in which the pressure was measured during propellant fires in two vented enclosures. Two useful conclusions were drawn concerning the maximum pressures and the maximum rates of pressure rise obtained in such events. These conclusions are in the form of empirical laws valid within the tested conditions.

Another, more general, conclusion concerns the initial part of the fire when flames are still propagating on the surface of the propellant bed. One can define an induction time for this part of the event and estimate that time as the initial nonlinear part of the pressure curve. The test data shows a dependence of the induction time on the diameter (or surface area) of the propellant stack.

An analysis of the present results and conclusions with respect to theoretical considerations would likely provide further insight in the observed behaviors. This analysis would have to look at these events with the help of thermodynamics and gas dynamics. The result would either be more general estimation tools, in the form of semi-empirical laws, or

complete numerical models at the limit. The general relationships derived in this study can already be applied to many cases encountered in the propellant industry. With the addition of prediction tools for flame propagation and radiant heat flux, designers will be able to build facilities that provide a better fire safety.

Chapter 5

Conclusion

"Music is the arithmetic of sounds as optics is the geometry of light."

Claude Debussy

Previous chapters attempted to look at the various facets of the propellant fire problem. It is undeniable that due to the variety of products studied, the problem can be complex. Through a sequence of theoretical derivations, empirical studies and statistical analyses, certain fundamental rules were obtained. In a sense, a number of theoretical considerations guided the analysis of experimental results which could confirm or invalidate the starting hypotheses. The endpoints of the chapters were models based on the sum of both theoretical and empirical work. This symbiotic relationship between observation and theory is at the foundation of the scientific method.

In the same spirit, it is practical to summarize the milestone results in a concise methodology. The ultimate goal of these results is for users to apply them in real industrial settings. For this, a clear and easy to apply method is required. This is even more important in safety applications where users should be provided with simple guidelines and their domain of validity. In addition to guidelines, a synthesis of the physical aspects of the problem is

necessary. Arranging the information in various graphical aids can help users to better understand the products they are working with. This makes them more critical of the results obtained from the guidelines. It can also help in noticing areas where further research is required. It is also worthwhile to mention that the work performed here would be applied to the risk evaluation part of the global risk assessment process, as shown in Figure 5.1 [76]. The basic hazards identified in this case are the heat fluxes and pressures generated.

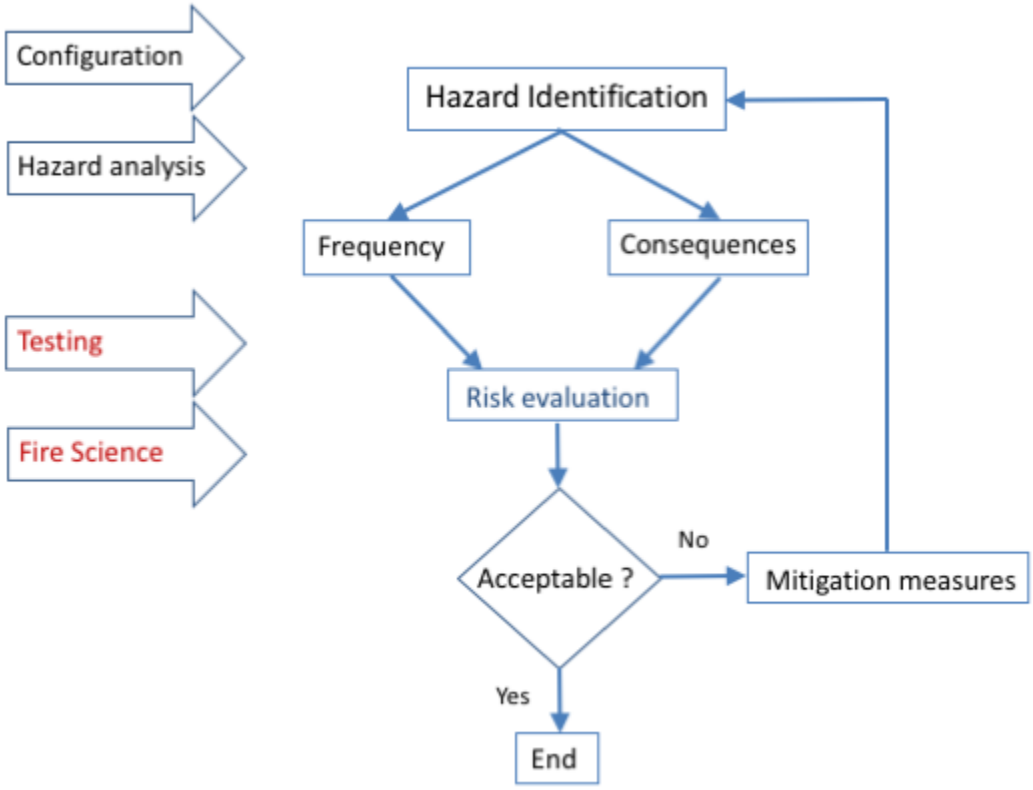

Figure 5.1: The risk assessment process [76]. This work would be part of the testing and fire science used in the risk evaluation step.

This chapter will provide a synthesis of the knowledge learned. The methodology needed to apply the results in real problems will be presented. Examples of such applications will finally be given. This should provide appropriate starting points for more detailed applications in the future. A summary of the contribution that this work provides to the field, along with possible future research, will then be discussed before concluding.

5.1 Synthesis

Based on the findings presented here, the procedure required to answer these questions would be as follows:

Flame propagation:

- Perform the basic burning rate tests (linear burning rate on a strand and 2 m horizontal burning test).
- Calculate the burning volume and height scaling factors ($\bar{V}$ and $\bar{h}$ respectively).
- Calculate the power using $\dot{Q}_m = \bar{V}\dot{Q}_{test}$.
- Calculate the horizontal propagation rate using $v_x = \bar{h}v_{test}$.
- Calculate the combustion rate using $\dot{m}_{gen} = \frac{\dot{Q}_m}{E}$.
- Estimate the event induction and maximum times using Eq. (16).
- Calculate the scaled power as $\bar{Q} = \frac{\dot{Q}_m}{m}$.
- Calculate the time ratio, $\bar{t} = \frac{t_{burn}}{t_{flight}}$.
- Determine the main propagation mode using the decision tree shown in Figure 2.20.
- Calculate the maximum fire diameter using the decision tree shown in Figure 2.20.
- Calculate the maximum flames height using the decision tree shown in Figure 2.20.

Radiant heat flux:

- If the propellant is arranged in a stack with a height of less than 0.20 m, apply Eq. (49).
- If the propellant is arranged in a stack with a height above 0.20 m, apply Eq. (39) or Eq. (47).

Pressure generation:

(1) Compute χ to verify the lumped parameter use assumption.

(2) Calculate X and determine the equation of state (ideal or Nobel-Abel).

(3) Calculate the theoretical maximum pressure.

(4) Calculate the maximum possible Mach number from the maximum pressure.

(5) Calculate the predicted maximum pressure, P_{max}, using one of the following:

- If the enclosure has a venting area of less than 0.5 m^2 and the propellant is not restrained in an open container, apply Eq. (82).
- If the enclosure has a venting area of less than 0.5 m^2 and the propellant is restrained in an open container, apply Eq. (90).
- If the enclosure has a venting area above 0.5 m^2, apply Eq. (91).
- The numerical model can be applied in all these cases with the proper discharge coefficient.

(6) Calculate the maximum rate of pressure rise, $\left(\frac{dP}{dt}\right)_{max}$, using Eq. (93).

The methodology is illustrated in the flowchart shown as Figure 5.2. Furthermore, the flame propagation mode selection is shown in a graphical manner in Figure 5.3. This last graphical tool provides the same information as Figure 2.20 but would enable one to compare various specific propellants in an easy and illustrative manner. It is expected that the models used here would be applicable to other granular propellant types. One must, however, remember that the general models are better suited to new conditions (as opposed to the statistical models). It is therefore important to determine what conditions are applicable in selecting a proper model.

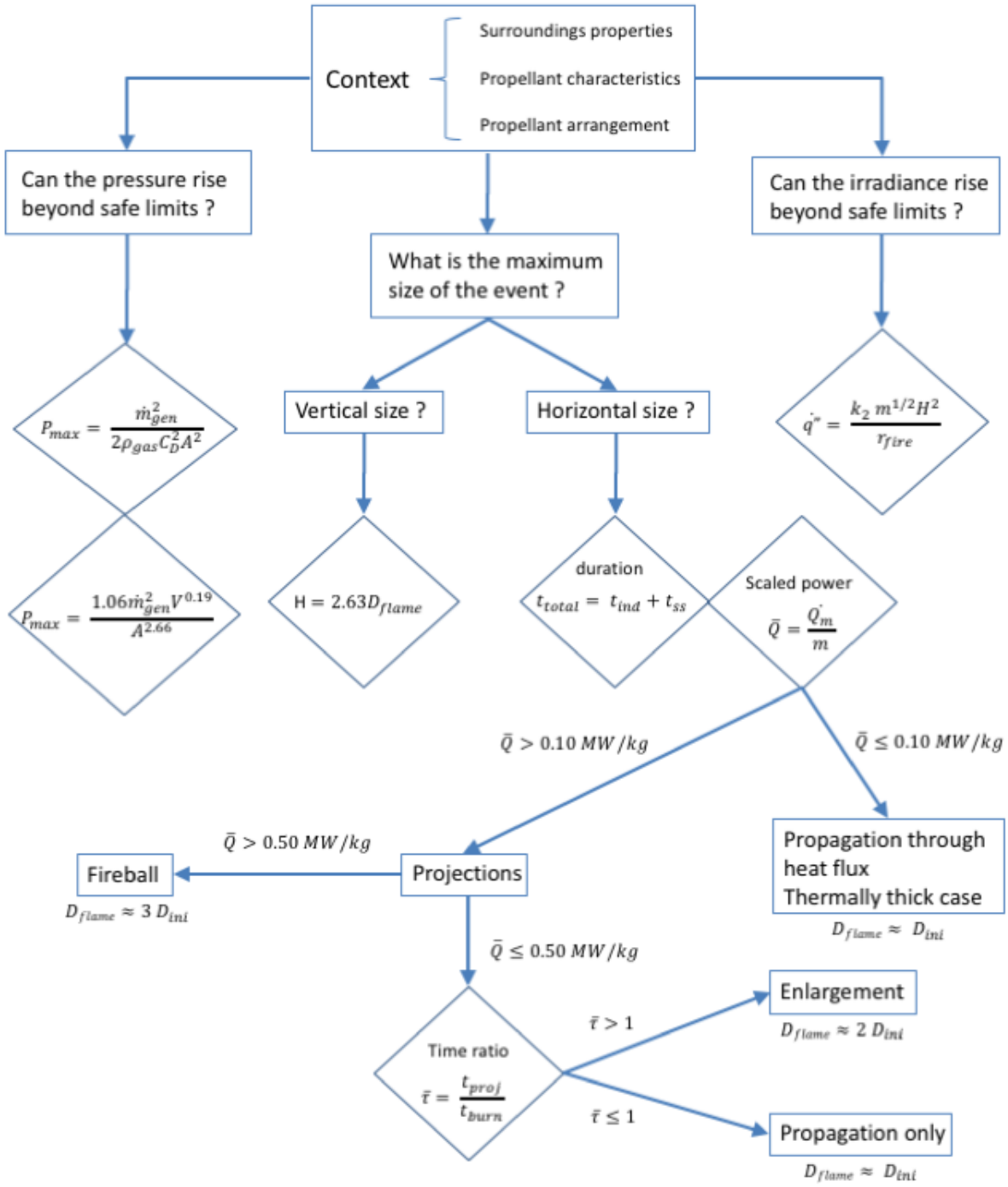

Figure 5.2: Decision tree to select the proper flame propagation mode.

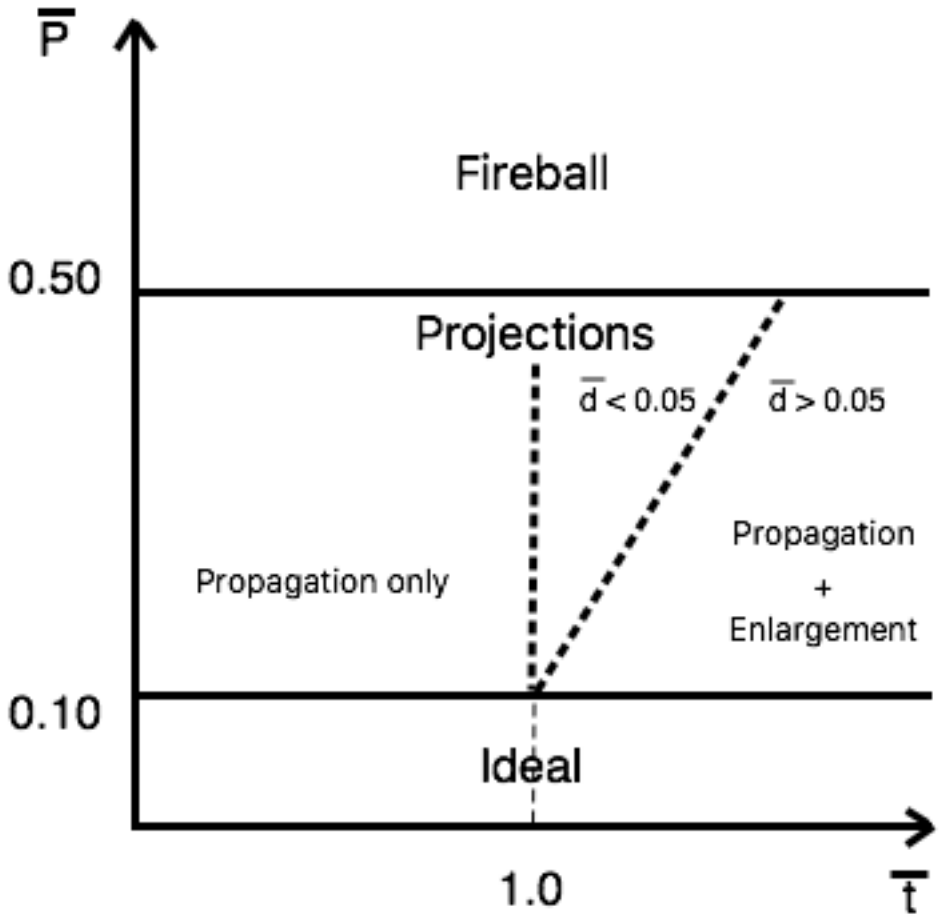

Figure 5.3: Graphical flame propagation characterization tool.

5.2 Contribution

At the beginning of this effort, very little information was available concerning propellant fire safety. Some succinct efforts have been led in order to solve very specific problems. The largest body of information available was from studies done with other fuels. Fire is indeed an important safety concern in any environment. Therefore, the body of related references available is important, both in empirical and theoretical information. As was shown initially, propellant can span a large range of combustion behaviours (a range taken by many different substances). This complexifies the analysis of potential fire hazards in facilities handling propellants. Perhaps one of the most important contributions of the present work was in recognizing how propellants span such a large range of behaviours, and devising the following methodology to analyze propellant fires:

- To decompose the global propellant fire event into its various associated behaviours.
- To design a classification scheme based on commonalities between the behaviours.
- To design predictive models that quantify some of these behaviours.

The result is a system which resembles the Cartesian method of subdividing a complex problem into simpler sub-problems and addressing them one by one [77]. It is therefore argued that the methodology is the greatest legacy of this work. An example of applying this method is the classification scheme designed for propellant fires propagation and how the estimated maximum size of the events can be linked to each class.

In the same way, the scheme used to solve individual problems is of greater importance than the actual solution. The general scheme was presented in the introduction of this work and applied throughout as follows:

- Derivation of a theoretical model (which may or may not involve numerical modeling).

- Experimental measurements performed on a limited number of configurations.
- Statistical analysis of the empirical results.
- Comparison with the empirical model and determination of unknown parameters.

In some cases, the statistical analysis agrees well with the theoretical model. In other cases, the limitations in experimental possibilities mean that the statistical interpretation can yield a less general model. It is important to recognize the latter case and use theoretical knowledge supported by the body of previous work in designing the best model. This second, more detailed scheme is, however, not as important a contribution as the first. The reason is that this second methodology is more akin to the expected regular conduct of scientific research.

The individual specific models derived are also important contributions. In the case of radiant heat transfer from propellant fires, two models are proposed: an empirical law based on a number of experiments and a more general theoretical result. In this case the two models are very similar. The empirical law has the advantage of having a single equation which uses variables that are often measured in the propellant industry. The theoretical model offers more control over some of the variables and thus additional precision. More work is, however, required to apply this model, as some calculations must be performed to apply the equation. In many industrial applications, the complimentary features of the theoretical model are not necessary and beyond the required range of precision. In these cases, the simpler empirical law can suffice.

The case of pressure generation has some similarities with the previous radiant heat flux situation. In this case, an empirical and a theoretical expression were derived. However, it was shown that the empirical equation is not expected to apply well at different scales. By using the experimental data with the help of a numerical solution of the theoretical model, it was possible to assess the effect of scale change on the variables. A relatively

simple expression which compares well with the experimental results followed. Because the empirical model has a limited range of validity, the two choices available are between the expression derived using the combination of empirical and numerical results, or the use of the fully numerical model. As in the previous case, one method provides for a relatively simple equation which uses variables commonly measured in the propellant industry. The other method, in this case the purely numerical model, is a bit more complex to use, but provides a more generally applicable scheme.

In all these cases, there are no clear standards or published methods to use in order to solve a problem. Most specialists in the field can somewhat describe what might happen and apply some basic principles to obtain a rough approximation. In many cases, how to proceed depends on rules of thumb used within an organization or department. The Lucotte irradiance model is perhaps the only previously available model [46]. The current work has shown that the law provides a good approximation, but can be improved by considering various geometrical aspects of the fires. The act of writing on the subject thus also constitutes an important contribution, as no formal treatment on propellant fire science has already been published (beyond the work of Lucotte and the results of a few experimental studies). This work is therefore valuable both in the new results derived and in its general scope.

5.3 Future work

For any studies, there are boundaries to follow. Early in the work, limitations in the range of some of the variables are set as a way to limit the amount of work and time required. In the present case, the limitations were as follows:

(1) Granular propellants.

(2) Combustion and pressure regimes no higher than what would be tolerated inside

buildings.

(3) Experimental scale within the budget of the supporting partner.

The last limitation is of lesser importance, as theoretical considerations are used to increase the applicability boundaries of the models. It would, however, be of interest to still perform a limited number of experimental trials at larger scales to verify the results and adjust them as necessary. Given that safety is an endeavor shared by all of the industry, these costlier tests could be supported by more than one partner in order to minimize the costs to an individual organization. In addition, if some of these results are eventually to become part of some kind of standard, further experimental verifications would likely be required. The methodology developed here would be of great use.

The first of the stated limits means that one must be careful when applying the results to propellants shaped as rocket motors. Although the same chemical ingredients are used in their manufacture, their geometry will alter the behaviour of the fire. In this case, propellant grain protection can reach the extreme limit, where the initial stack will not keep its integrity through the fire. This raises new questions, such as: when can a grain be considered as self propelling and how far can such a projection travel? Theoretical tools could be derived based on the propellant combustion dynamics, but experimental tests in controlled environments would be required. Future work on this topic would expand the classification model derived here for propellant fire propagation.

The second limitation is of great concern in the propellant industry. Most process equipment involves confining the propellant at a density that goes above those studied here. These densities are still below what can be found in most applications, but high enough to generate dangerous pressures. Additional theoretical and empirical work is thus needed in vented enclosure propellant fires. As pressures become higher, the constant burning rate assumption can no longer be used. Tests performed in closed vessels and pressurized strand burners would therefore be required to better quantify the burning rate at these pressure

levels. The extreme limit is the case when a propellant can detonate if specific conditions are met. Many previous studies have been published concerning the transition from deflagration to detonation of propellants. There are, however, no clear guidelines available to the industry on the matter.

Although it has not been stated as a limitation, granular propellants at manufacturing stages prior to the drying process is also of interest. The results of the present work are expected to be applicable to these cases as well. The only difference in the propellant prior to its drying is a concentration of solvent. This solvent will affect the heat of explosion and burning rate of the propellant. Experimental work would therefore be required to characterize these variables for solvent containing propellants, if the techniques derived here are to be applied. In addition, some of the processing solvents are flammable and volatile. The flame propagation of these slower burning propellants will likely be governed by the flame propagation rate of the solvent air mixture located at the surface of the propellant stack. Further studies in this direction would, again, expand the classification scheme derived here for flame propagation.

5.4 Concluding remarks

The goal of this study was to design models pertaining to propellant fire dimensions, radiant heat flux emissions and pressure generation. Quantitative methods that predict the maximum values and time required to reach these maximums were required. Through a series of theoretical and empirical analyses, these goals have been fulfilled. In addition, a classification model which qualitatively describes how a fire will evolve has also been designed. Given both the methods designed and the results obtained, this study can be considered a success with respect to the initial goals. As is the case in any work of this nature, there is always room for improvement and future considerations. The current results are, however, satisfactory with respect to the industry for which they are designed.

Fire safety is always an important preoccupation in any industry. The propellant industry is even more concerned as the materials used are highly flammable and energetic. The author of this study has worked in a propellant manufacturing facility for over a decade. During this tenure, several fires and near misses occurred in different parts of the process. Fortunately, none of these events caused any harm. The investigation reports of fatal fires which occurred in previous decades give a chilling account of what can go wrong when handling propellants [78]. Sadly, most of these dramatic events took place due to a failure in recognizing and understanding some of the basic behaviours and characteristics of propellants (both in their sensitivity to ignition and fire characteristics). The accounts and memories of those that were present during these events are constant reminders to never take safety for granted and never underestimate the power contained in propellants. It is the duty of those who work in this industry to always remember those who paid the ultimate price, and ensure that all the knowledge available is applied in minimizing the risks of future incidents. In the end, this is the fundamental goal of this effort.

Bibliography

[1] L. N. Cooper. *An introduction to the meaning and structure of physics*. Harper & Row, 1970.

[2] R. P. Feynman, R. B. Leighton, and M. L. Sands. *The Feynman Lectures on Physics*. Addison-Wesley, 1963.

[3] N. Kubota. *Propellants and Explosives: Thermochemical Aspects of Combustion*. John Wiley & Sons, 2015.

[4] D. E. Carlucci and S. S. Jacobson. *Ballistics: Theory and Design of Guns and Ammunition, Second Edition*. CRC Press, 2013.

[5] J. S. Merola. How do air bags work. *Scientific American*, October 1999.

[6] J. Wilson. Solid Rocket Boosters. http://www.nasa.gov/returntoflight/system/system_SRB.html.

[7] J. Corner. *Theory of the interior ballistics of guns*. Wiley, 1950.

[8] T. Urbański. *Chemistry and technology of explosives*. Pergamon Press, 1983.

[9] W. M. Haynes. *CRC Handbook of Chemistry and Physics, 93rd Edition*. CRC Press, 2016.

[10] K. K. Kuo. *Principles of combustion*. John Wiley, 2005.

[11] S. Gordon, B. McBride, and F. J. Zeleznik. *Computer program for calculation of complex chemical equilibrium compositions and applications. Supplement 1: Transport properties*. National Space and Aeronautics Administration, 1984.

[12] Sandia National Laboratory. *CHEMKIN Release 3.6.2*. Reaction Design, 2001.

[13] L. E. Fried, W. M. Howard, and P. C. Souers. Cheetah 2.0. Technical report, Lawrence Livermore National Laboratory, 1998.

[14] F. Paquet and H. D. Ng. A simple method for initial condensed-phase combustion reactions predictions. *Applied Spectroscopy Reviews*, 46(2):132–139, 2011.

[15] J. G. Quintiere. *Fundamentals of fire phenomena*. John Wiley, 2006.

[16] Health and Safety Executive. Explosive Incident Database Advisory Services, quarterly accident listing – 21st edition. http://www.hse.gov.uk/explosives/eidas.htm, 2015.

[17] V. Novozhilov, B. Moghtaderi, D. F. Fletcher, and J. H. Kent. Computational fluid dynamics modelling of wood combustion. *Fire Safety Journal*, 27(1):69–84, 1996.

[18] M. J. Gollner, F. A. Williams, and A. S. Rangwala. Upward flame spread over corrugated cardboard. *Combustion and Flame*, 158(7):1404–1412, 2011.

[19] M. Sibulkin and A. G. Hansen. Experimental study of flame spreading over a horizontal fuel surface. *Combustion Science and Technology*, 10(1-2):85–92, 1975.

[20] D. Bjerketvedt, J. R. Bakke, and K. Van Wingerden. Gas explosions handbook. *Journal of Hazardous Materials*, 52(1):1–150, 1997.

[21] R.K. Eckhoff. *Dust Explosions in the Process Industries: Identification, Assessment and Control of Dust Hazards*. Elsevier Science, 2003.

[22] A. T. Modak. Thermal radiation from pool fires. *Combustion and Flame*, 29:177–192, 1977.

[23] F. Diaz Alonso, E. Gonzalez Ferradas, J. F. Sanchez Perez, A. Minana Aznar, J. Ruiz Gimeno, and J. Martinez Alonso. Characteristic overpressure-impulse-distance curves for the detonation of explosives, pyrotechnics or unstable substances. *Journal of Loss Prevention in the Process Industries*, 19(6):724–728, 2006.

[24] D. Price and R. R. Bernecker. DDT behavior of porous columns of simple propellant models and commercial propellants. *Combustion and Flame*, 42:307–319, 1981.

[25] V. Babrauskas. A closed-form approximation for post-flashover compartment fire temperatures. *Fire Safety Journal*, 4:63–73, 1981.

[26] P. Amyotte. *An Introduction to Dust Explosions: Understanding the Myths and Realities of Dust Explosions for a Safer Workplace*. Butterworth-Heinemann, 2013.

[27] Merriam-Webster. *The Merriam Webster Dictionary*. Demco Media, 1994.

[28] National Fire Protection Association. *NFPA 68: Venting of Deflagrations*. National Fire Protection Association, 1988.

[29] S. Singh, Q. Kwok, R. Turcotte, and M. Paquet. Thermal and Mechanical Hazards of Nitrocellulose and its Mixture with Nitroglycerin. In *Proceedings of the 7th International Nitrocellulose Symposium*, Montreal, Canada, May-June 2016.

[30] J. H. Lienhard IV and J. H. Lienhard V. *A Heat Transfer Textbook*. Dover Publications, 2011.

[31] M. S. Miller. Thermal Conductivities and Diffusivities of Solid Gun Propellants. *Combustion Science and Technology*, 100(1-6):345–354, 1994.

[32] J. E. Hay and R. W. Watson. Scaling studies of thermal radiation flux from burning propellants. In *Proceedings of the 25th DOD Safety Seminar*, Anaheim, California, August 1992.

[33] A. I. Atwood, K. P. Ford, and C. J. Wheeler. High-pressure burning rate studies of solid rocket propellants. *EUCASS Proceedings Series*, 4:3–14, 2013.

[34] W. F. Oberle and D. E. Kooker. BRLCB: A Closed-Chamber Data Analysis Program. Part 2. Theory and User's Manual (Appendices D-M). Technical report, 1993.

[35] North Atlantic Treaty Organization. STANAG 4115 - Definition And Determination Of Ballistic Properties Of Gun Propellants, 1997.

[36] M. R. S. Nair and M. C. Gupta. Burning velocity measurement by bomb method. *Combustion and Flame*, 22(2):219–221, 1974.

[37] W. Swiderski, M. Miszczak, and A. Panas. A novel technique for the continuous evaluation of a burning rate of solid rocket propellant by using IR thermography. *Quantitative InfraRed Thermography Journal*, 8:111–114, 2011.

[38] H. F. R. Schöyer and P. A. O. G. Korting. Low Pressure Combustion of Composite Propellant. *Propellants, Explosives, Pyrotechnics*, 9(5):149–156, 1984.

[39] D. Drysdale. *An Introduction to Fire Dynamics*. John Wiley & Sons, 2011.

[40] M. Sibulkin, J. Kim, and J. V. Creeden. Dependence of flame propagation on surface heat transfer - 1. downward burning. *Combustion Science and Technology*, 14(1-2):43–56, 1976.

[41] F. Lees. *Lees' Loss Prevention in the Process Industries: Hazard Identification, Assessment and Control*. Butterworth-Heinemann, 2012.

[42] T. Hastie, R. Tibshirani, and J. Friedman. *The Elements of Statistical Learning*. Springer New York, 2009.

[43] V. I. Blinov and G. N. Khudyakov. Diffusion Burning of Liquid. *U.S. Army Engineering Research and Development Laboratories, T-1490 a-c, ASTIA AD296*, 762, 1961.

[44] J. G. Quintiere and B. S. Grove. Correlations for fire plumes. *NASA Report*, (19980209794), 1998.

[45] G. Heskestad. Luminous heights of turbulent diffusion flames. *Fire Safety Journal*, 5(2):103–108, 1983.

[46] L. P. Lucotte. Measurement and prediction of heat flux in gun propellant fires. In *Proceedings of the 20th DOD Safety Seminar*, Norfolk, Virginia, 1982.

[47] R. Merrifield and R. Wharton. Measurement of the size, duration and thermal output of fireballs produced by a range of propellants. *Propellants, Explosives, Pyrotechnics*, 25(4):179–185, 2000.

[48] R. A. Serway, C. J. Moses, and C. A. Moyer. *Modern Physics*. Brooks Cole, 2004.

[49] L. Boltzmann. Ableitung des Stefan'schen Gesetzes, betreffend die Abhängigkeit der Wärmestrahlung von der Temperatur aus der electromagnetischen Lichttheorie. *Annalen der Physik*, 258(6):291–294, 1884.

[50] J. R. Howell, M. P. Menguc, and R. Siegel. *Thermal Radiation Heat Transfer*. CRC Press, 2010.

[51] F. L. Pedrotti and L. S. Pedrotti. *Introduction to Optics*. Prentice Hall, 1993.

[52] H. Krier and M. Summerfield. *Interior ballistics of guns*, volume Progress in Astronautics and Aeronautics 66. American Institute of Aeronautics and Astronautics, 1979.

[53] M. Shokri and C. L. Beyler. Radiation from Large Pool Fires. *Journal of Fire Protection Engineering*, 1(4):141–149, 1989.

[54] A. Dayan and C. L. Tien. Radiant Heating from a Cylindrical Fire Column. *Combustion Science and Technology*, 9(1-2):41–47, 1974.

[55] W. S. N. Tinkler. Quantity-distances for hazard division 1.3 mass fire explosives. In *Proceedings of the 20th DOD Safety Seminar*, Norfolk, Virginia, 1982.

[56] J. R. Taylor. *An Introduction to Error Analysis: The Study of Uncertainties in Physical Measurements*. University Science Books, 2nd edition, 1997.

[57] N. J. Miller and J. C. Miller. *Statistics and chemometrics for analytical chemistry*. Prentice Hall/Pearson, Harlow, England; New York, 6th edition, 2010.

[58] R Core Team. *R: A Language and Environment for Statistical Computing*. R Foundation for Statistical Computing, Vienna, Austria, 2013.

[59] M. Racette, D. Brousseau, and C. Valliere. Rapport d'essais - transition de deflagration a detonation. Technical Report CEEM04-067, Centre d'essais et d'experimentation en munition, 2004.

[60] D. A. White, C. L. Beyler, F. W. Williams, and P. A. Tatem. *Fire Saf. J.*, 34(4):321–341, 2000.

[61] C. E. Joachim. KA-111, Phase C, M-1 Propellant Tests: Deflagration in Partial Confinement. Technical Report SL-91-11, USAE Waterways Experiment Station, Structural Laboratory, 1991.

[62] M. A. Polcyn and S. A. Mullin. Propellant loads testing application to facility design. In *Proceedings of the 28th DOD Safety Seminar*, Orlando, Florida, August 1998.

[63] K. J. Graham. *Explosive Response to Fragments: Venting Studies*. Naval Weapons Center, China Lake, California, 1986.

[64] B. Porterie, M. Larini, F. Giroud, and J. C Loraud. Solid-propellant fire in an enclosure fitted with a ceiling safety-vent. *International Journal of Heat and Mass Transfer*, 39(3):575–601, 1996.

[65] R. Frauenfelder. Experiments on the transition deflagration-detonation of propellants. *Propellants, Explosives, Pyrotechnics*, 8(6):193–198, 1983.

[66] R. Frauenfelder. Testing of a new concept for the storage of granular propellant. *Propellants, Explosives, Pyrotechnics*, 8(4):102–108, 1983.

[67] R. Merrifield and S. Myatt. The risks associated with the storage of small quantities of gunpowder and shooters powders in containers and buildings. In *Proceedings of the 28th DOD Safety Seminar*, Orlando, Florida, August 1998.

[68] R. K. Wharton and S. A. Formby. *J. Hazard. Mater.*, 79(1-2):31–39, 2001.

[69] R. K. Eckhoff. Chapter 2 - Gas and Vapor Cloud Explosions. In *Explosion Hazards in the Process Industries*, pages 11–148. Gulf Publishing Company, 2005.

[70] National Fire Protection Association. *NFPA 68: standard on explosion protection by deflagration venting, 2007 edition*. National Fire Protection Association, 2010.

[71] E. A. Ural. A simplified development of a unified dust explosion vent sizing formula. *Process Safety Progress*, 20(2):136–144, 2001.

[72] F. Tamanini. Scaling parameters for vented gas and dust explosions. *Journal of Loss and Prevention in the Process Industries*, 14(6):455–461, 2001.

[73] R. Bauwens and J. Chaffee. *Combust. Sci. Tech.*, 182(11):1915–1932, 2010.

[74] J. E. A. John and T. G. Keith. *Gas Dynamics*. Pearson Prentice Hall, 2006.

[75] P. L. Smith and M. Van Winkle. Discharge coefficients through perforated plates at reynolds numbers of 400 to 3,000. *AIChE Journal*, 4(3):266–268, 1958.

[76] G. Ramachandran and D. Charters. *Quantitative Risk Assessment in Fire Safety*. Routledge, 2011.

[77] R. Descartes and D. A. Cress. *Discourse on Method (Third Edition)*. Hackett Publishing, 1998.

[78] Commission de la santé et de la sécurité du travail du Québec. Rapport d'enquête d'accident : accident survenu le 26 octobre 1993 au séchoir de l'usine Les Produits chimiques Expro inc. à St-Timothée, causant la mort de deux travailleurs et des brûlures à deux autres travailleurs. Investigation report CAEQ 3793, CSST, 1994.

Appendix A

Experimental pressure - time traces (1800-L)

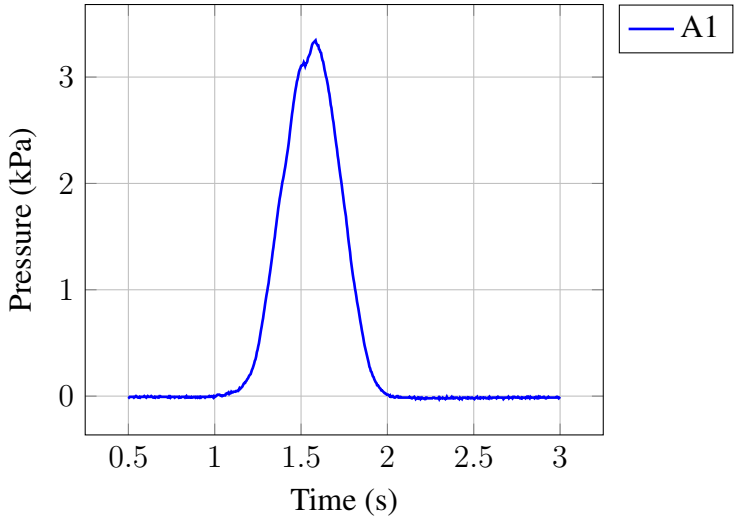

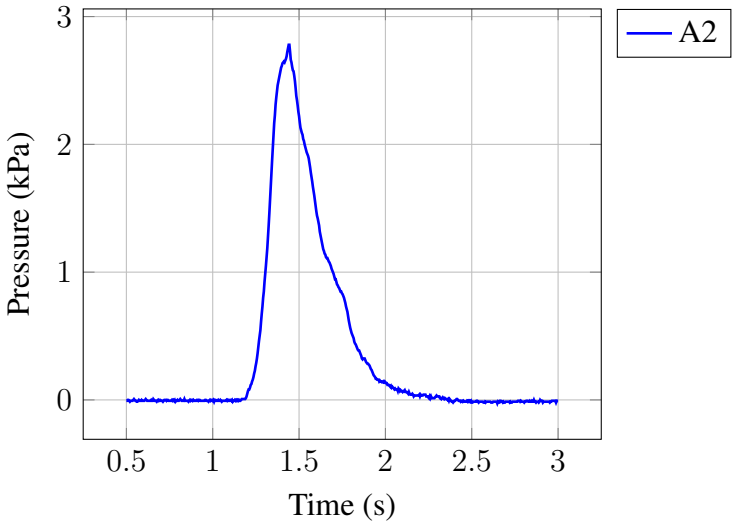
A2
Pressure (kPa)
Time (s)
0
1
2
3
0.5
1
1.5
2
2.5
3

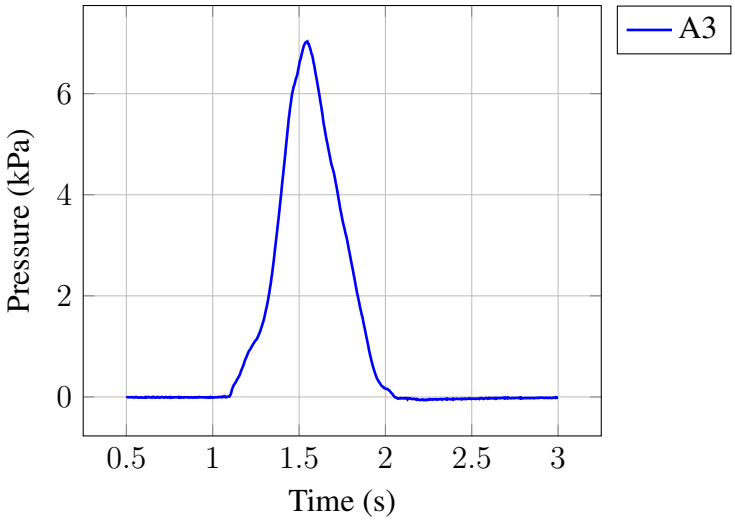
A3
Pressure (kPa)
Time (s)
0
2
4
6
0.5
1
1.5
2
2.5
3

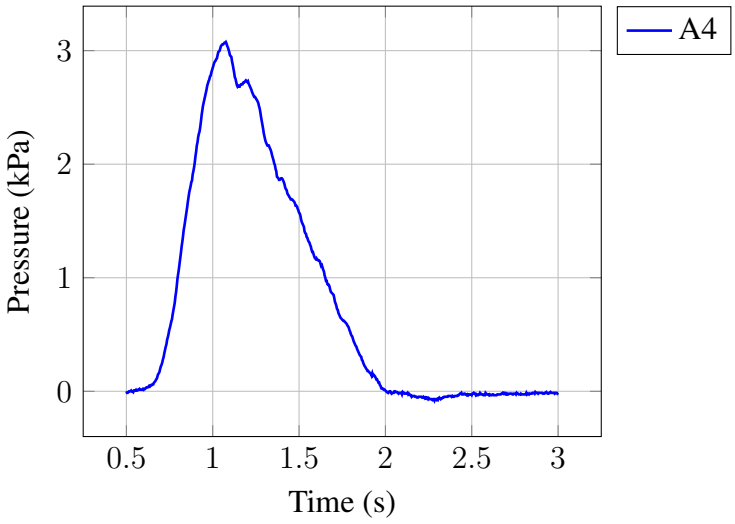
A4
Pressure (kPa)
Time (s)
0
1
2
3
0.5
1
1.5
2
2.5
3

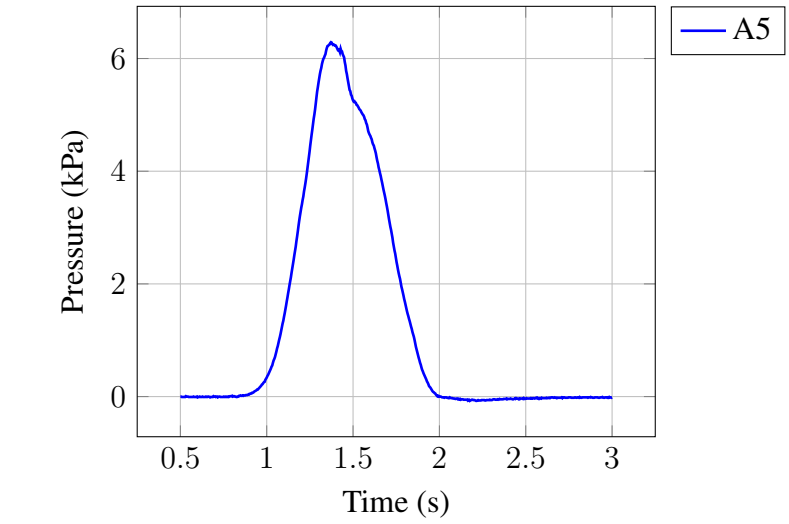
A5
Pressure (kPa)
Time (s)
0
2
4
6
0.5
1
1.5
2
2.5
3

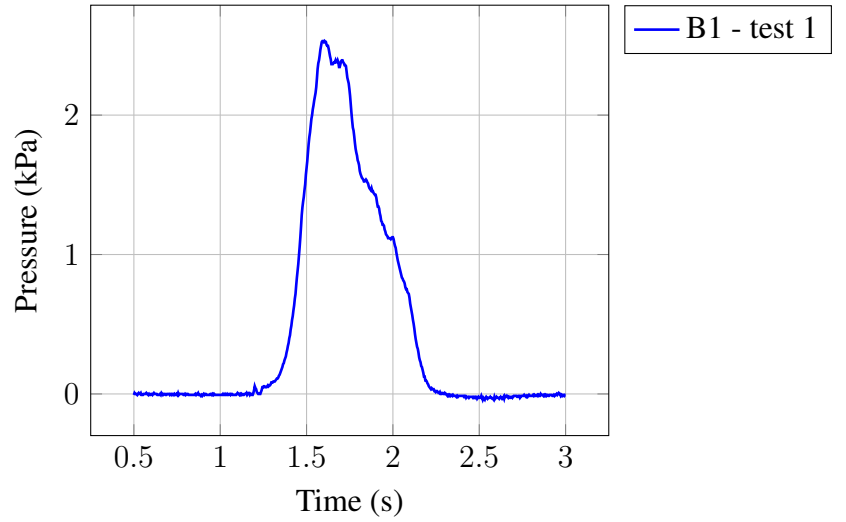
B1 - test 1
Pressure (kPa)
Time (s)
0
1
2
0.5
1
1.5
2
2.5
3

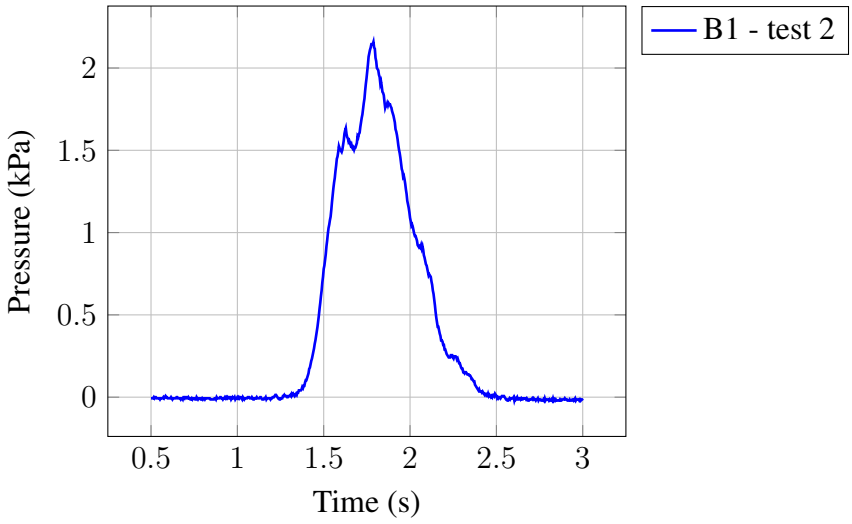
B1 - test 2
Pressure (kPa)
Time (s)
0
0.5
1
1.5
2
0.5
1
1.5
2
2.5
3

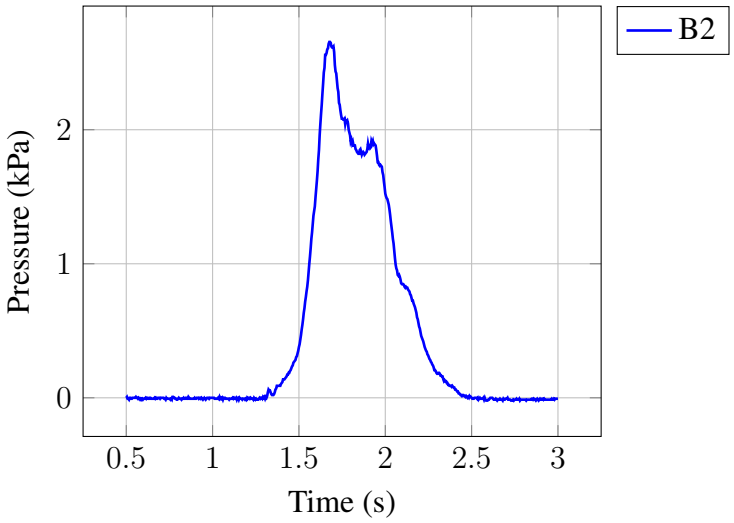
B2
Pressure (kPa)
Time (s)
0
1
2
0.5
1
1.5
2
2.5
3

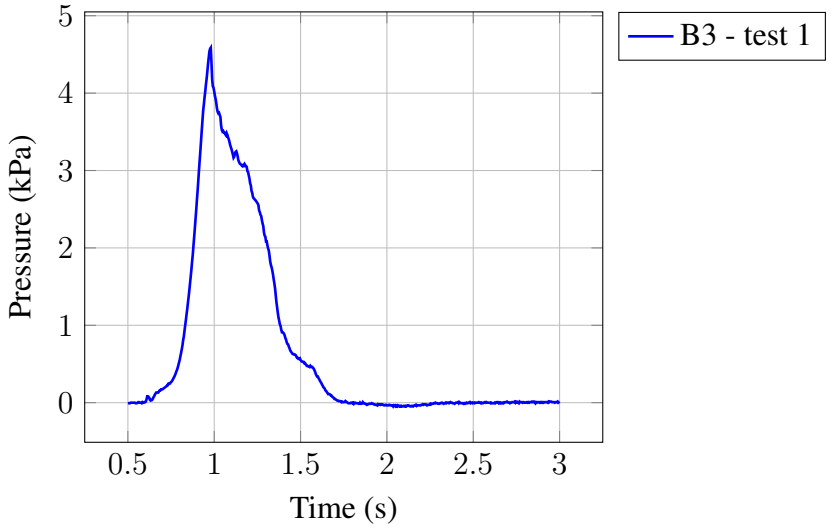
B3 - test 1
Pressure (kPa)
Time (s)
0
1
2
3
4
5
0.5
1
1.5
2
2.5
3

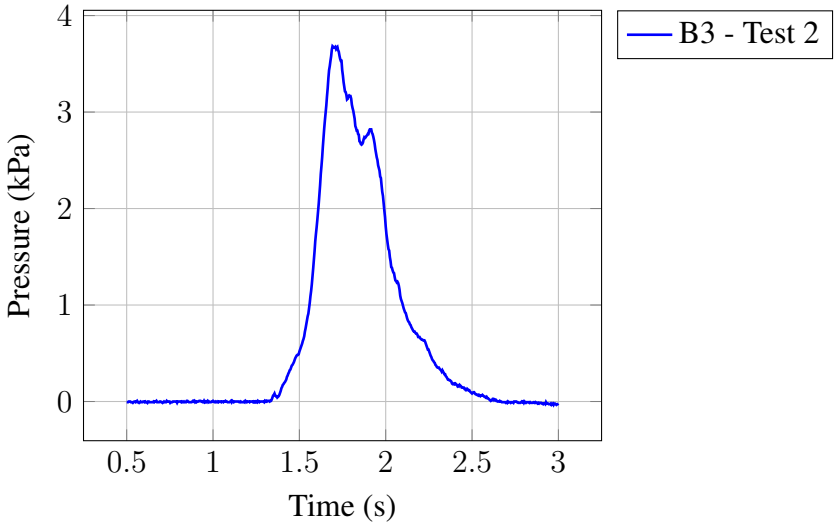
B3 - Test 2
Pressure (kPa)
Time (s)
0
1
2
3
4
0.5
1
1.5
2
2.5
3

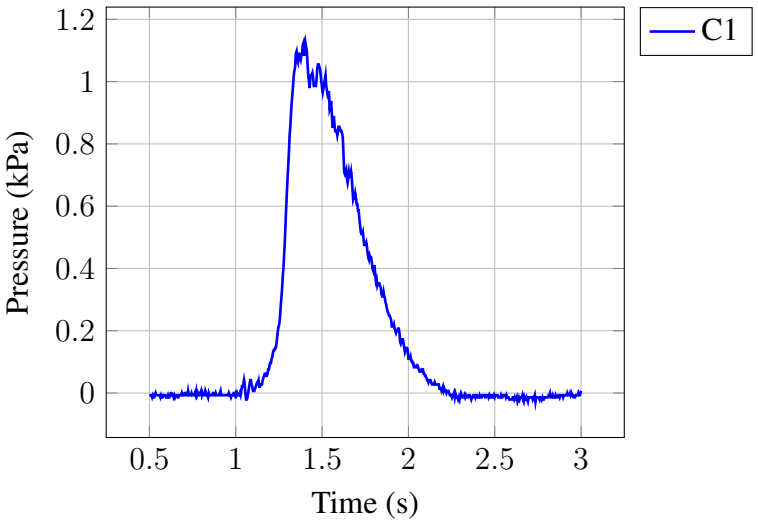
C1
Pressure (kPa)
Time (s)
1.2
1
0.8
0.6
0.4
0.2
0
0.5
1
1.5
2
2.5
3

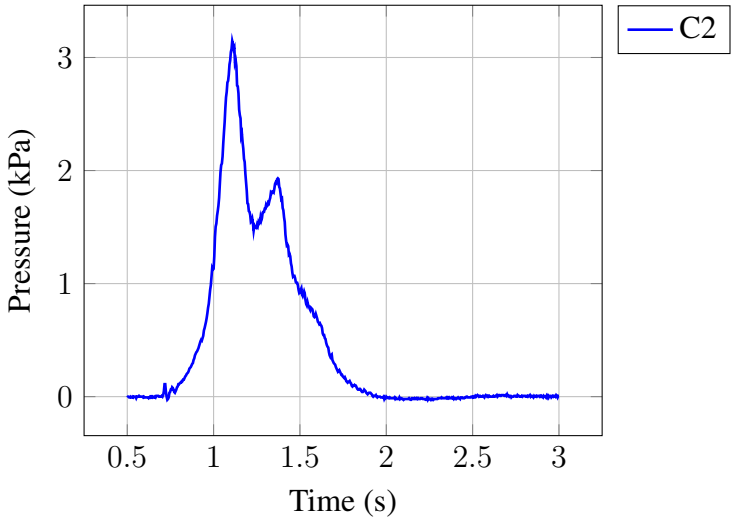
C2
Pressure (kPa)
Time (s)
3
2
1
0
0.5
1
1.5
2
2.5
3

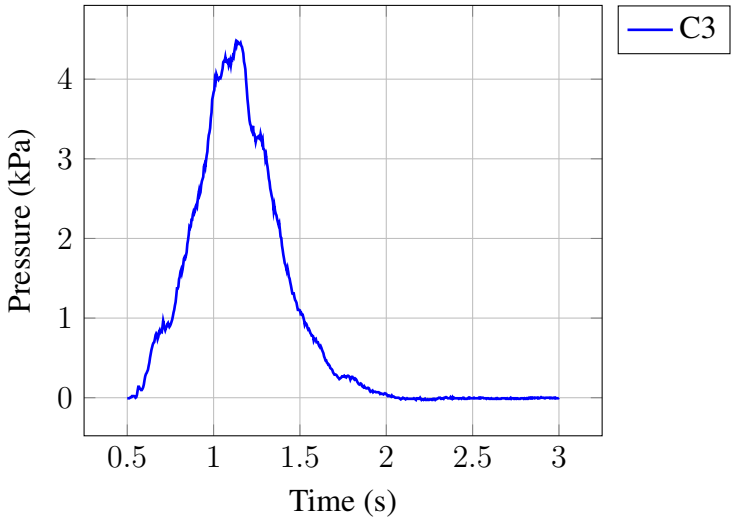
C3
Pressure (kPa)
Time (s)
4
3
2
1
0
0.5
1
1.5
2
2.5
3

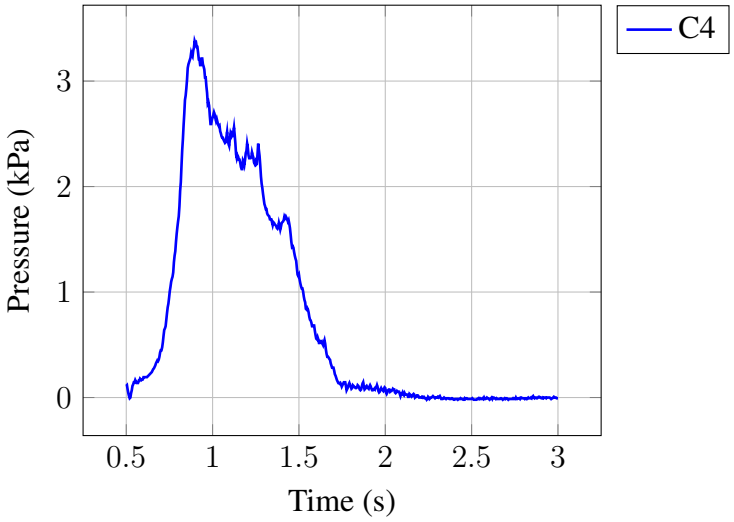
C4
Pressure (kPa)
0
1
2
3
0.5
1
1.5
2
2.5
3
Time (s)

Appendix B

Experimental irradiance - time traces

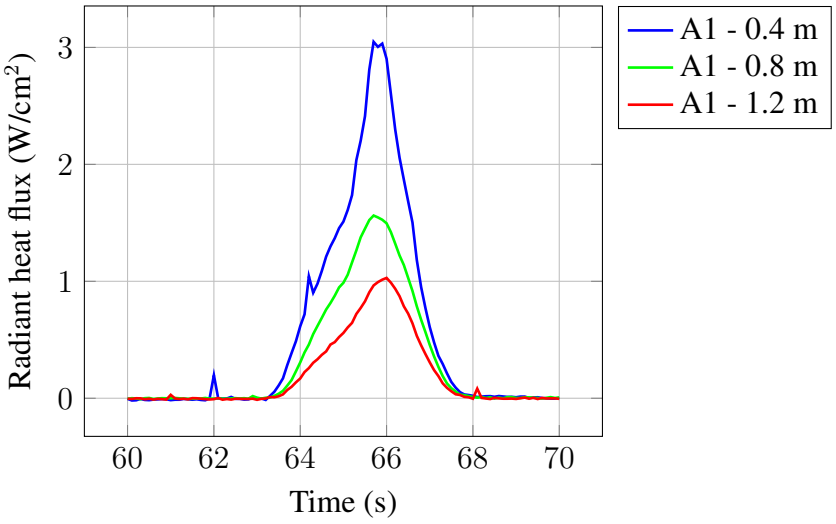

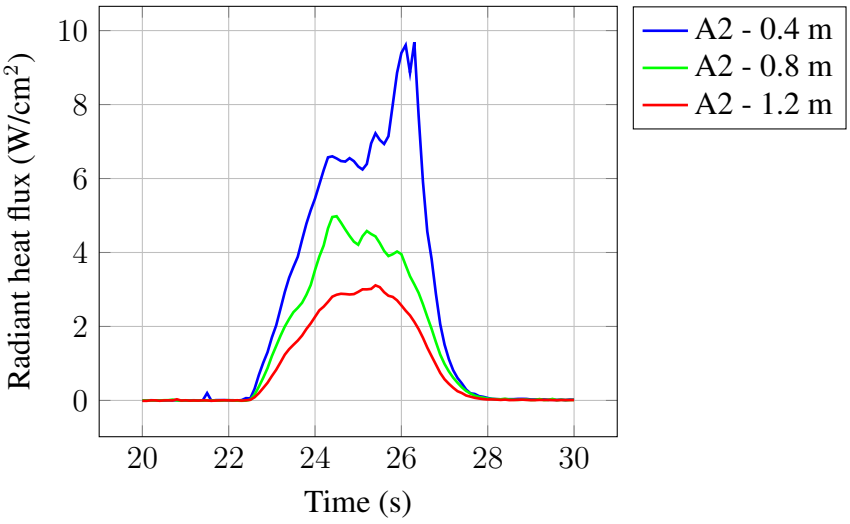
A2 - 0.4 m
A2 - 0.8 m
A2 - 1.2 m
Radiant heat flux (W/cm^2)
Time (s)
0
2
4
6
8
10
20
22
24
26
28
30

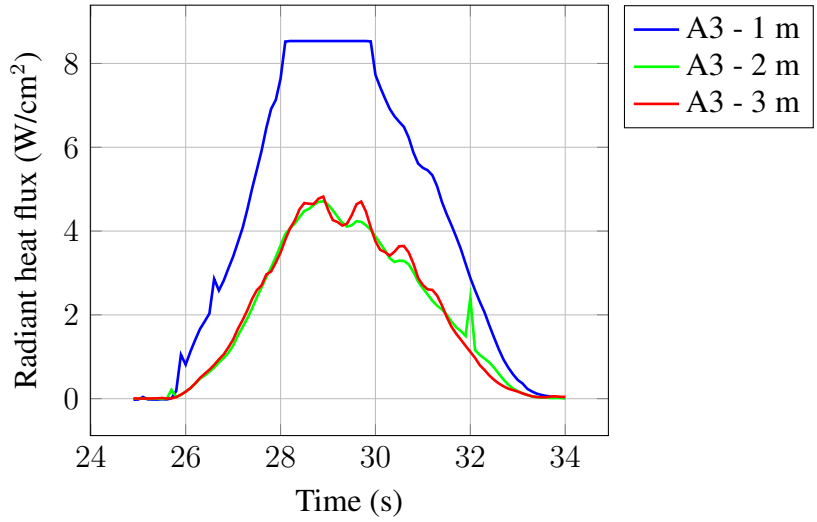
A3 - 1 m
A3 - 2 m
A3 - 3 m
Radiant heat flux (W/cm^2)
Time (s)
0
2
4
6
8
24
26
28
30
32
34

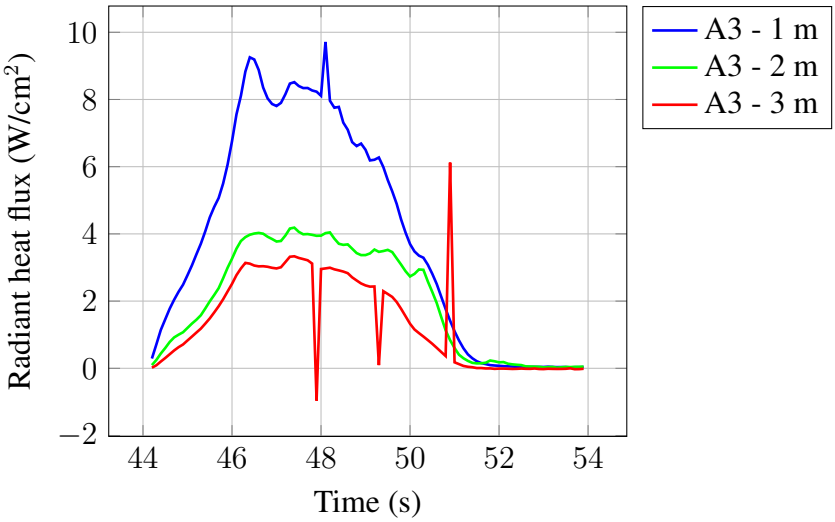
A3 - 1 m
A3 - 2 m
A3 - 3 m
Radiant heat flux (W/cm^2)
Time (s)
−2
0
2
4
6
8
10
44
46
48
50
52
54

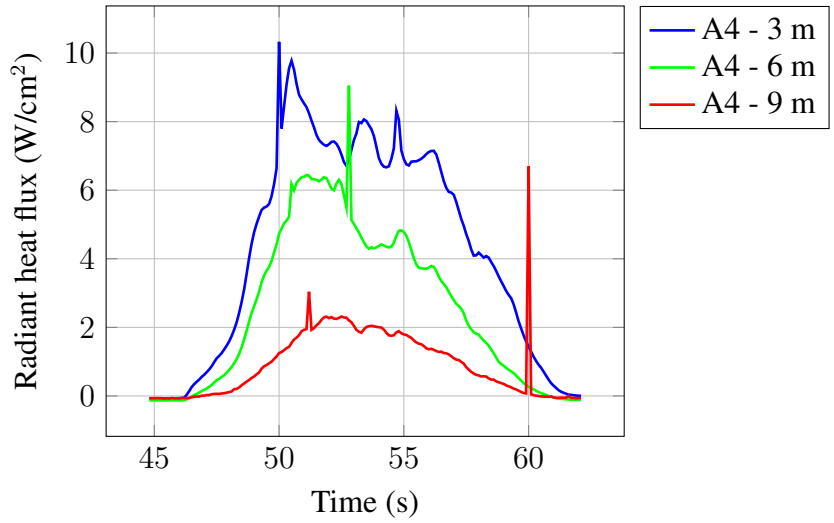
A4 - 3 m
A4 - 6 m
A4 - 9 m
Radiant heat flux (W/cm^2)
Time (s)
0
2
4
6
8
10
45
50
55
60

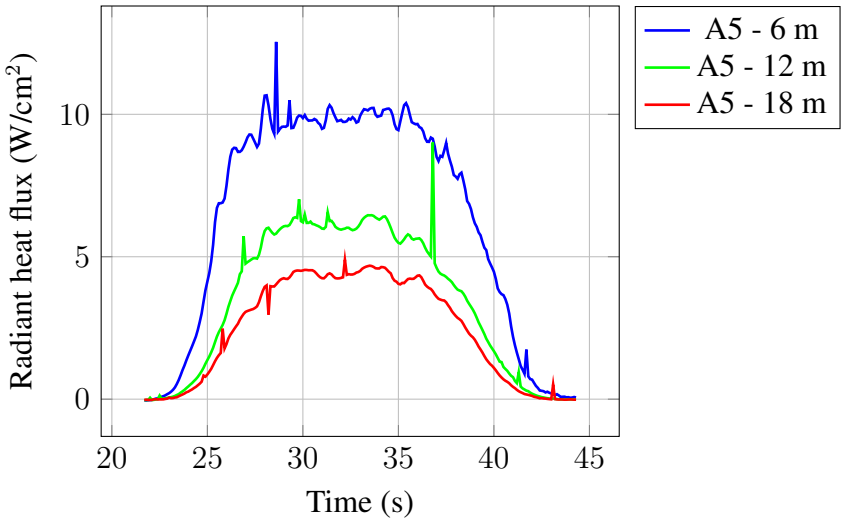
A5 - 6 m
A5 - 12 m
A5 - 18 m
Radiant heat flux (W/cm^2)
Time (s)
0
5
10
20
25
30
35
40
45

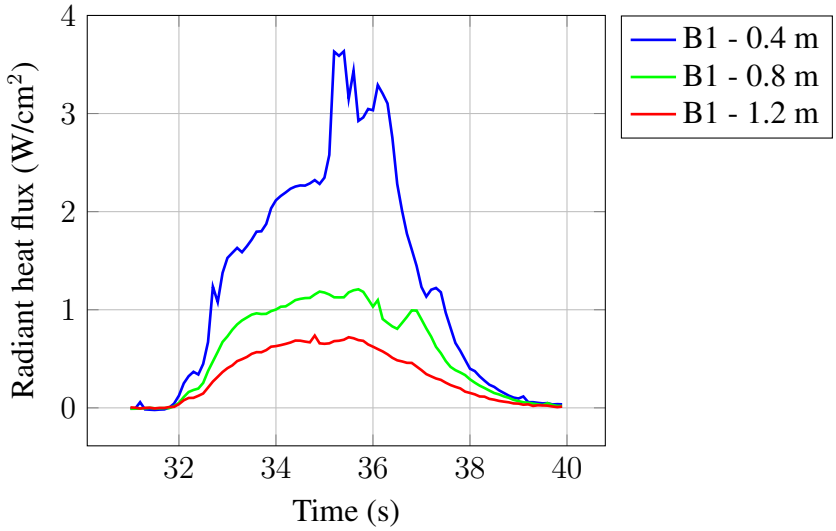
B1 - 0.4 m
B1 - 0.8 m
B1 - 1.2 m
Radiant heat flux (W/cm^2)
Time (s)
0
1
2
3
4
32
34
36
38
40

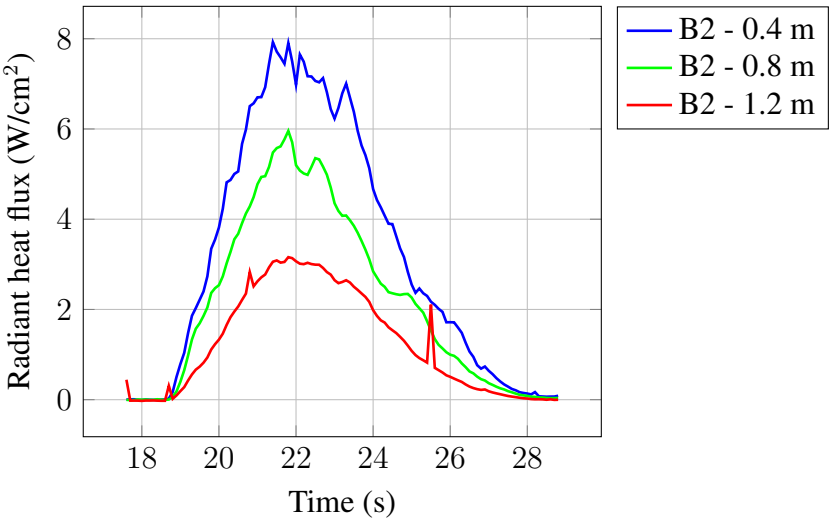
B2 - 0.4 m
B2 - 0.8 m
B2 - 1.2 m
Radiant heat flux (W/cm^2)
Time (s)
0
2
4
6
8
18
20
22
24
26
28

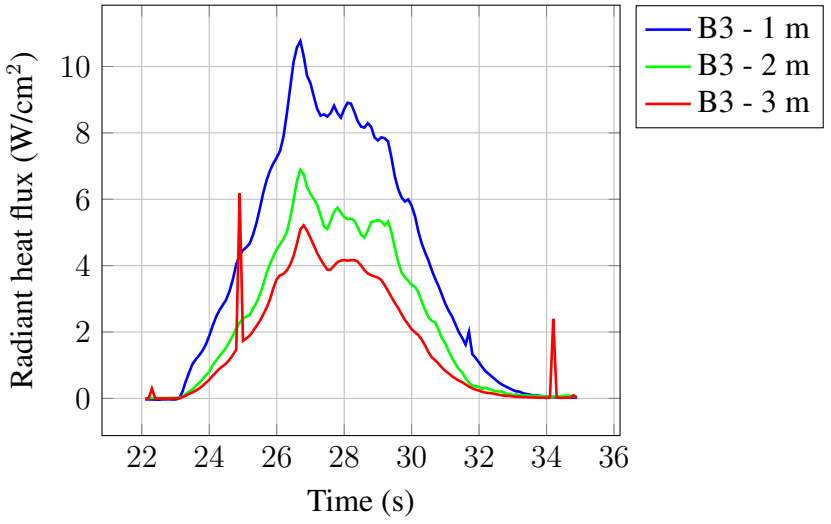
B3 - 1 m
B3 - 2 m
B3 - 3 m
Radiant heat flux (W/cm^2)
Time (s)
0
2
4
6
8
10
22
24
26
28
30
32
34
36

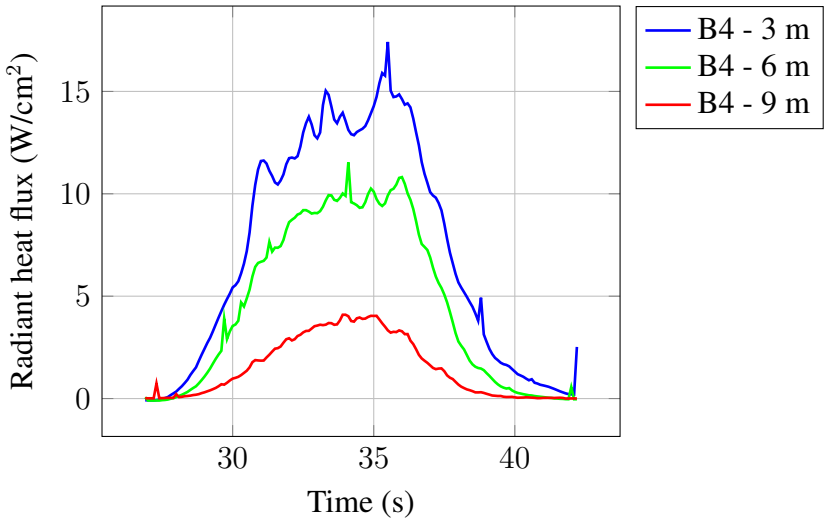
B4 - 3 m
B4 - 6 m
B4 - 9 m
Radiant heat flux (W/cm^2)
Time (s)
0
5
10
15
30
35
40

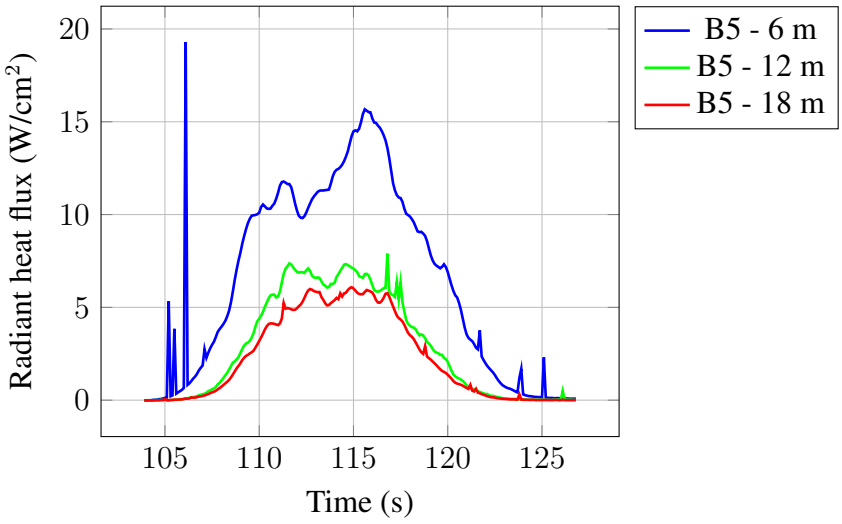
B5 - 6 m
B5 - 12 m
B5 - 18 m
Radiant heat flux (W/cm^2)
Time (s)
0
5
10
15
20
105
110
115
120
125

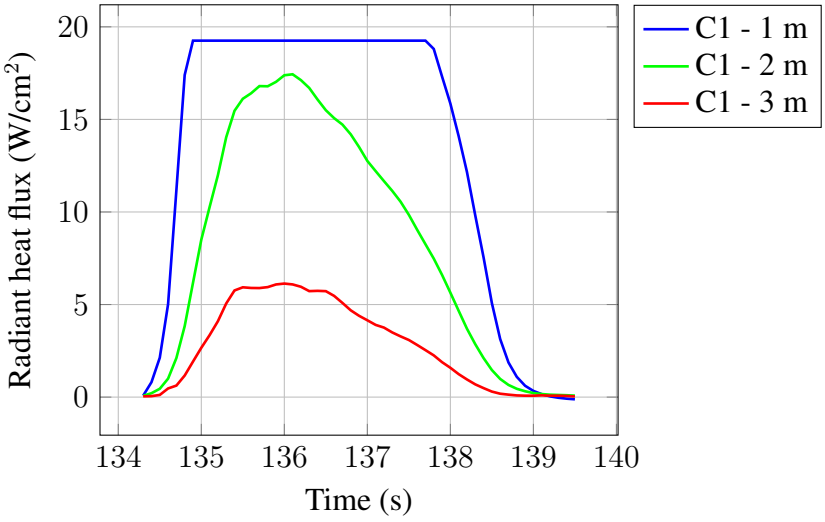
C1 - 1 m
C1 - 2 m
C1 - 3 m
Radiant heat flux (W/cm^2)
Time (s)
0
5
10
15
20
134
135
136
137
138
139
140

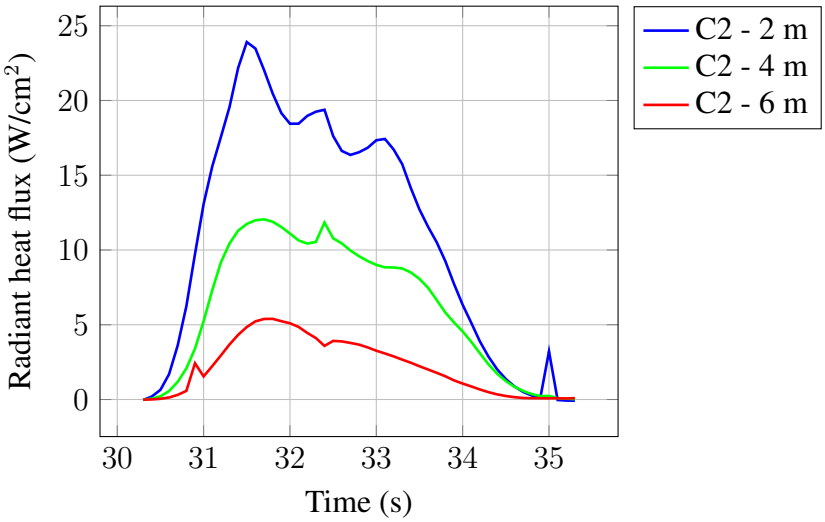
C2 - 2 m
C2 - 4 m
C2 - 6 m
Radiant heat flux (W/cm^2)
Time (s)
0
5
10
15
20
25
30
31
32
33
34
35

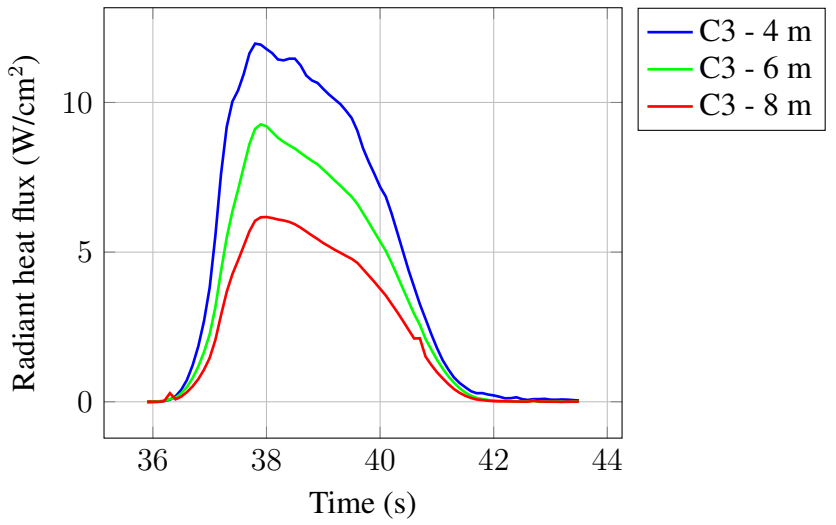
C3 - 4 m
C3 - 6 m
C3 - 8 m
Radiant heat flux (W/cm^2)
0
5
10
36
38
40
42
44
Time (s)

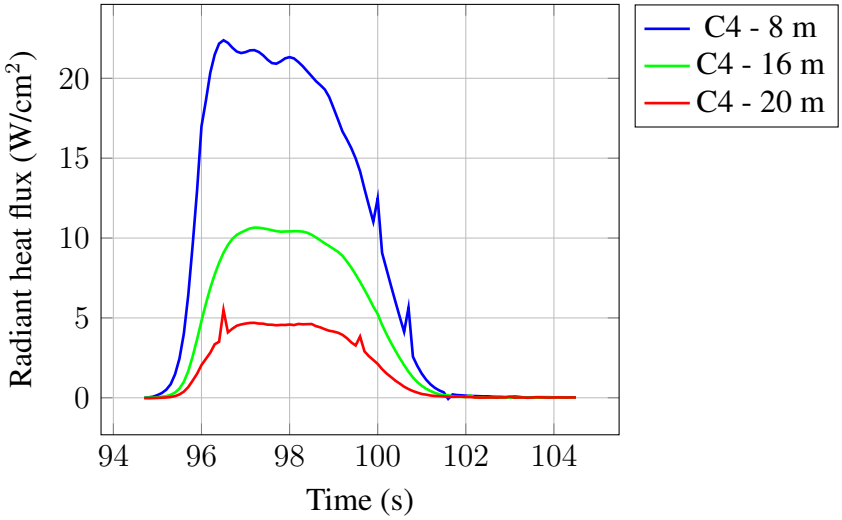
C4 - 8 m
C4 - 16 m
C4 - 20 m
Radiant heat flux (W/cm^2)
0
5
10
15
20
94
96
98
100
102
104
Time (s)

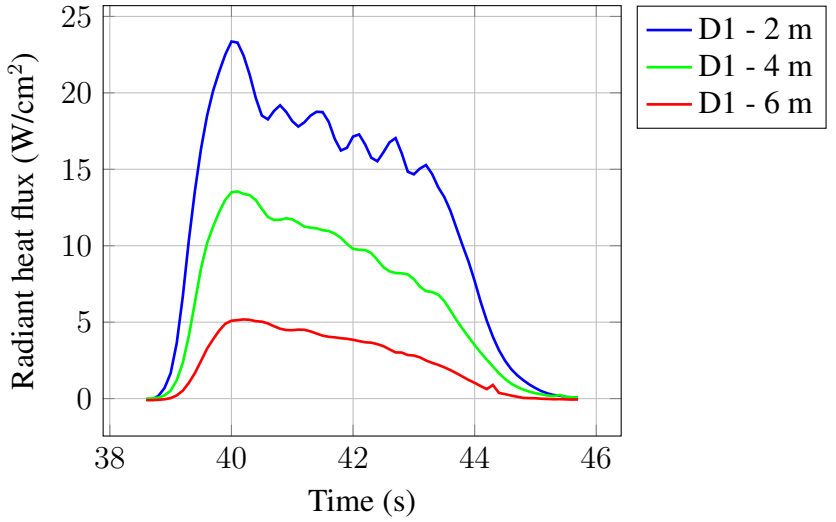
D1 - 2 m
D1 - 4 m
D1 - 6 m
Radiant heat flux (W/cm^2)
0
5
10
15
20
25
38
40
42
44
46
Time (s)

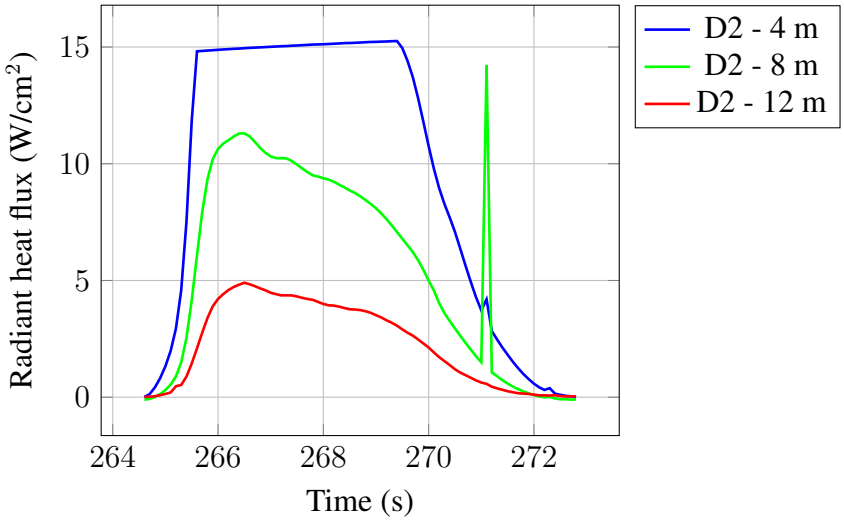
Radiant heat flux (W/cm^2)
15
10
5
0
264
266
268
270
272
Time (s)
D2 - 4 m
D2 - 8 m
D2 - 12 m

Appendix C

Pressure generation numerical tool

```
% Pressure generation in enclosure (Matlab code)

clear

robulk = 950; % kg/m3
rho(1) = 1.2; % kg/m3
MW = 0.026;  % kg/mol
T(1) = 291; % K
R = 8.314; % si-mks
HOE = 5200000; % J/kg
cv = 1100; % J/kg/K
Patm = 101300; % Pa

mi = 50; % kg
Venc = 100; % m3
Avent = 0.5; % m2
%Cd = (Avent/0.016)^0.5 * Avent^0.5; % Discharge coeff (auto)
Cd = 0.80; % Discharge coeff (man)
```

```
%mgendot = mi/0.3;
mgendot = mi/4;

n = 1;  % unitless
nmax = 60000;  % unitless
dt(1:nmax) = 0.0001;  % s
t = 0;
mstart = pi * Df^2 / 4 * H * robulk;
mburn = 0;

okerror = .0000001;

vvent(1) = 0;
mventdot(1) = 0;
mvent(1) = 0;
mventtot(1) = 0;
Pgen(1) = 0;
Pgeng(1) = Patm;
N(1) = 0;
time(1) = dt(1);
dummy1 = 0;

for n = 1:nmax;

    if mburn < 0.999*mi
        time(n) = t;

        if n > 1

            T(n) = T(n-1) + (HOE * mgendot * dt(n-1)) / (cv * (m(n-1) +...
            ... rho(1) * Venc)) - mventdot(n-1)*dt(n-1)*cv*T(n-1) ...
```

```
        ... / (cv * (m(n-1) + rho(1) * Venc));

        rho(n) = (Pgeng(n-1)) * MW / R / T(n-1);

        mburndot(n) = mgendot;
        vvent(n) = (2 * Pgen(n-1) / rho(n))^0.5;
        mventdot(n) = Cd .* vvent(n) .* Avent .* rho(n);

        mvent(n) = mventdot(n) .* dt(n);
        mventtot(n) = sum(mvent);
        mburn(n) = mgendot * time(n-1);

    else
        mburn(n) = mgendot * time(n);

    end

    m(n) = mburn(n) - mventtot(n);
    N(n) = m(n) ./ MW;
    Pgen(n) = N(n) .* R .* T(n) ./ Venc;
    Pgeng(n) = Pgen(n) + Patm;

    %n = n + 1;
    t = t + dt(n);
else

     T(n) = T(n-1) - mventdot(n-1)*dt(n-1)*cv*T(n-1) ...
     ... / (cv * (m(n-1) + rho(1) * Venc));

     rho(n) = (Pgeng(n-1)) * MW / R / T(n-1);

     time(n) = t;
```

```
        vvent(n) = (2 * Pgen(n-1) / rho(n))^0.5;
        mventdot(n) = Cd .* vvent(n) .* Avent .* rho(n);
        mvent(n) = mventdot(n) .* dt(n);
        mventtot(n) = sum(mvent);
        mburn(n) = mburn(n-1);

        m(n) = mburn(n) - mventtot(n);
        N(n) = m(n) ./ MW;
        Pgen(n) = N(n) .* R .* T(n) ./ Venc;
        Pgeng(n) = Pgen(n) + Patm;
        t = t + dt(n);
    end

end
```